National Defence
Research and Development Branch

Défense nationale
Bureau de recherche et développement

TECHNICAL MEMORANDUM 90/204
August 1990

EXAMPLES MANUAL FOR PROGRAM **MAVART**

G. W. McMahon - E. L. Skiba

Defence Research Establishment Atlantic

Centre de Recherches pour la Défense Atlantique

Canada

UNLIMITED DISTRIBUTION

National Defence
Research and Development Branch

Défense nationale
Bureau de recherche et développement

EXAMPLES MANUAL FOR PROGRAM **MAVART**

G. W. McMahon * - E. L. Skiba †

August 1990

Approved by P. Bhartia
Director / Sonar Division

Distribution Approved by

Director / Sonar Division

TECHNICAL MEMORANDUM 90/204

Defence Research Establishment Atlantic

Centre de Recherches pour la Défense Atlantique

Canada

* Defence Research Establishment Atlantic
† Acres International

ABSTRACT

This document is the third in a set of documents that provides information on the Finite Element **M**odel for the **A**nalysis of **V**ibration and **A**coustic **R**adiation of **T**ransducers (MAVART). The set comprises: 1. Theoretical Manual for Program MAVART, 2. User's Manual for Program MAVART, and 3. Examples Manual for Program MAVART. The program MAVART is resident at the Defence Research Establishment Atlantic (DREA) and has been developed under several research contracts to Canadian industry from 1976 to the present (1990). The original set of documents formed Contractor Report DREA CR/87/442 and they are now being extensively revised.

This Examples Manual attempts to demonstrate and exercise all of the capabilities and features of MAVART. As well, the DREA postprocessing program GRAF1 has been used to display the data for the example problems.

RESUME

Ce document est le troisième d'un ensemble de documents qui fournit des renseignements sur le modèle à éléments finis d'analyse des vibrations et du rayonnement acoustique des transducteurs (MAVART). L'ensemble compose: (1) du manuel des fondements théoriques, (2) du manuel de l'utilisateur, (3) et d'un recueil d'exemples.

Le programme MAVART est un programme résidant au Centre de recherches pour la Défense Atlantique (CRDA) développé par des industries canadiennes sous plusieurs contrats de recherches durant la période de 1976 à 1990. L'original de cet ensemble de documents, "Contractor Report DREA CR/87/442", est présentement en révision.

Ce recueil d'exemples essaie de démontrer et de mettre en pratique toutes les caractéristiques et le potentiel du code MAVART. De plus, le code pour traitement ultérieur, GRAF1 du CRDA, a été utilisé pour visualiser les données pour les problèmes exemples.

TABLE OF CONTENTS

TABLE OF CONTENTS (cont'd) **Page**

LIST OF FIGURES

LIST OF FIGURES (Cont'd)

LIST OF FIGURES (Cont'd)

LIST OF FIGURES (Cont'd)

LIST OF FIGURES (Cont'd)

1 INTRODUCTION

MAVART is a two-dimensional, dynamic finite-element code developed for DREA under research contracts to Canadian industry. It has been developed primarily for analysis of axisymmetric electroacoustic transducers, and the name is an acronym for the code's function, that is, a **M**odel to **A**nalyze the **V**ibrations and **A**coustic **R**adiation of **T**ransducers. It was first implemented in 1976, under a contract with Acres Consulting Services, Niagara Falls, Ontario. It has been revised and improved a number of times over the years, the latest version (MAVART9 - 1989) resulting from a contract with Ortech International, Mississauga. The main revision introduced in MAVART9 is the installation of the Waterloo University's SPARSPAK solver package, replacing the profile solver used in the previous version. Other new features are the addition of torsional analysis capability and the ability to conduct a resonance search on any specified degree-of-freedom.

This document is a revised edition of the 1987 Examples Manual, issued by Ortech International as part of DREA Contractor Report CR/87/442 [Ref. 1.1]. It now features graphic data display generated by the DREA program GRAF1 [1.2, 1.3], rather than Ortech's SDRC post-processing system. Also added are a torsional structure example and a corrected viscous fluid example, which can be analysed only with MAVART9.

Companion Theoretical [1.1b] and User's Manuals [1.1a] complete the manual set. In addition to the tests reported in this Examples Manual, some special testing of MAVART's capabilities and limitations have been conducted. These tests are reported separately and are referenced in this document when they are relevant to an example problem.

The purposes of this revised Examples Manual are:

- to aid MAVART users in model development, and data input and output interpretation;
- to provide comprehensive new user training;
- to exercise and demonstrate all elements and features of MAVART;
- to provide a set of problems to validate proper operation of the program after modifications are made;
- to help in establishing timing benchmarks for reference after modifications are made; and
- to exercise and demonstrate features of the post-processor GRAF1.

The pre-processor programs available at DREA for MAVART data preparation are GRID [1.4], to create a F. E. grid using a digitizing table, MOD [1.5] to modify node and element data created by GRID, and MATER [1.6], [1.7] to compute the material properties. Several changes to these programs have taken place since their initial development and other reports have documented these changes [1.8], [1.9].

All of the programs in the MAVART package at DREA are written in Fortran-77. All recent versions of MAVART have been developed on VAX computers and have been installed on the DEC 2060 computer at DREA and on a HP 9000 computer at Hermes Electronics, Dartmouth. MAVART9 is presently installed only on the μVax 3900 at DREA.

2 TEST PROBLEM DEFINITION

Most test problems come from DREA experience with simple, typical transducer designs that have special features or are of special interest. They have been selected so as to exercise all MAVART features.

2.1 LIST OF PROBLEMS

The problems that have been included in the manual are grouped below by principal element type and are individually numbered.

Series 1 Problems - PAR Piezoelectric Spherical Shell:

1. STATC - pressure load (hydrophone sensitivity, stresses)
2. EIGEN - resonance
3. EIGEN - antiresonance
4. CAPAC - frequency sweep
5. CAPAC - transient
6. DRIVE - frequency sweep (stresses at resonance)

Series 2 Problems - PT Piezoelectric Ring:

7. EIGEN - resonance (m = 2,0)
8. CAPAC - frequency sweep (m = 0)
9. DRIVE - resonance search, with and without extra DOF's carried

Series 3 Problems - PAR, SOLID and SLIDER Trilaminar Bender Disk:

10. STATC - electric stress
11. STATC - thermal stress
12. CAPAC - deformations, with and without slider softening

Series 4 Problems - SHELL Thin Disk/Tube:

13. EIGEN - flexural and extensional resonances
14. STATC - transverse temperature differential, and nodal load

Series 5 Problem - Analytical FLUID and FTOS:

15. DRIVE - piston in infinite hard baffle

Series 6 Problem - MEMBRANE, FLUID, and FTOS:

16. DRIVE - MEMBRANE on spherical air bubble

Series 7 Problem - RING and SHELL:

17. EIGEN - RING-stiffened SHELL with added nodal mass

Series 8 Problem - DAMPING Applications:

18. DRIVE - complex modulus and viscous damping in PT ring

Series 9 Problems - Ring Array and RIGID Node Application:

19. DRIVE - Two Free-flooding PT Rings and SOLID Spacer Ring
20. DRIVE - RIGID node replacing Spacer Ring

Series 10 Problem - Torsional Applications

21. STATC - SOLID cylinder with torsional loading (m=0)
22. EIGEN - SOLID cylinder torsional resonance

2.2 PROBLEM / FEATURE MATRIX

Figure 2.2.1 provides a cross-reference chart of significant program features and test problems. It allows the MAVART user to quickly find which example problem demonstrates a given problem type, element type, node type, or other program feature. The listed problems attempt to exercise all of the features to an adequate degree, biased towards the normal use of the program.

Most features of GRAF1 are also exercised by these example problems, although no cross-reference chart is presented.

Figure 2.2.1: Problem / Feature Matrix

FEATURE		Problem #																					
		1	2	3	4	5	6	7	8	9	10	11	12	13	14	15	16	17	18	19	20	21	22
PROBID	EIGE		*	*				*						*				*					*
	STAT	*									*	*			*							*	
	CAPA				*	*			*				*										
	DRIV						*			*						*	*		*	*	*		
	FOUD					*																	
Phase	TRAN					*																	
ELEMENTS	SOLID(Q)										*	*	*		*					*		*	
	PAR(Q)	*	*	*	*	*	*				*	*	*										
	PT(Q)							*	*	*									*	*	*		
	FLUID(Q)						*			*						*	*		*	*	*		
	MEMB																*						
	FTOS	*					*			*						*	*		*	*	*		
	FTOF						*			*						*	*		*	*	*		
	SILV	*	*	*	*	*	*																
	SLIDER										*	*	*										
	SHELL													*	*	*		*					
	RING																	*					
	VISC																		*				
NODES	S							*	*	*	*	*	*						*	*	*	*	
	R																				*		
	A	*	*	*	*	*	*				*	*	*										
	H													*	*	*		*					
	E							*	*	*									*	*	*		
	F	*					*			*						*	*		*	*	*		
	Load														*							*	
	Mass																	*					
Fourier m>0								*															
Torsion m=0																						*	*
Damping																			*				
Thermal Load											*			*									
Frequency Sweep					*		*		*														
Resonance Search										*													

3 GENERAL APPROACH TO PROBLEM ANALYSIS

The problem analysis, performed using Ortech's Vax 11/6210 computer, followed the sequence:

- pre-processing, i.e. finite element model and input data preparation;
- execution in MAVART; and
- post-processing, to interrogate results of the analysis.

To facilitate the pre- and post-processing tasks at Ortech, the Structural Dynamics Research Corporation (SDRC) Integrated Design Engineering and Analysis System (I-DEAS) was used. This software is not available at DREA nor at Acres International, where MAVART improvements are now (1990) taking place under contract.

For this edition of the Examples Manual, the problems have been re-run on DREA's μVax 3900. Some of the problems' input data were changed slightly for various reasons, and these changes are documented where they occur.

3.1 MODEL DEVELOPMENT

The path taken to prepare the finite element (F.E.) model for a problem was consistent with capabilities offered by SUPERTAB - the finite element modeller, part of the I-DEAS software used at Ortech. The procedure followed the steps:

- coordinate systems and node creation;
- generation of linear elements;
- element order change from linear to parabolic; and
- minimization of the model's bandwidth, which explains some peculiarities of node and element numbering.
- translation of data into a MAVART input file.

3.2 PROBLEM SOLVING

Each MAVART execution produces a lexical output file §MAV.DAT, where "§" represents a user identification character input on start-up. A binary data file §IN32.DAT, required for GRAF1 input, is also generated. A portion of the data in §MAV.DAT is output to the terminal, or to a Batch LOG file so that the operation of the job can be monitored.

3.3 DATA PRESENTATION

Each MAVART input file created at the pre-processing stage bears a name compatible with the problem annotation, e.g. for Problem 9 the corresponding input file is D09.DAT . MAVART execution produces one or more files named §MAV.DAT;x, where x is a revision level. To facilitate their identification, the output files were renamed for compatibility with the corresponding problem description, e.g. §MAV.DAT;3 for Problem 9 was renamed E09_V03.RES;1. The files D**.DAT and E**.RES for each problem were copied to magnetic tape for delivery to DREA. As well, files F**.LOG and E**.LOG for each problem were written to the tape; these monitor MAVART runs using the old profile solver and the new SPARSPAK solver,respectively. In general, the SPARSPAK solver provides a substantial improvement in execution time.

Each section of the following chapters contain details pertinent to a particular problem solved. Besides the lexical output files, stored on the tape, some significant results of the analysis are shown in the form of plots generated using GRAF1, such as:

- model grids;
- stress and strain contours;
- pressure and pressure gradient contours;
- displacements of solid boundaries;
- directional response of acoustic output; and
- plots of various parameters versus frequency.

Most of the graphic output presented in this edition was generated by DREA's GRAF1 program, but some minor editing was done in the MacDraw II application on the Macintosh computer. Note that the direction of the positive R-axis is reversed from that used in the earlier editions. This now conforms to most scientific and engineering practice, except for Civil Engineering.

4 SERIES 1: PAR PIEZOELECTRIC SPHERICAL SHELL

A cross-sectional diagram of the radially-poled piezoelectric spherical shell, made of Clevite PZT-4 material [4.1] and immersed in sea water, is shown in Figure 4.0.1. The inner and outer radii of the shell are 0.911 m and 1.0 m, respectively. The outer radius of the near-field sea water sphere used in the analysis is 2.0 m.

Due to symmetry of the problem, only the upper hemisphere has been analyzed. The mesh of the F.E. model is shown in Figure 4.0.2 . The Z and R axes of the model system of cylindrical coordinates coincide respectively with the Z and X axes of the coordinate system shown. Element numbers are printed just above the centroid of the element.

Figures 4.0.3 (a,b) and 4.0.4 (a,b) give details of node and element numbering of the F.E. model. Note that the fluid node numbers are printed by GRAF1 just above the node position and solid node numbers are printed just below.

The elements grouped along the outer boundary of the fluid are FTOF, Type 7 elements. The outer surface of the shell is "covered" with SILV, Type 8 elements. These are necessary for antiresonance analysis of a PAR piezoelectric structure, but can be useful whenever Type A (PAR) nodes must be connected together electrically. Also along the outer surface of the shell are FTOS, Type 6 elements that connect the solid structure to the fluid.

The horizontal symmetry plane requires proper boundary conditions for solid elements: the cross plane displacements for Nodes 1,3, and 4 are restrained in the Z-direction, i.e., JFIX(1)=1.

Figure 4.0.1: Series 1 Problems - Model Diagram

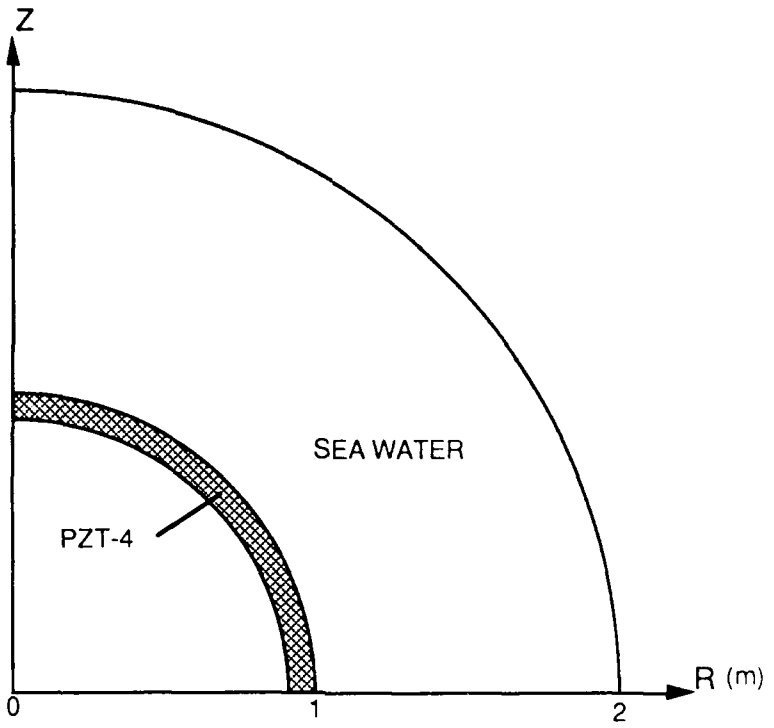

Figure 4.0.2: Series 1 Problems - Full F.E. Model

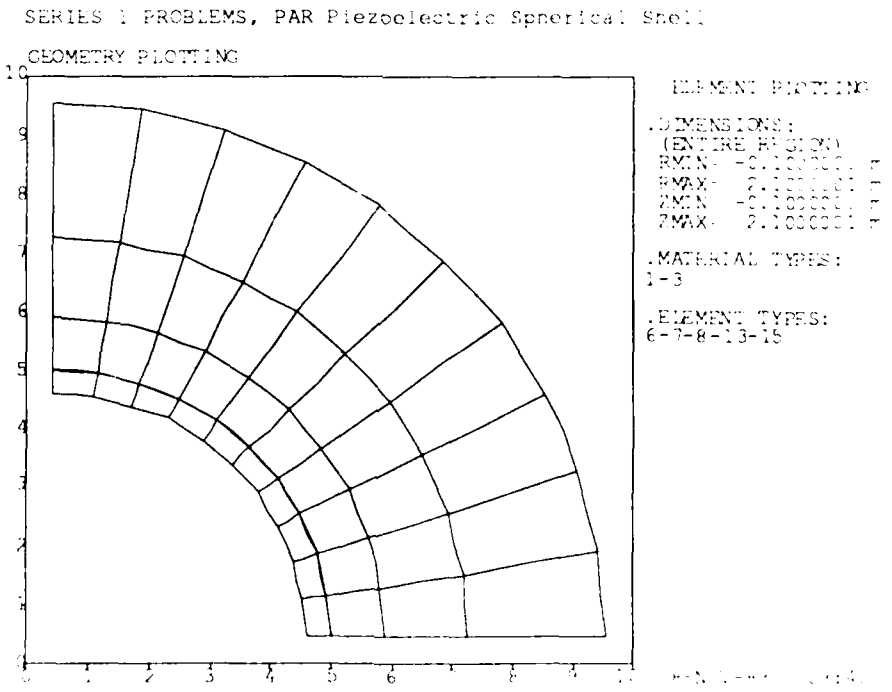

Figure 4.0.3 (a): Series 1 Problems - Fluid Node Numbering

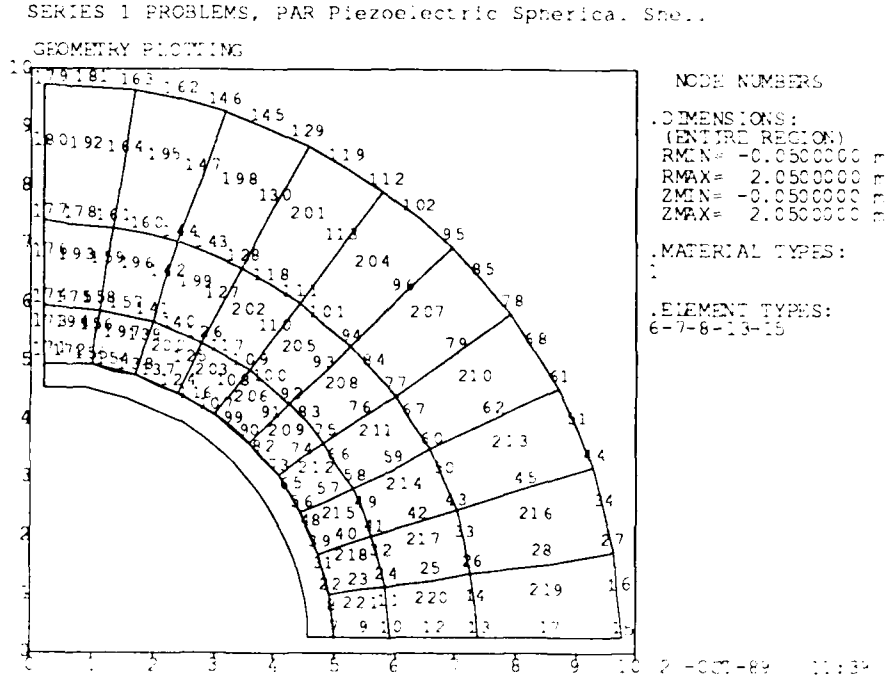

Figure 4.0.3 (b): Series 1 Problems - Solid and Connecting Fluid Node Numbering

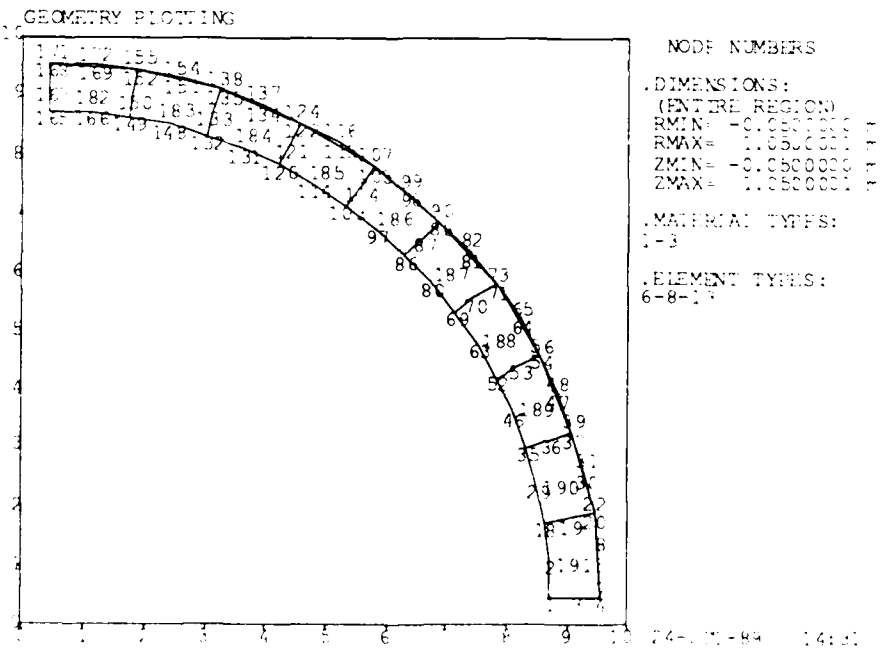

Figure 4.0.4 (a): Series 1 Problems - FLUID and FTOF Element Numbering

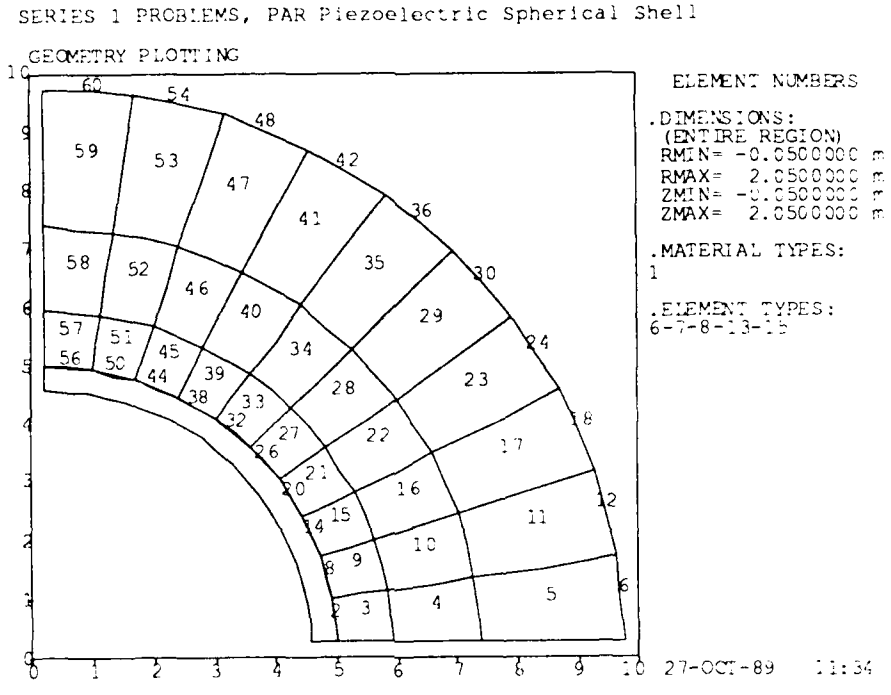

Figure 4.0.4 (b): Series 1 Problems - SOLID and SILV Element Numbering

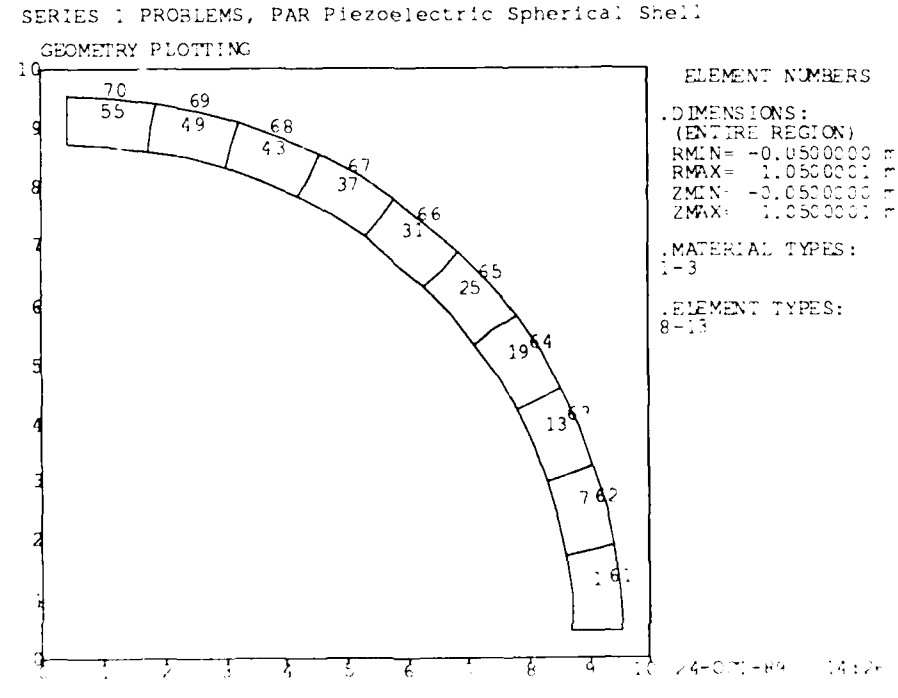

4.1 PROBLEM 1

Analysis Type: STATC - pressure load (hydrophone sensitivity, stresses)

Input File: D01.DAT

The F.E. model, a subset of the full model from Figure 4.0.1 , contains PARQ, FTOS and SILV elements only. The nodes used are shown in Figure 4.0.3(b)

A uniform pressure of 1 Pa, applied to the F nodes of the FTOS elements, is shown in input data as a load fixity and shown graphically in Figure 4.1.1. The small "pins" pointing to the fixed nodes indicate non-zero fixities. Voltage on the internal surface of the PARQ elements is fixed at V = 0. GRAV and SPIN body forces (Card 13) are set to zero. The voltage node, to which the calculated hydrophone sensitivity is referred, is Node 5 and input pressure is 1 Pa (Card 14). It is important to notice that Node 5 is located on the silvered external surface of the piezoelectric shell.

Plots of selected output data are shown in Figures 4.1.2 through 4.1.4 . Note that the radial stress depicted in Figure 4.1.4 is cylindrically radial and not spherically radial.

The hydrophone receiving sensitivity printed on Figure 4.1.2 is valid at low frequencies, well below any resonances. Simple theory for thin spherical shells leads to the following expression for receiving sensitivity:

$$M = r\, d_{31} \,/\, \varepsilon_{33}^{T} \qquad (4.1)$$

where r = 0.9555 metre is the mean radius of the spherical shell,
d_{31} = –123.E–12 m/V is the transverse piezoelectric strain constant,
and ε_{33}^{T} = 1.15E–8 F/m is the dielectric permittivity at constant stress.
With these "book" values for PZT-4 [see Ref. 4.1], we calculate a receiving sensitivity of –159.98 dB re-1V/μPa, in good agreement with the value obtained by MAVART of –160.00 dB.

Figure 4.1.1: Problem 1 - Fixities

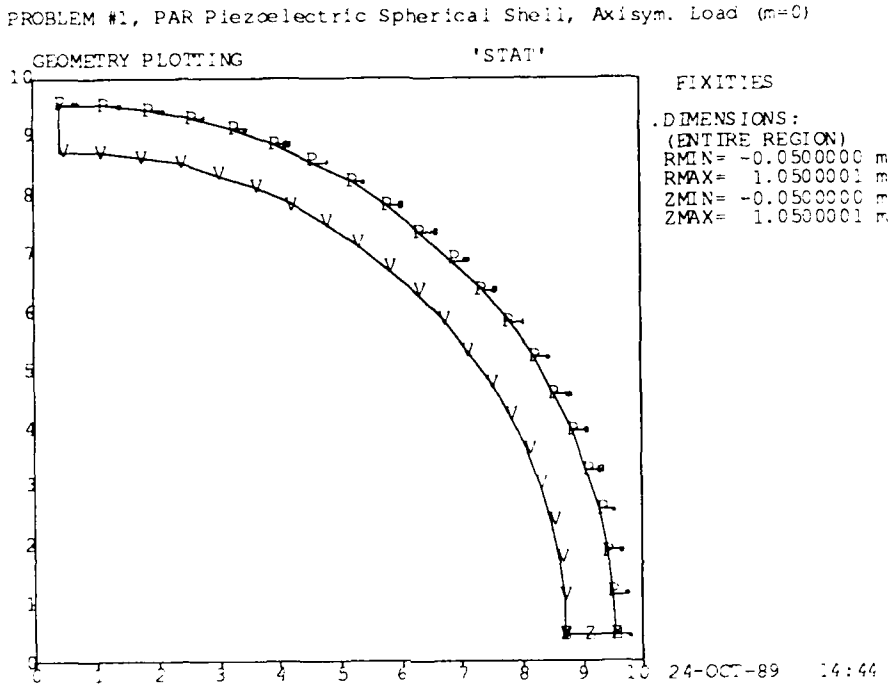

Figure 4.1.2: Problem 1 - Deformations

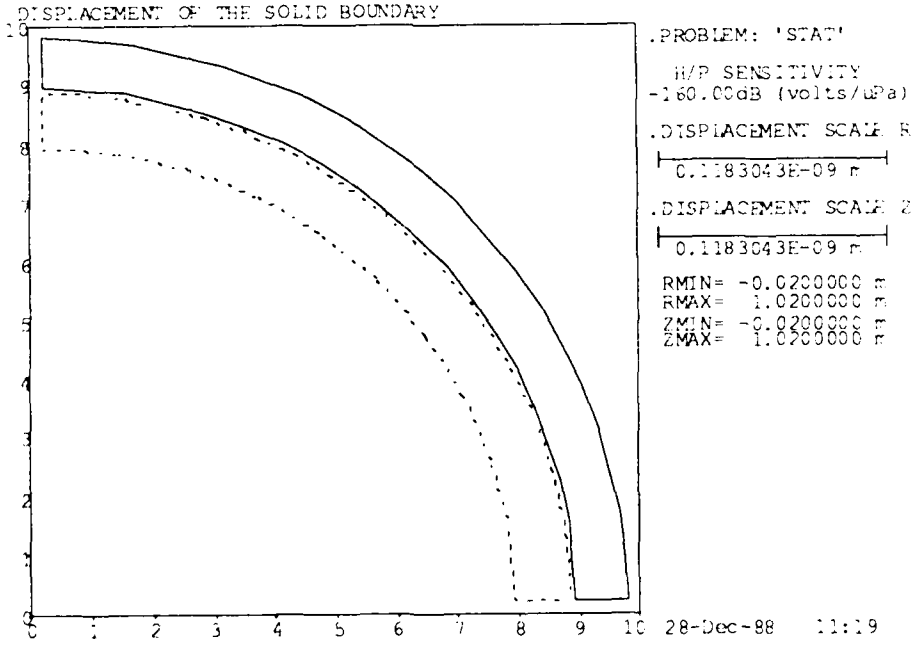

Figure 4.1.3: Problem 1 - Axial Stresses

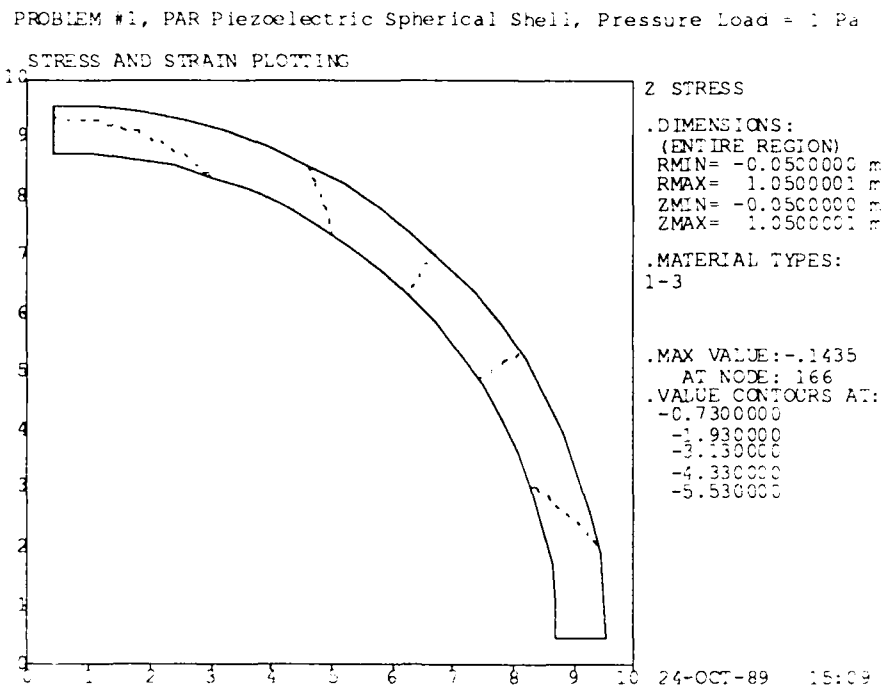

Figure 4.1.4: Problem 1 - Radial Stresses

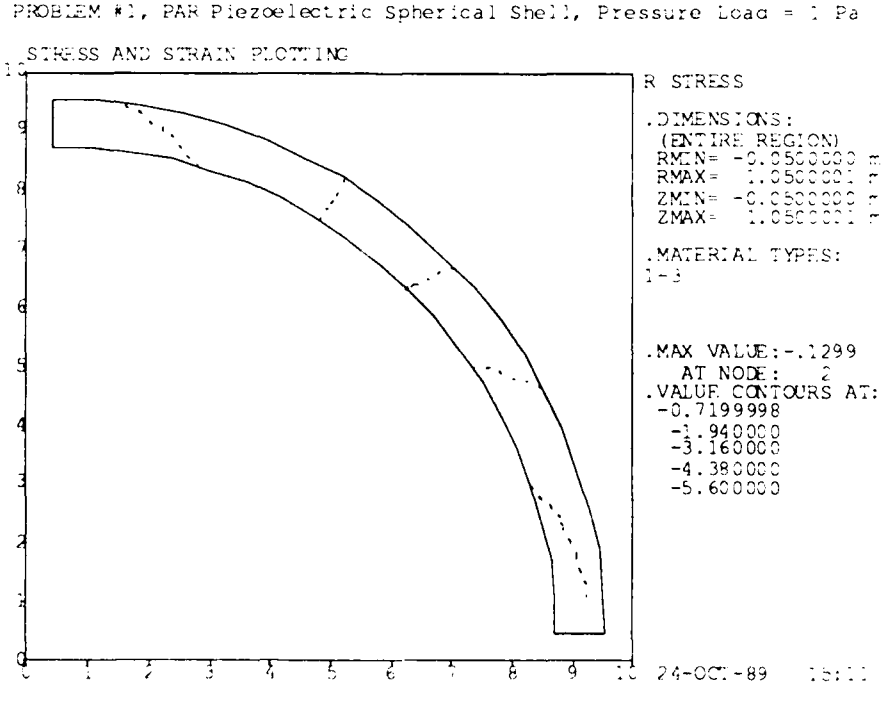

4.2 PROBLEM 2

Analysis Type: EIGEN - resonance

Input File: D02.DAT

The F.E. model, a subset of the full model from Figure 4.0.1 , contains PARQ, and SILV elements only.

As the resonance condition requires, a V = 0 fixity is applied to all of the nodes on the inner and outer surfaces of the shell (i.e., a short-circuit condition). Due to the presence of SILV elements, it is sufficient to apply V = 0 to Node 4, in order to assure a uniform potential of V = 0 on the entire external surface of the shell.

Lower and upper frequency estimates (Card 6) are set to 300 Hz and 1000 Hz respectively. The normalizing DOF number was chosen as 83 after a geometry check run to ensure that this is not a fixed DOF. The value of the normalizing DOF is set to 1.0E–6 . Values of ERVAL and ERVEC (Card 7) were each reduced to 1.0E–6 to ensure convergence to an accurate solution [See Ref. 4.2]

Plots of mode shape for the first four modes are shown in Figures 4.2.1 through 4.2.4. Mode 4, the "breathing" mode, is the only one of these modes that can be excited piezoelectrically with the (spherically) radial poling condition of Problem 2.

Analytical theory [4.3] for a thin-walled spherical shell gives the following expression for the resonance frequency (Mode 4):

$$f_r = (2\pi^2 r^2 \rho (s_{11} + s_{12}))^{-1/2} \qquad (4.2)$$

where r is the mean radius of the sphere, ρ is the density, and s_{11} and s_{12} are elastic compliance moduli of the material. The short-circuit elastic moduli are used for resonance calculation, and open-circuit moduli for antiresonance calculation, giving values of 947 Hz and 1162 Hz, respectively, using Clevite "book values" for the properties of PZT-4 [4.1].

Figure 4.2.1: Problem 2 - 1st Mode Shape

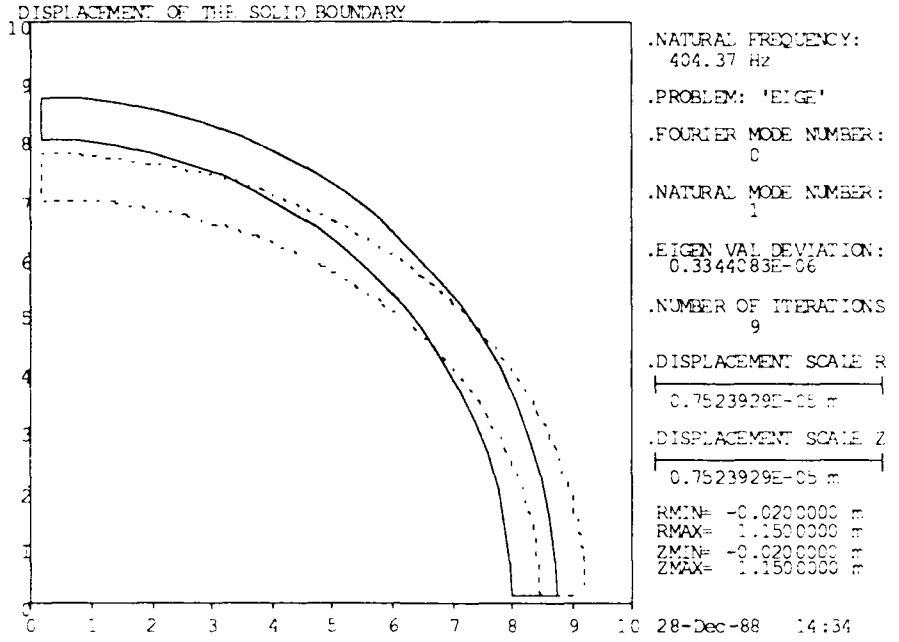

Figure 4.2.2: Problem 2 - Second Mode Shape

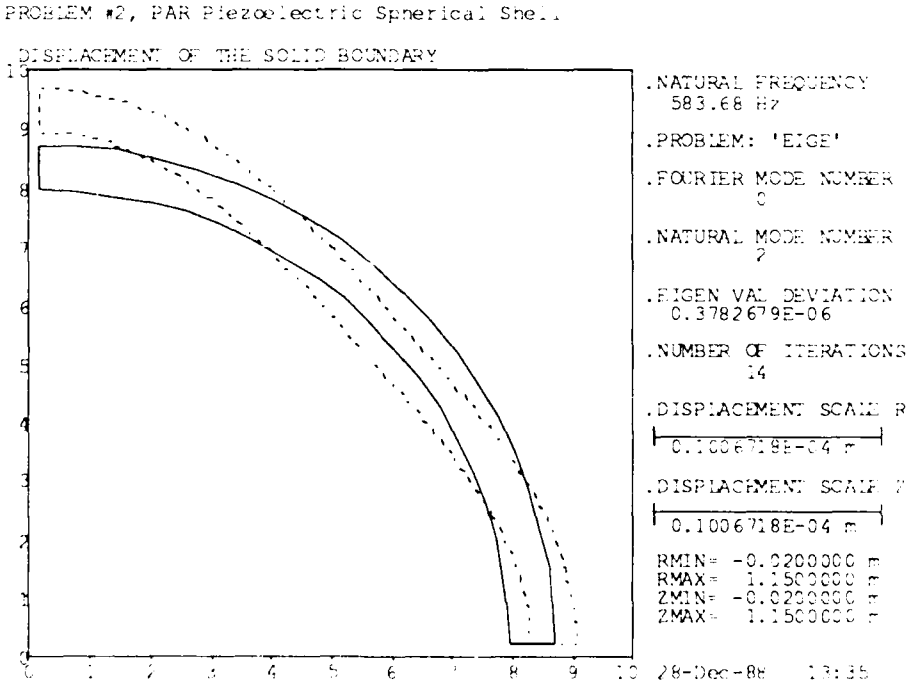

Figure 4.2.3: Problem 2 - Third Mode Shape

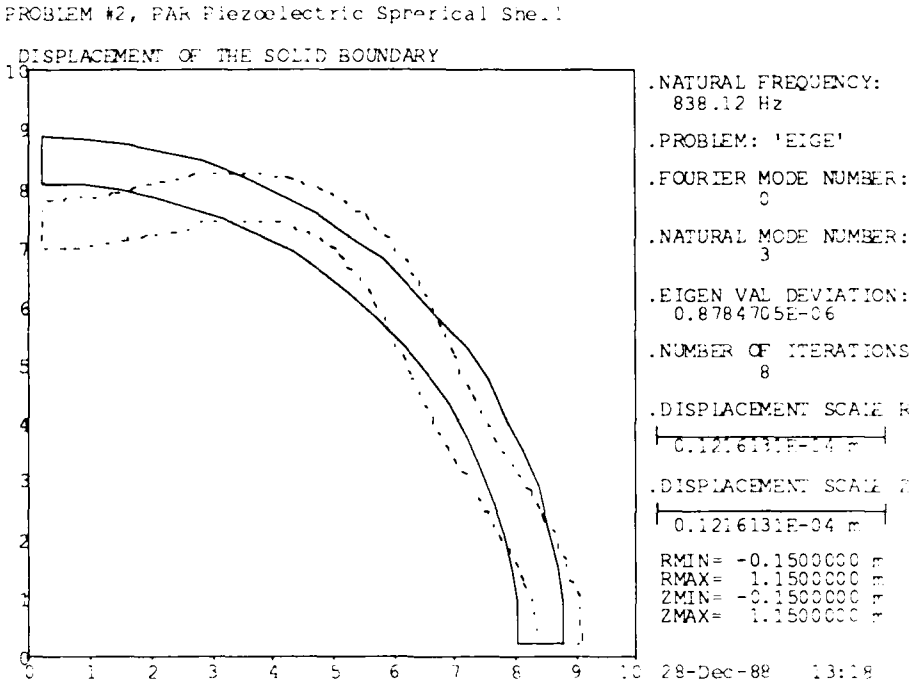

Figure 4.2.4: Problem 2 - Fourth Mode Shape

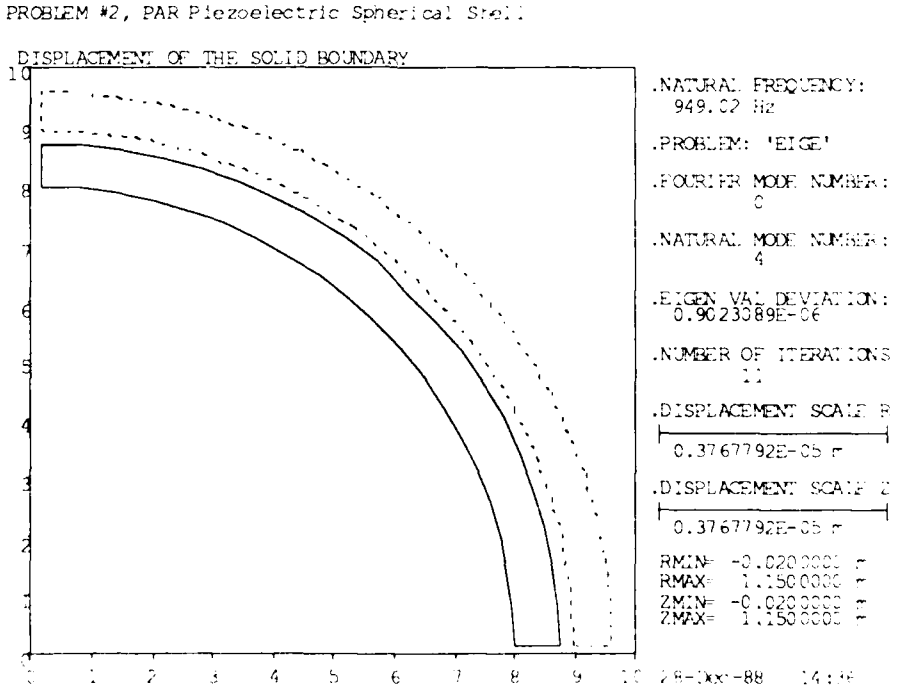

4.3 PROBLEM 3

Analysis Type: EIGEN - antiresonance

Input File: D03.DAT

The F.E. model, a subset of the full model from Figure 4.0.1 , contains PARQ, and SILV elements only.

For antiresonance analysis an open-circuit condition is required; hence, a V = 0 fixity is applied to one surface - in this case, the internal surface of the shell, while the outer silvered surface is free. The only change that is required to Problem 2 input data is to remove the fixity from Node 4.

The modal frequency analysis data (Card 6) are the same as for Problem 2. Two poling conditions, set by parameter POLANG, for the piezoelectric shell have been used in both resonance and antiresonance analyses: (a) Uniform radial (spherical) poling and (b) The upper five of the ten PARQ elements have their poling reversed. The first four mode shapes are essentially identical in all cases to those shown in Figures 4.2.1 to 4.2.4 for the resonance (a) condition. The frequencies obtained in the MAVART analysis are given in the following table for all cases:

	(a) FULL RADIAL POLING		(b) HALF REVERSED POLING	
Mode #	Resonance	Antires.	Resonance	Antires.
1	404.37	404.37	404.43	409.28
2	583.68	583.68	582.74	583.02
3	838.12	838.11	844.18	845.02
4	949.02	1146.8	948.54	974.37

Note that for condition (a), the antiresonance frequency differs from the resonance only for Mode 4, which is the mode of most interest acoustically. For condition (b), the antiresonance is always higher in frequency than the resonance, indicating that the other modes can now be excited piezoelectrically.

The resonance and antiresonance frequencies calculated using Eq. 4.2, 947 Hz and 1162 Hz, respectively, are in reasonable agreement with the MAVART predictions of 949 Hz and 1147 Hz, above.

4.4 PROBLEM 4

Analysis Type: CAPAC - frequency sweep

Input File: D04.DAT

The F.E. model, a subset of the full model from Figure 4.0.1, contains PARQ, and SILV elements only.

A V = 0 fixity is applied to all nodes on the internal surface of the shell. A sinusoidal driving voltage of 1 V amplitude is specified as a fixity at Node 4 on the silvered surface.

The same polarity of PARQ elements as in Problem 3, condition (b) is used, so that Mode 1 can be excited.

A frequency scan was conducted in the range of 400 Hz through 408 Hz, with frequency start points and increments specified according to Card 8 format. Ten element groups are used, one element per group. NSTAV, the 'number of staves' in the transducer is 2, as a hemisphere is being analyzed; for a full sphere, NSTAV would be 1.

Plots of deformations, obtained at 404 Hz excitation frequency for two different phase angles, are shown in Figures 4.4.1 and 4.4.2. Capacitance is plotted versus frequency in Figure 4.4.3. It should be noted that the capacitance values passed to the output files are the absolute values. It is necessary to use absolute values in the resonance search mode (see Problem 9) since the logarithm of the value is used. However, any negative (i. e. inductance) values should be restored before output. This will be corrected in a future revision of MAVART. Some of the capacitance values just above the resonance in Figure 4.4.3 may be negative.

Figure 4.4.1: Problem 4 - Deformations at 404 Hz, Phase = 0

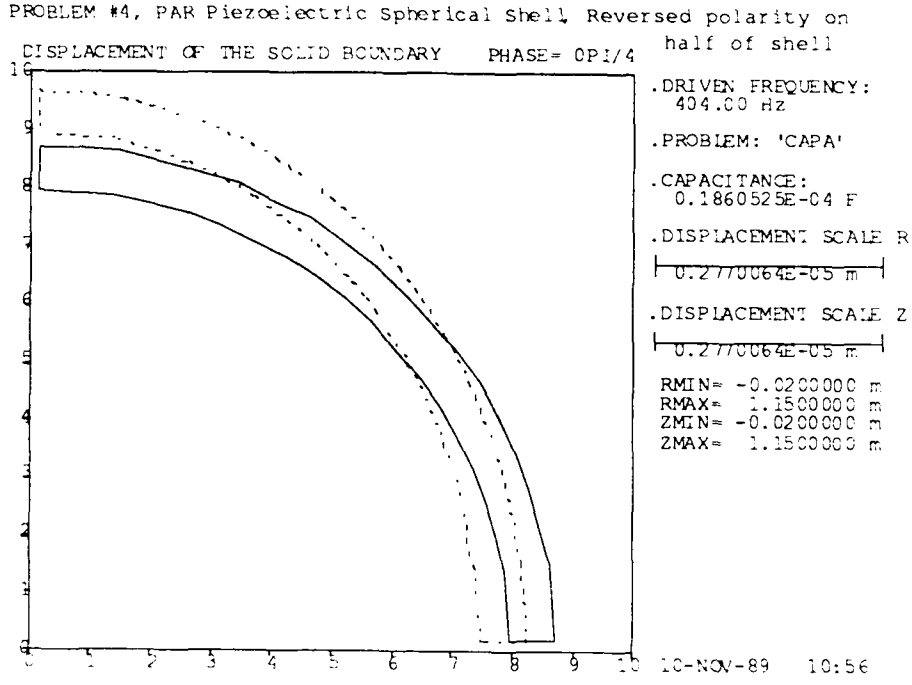

Figure 4.4.2: Problem 4 - Deformations at 404 Hz, Phase = π

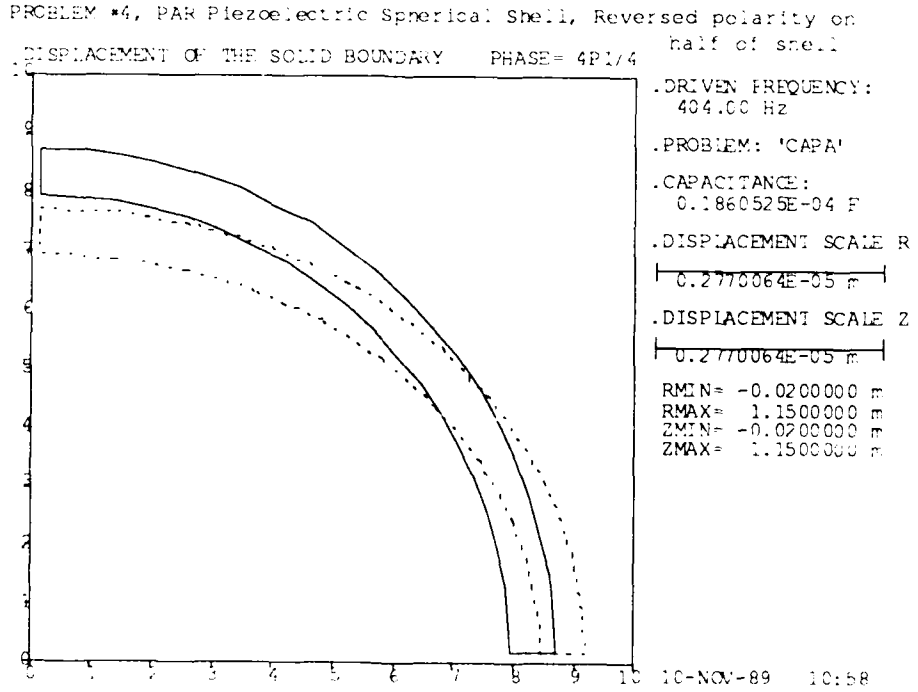

Figure 4.4.3: Problem 4 - Capacitance versus Frequency

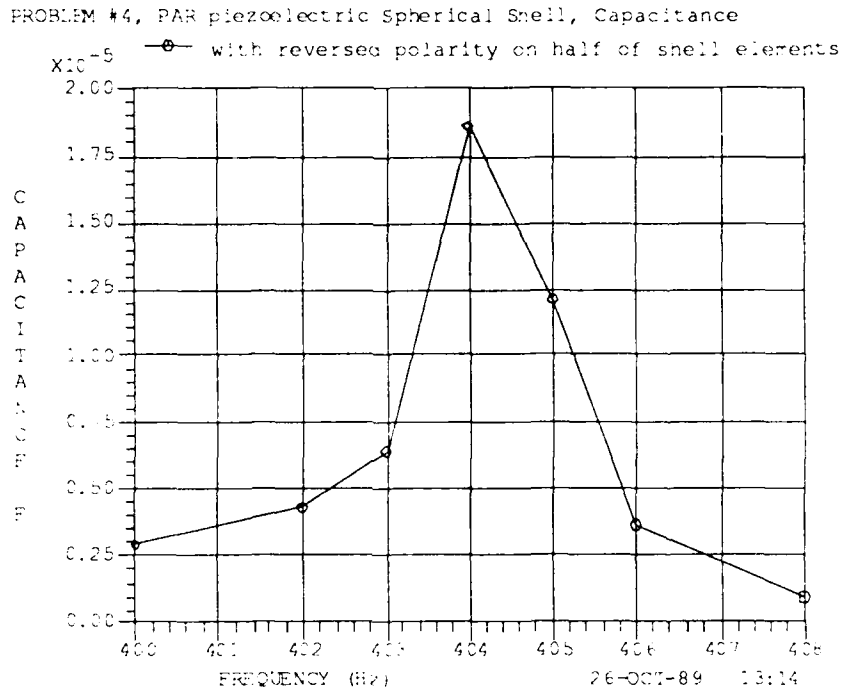

4.5 PROBLEM 5

Analysis Type: CAPAC - transient

Input File: D05.DAT

Auxiliary Input File: D05FOUD.DAT

Auxiliary Output File: FOUDC.DAT

The F.E. model, a subset of the full model from Figure 4.0.1 , contains PARQ, and SILV elements only.

Voltage fixities, the driving point and the polarity of PARQ elements are the same as in Problem 4 .

In order to obtain a time-dependent solution for an arbitrary forcing function, it is necessary to decompose the function first into the corresponding Fourier series using the Fourier Decomposition Pre-processor invoked by setting variable PROBID to "FOUD". At the end of the auxiliary input file D05FOUD.DAT, the Fourier decomposition data are given in a format specified by Cards 16 (a,b) . In this case there are sixteen equally spaced values in one cycle of a 1-volt-amplitude square wave (2 volts peak-to-peak) with a fundamental frequency of 134.7 Hz. Note that this drive is not a true "transient", but a repetitive, non-sinusoidal waveform.

MAVART execution with the file D05FOUD.DAT as input yields output files §MAV.DAT and FOUDC.DAT. The latter, containing Fourier coefficients, is used automatically in subsequent MAVART execution, with file D05.DAT serving as the main source of input data.

In file D05.DAT, the fundamental frequency, total number of harmonic frequencies and number of times at which displacements and stresses are to be computed are given according to Card 9 (a) . After inspection of data in file FOUDC.DAT, harmonic numbers 1, 3 and 5 were chosen and written into D05.DAT, as required by Card 9 (b) . Then, six equally spaced time instances, ranging from 7.5 ms through 10 ms, were specified as per Card 9 (c).

Plots representing snapshots of the deformation at the selected times are shown in Figures 4.5.1 through 4.5.6 .

Figure 4.5.1: Problem 5 - Deformations at 0.0075 s

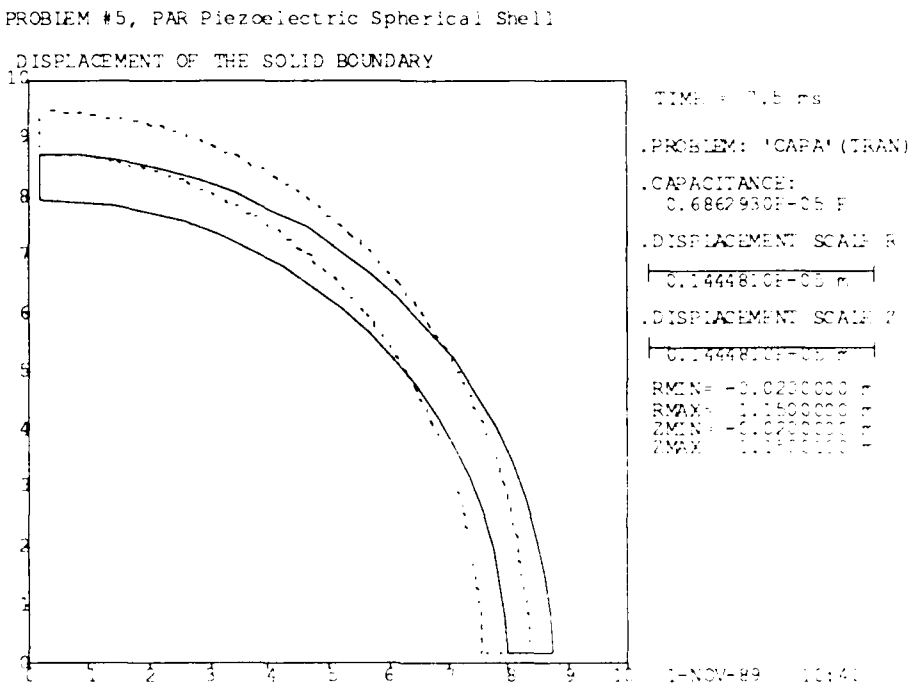

Figure 4.5.2: Problem 5 - Deformations at 0.0080 s

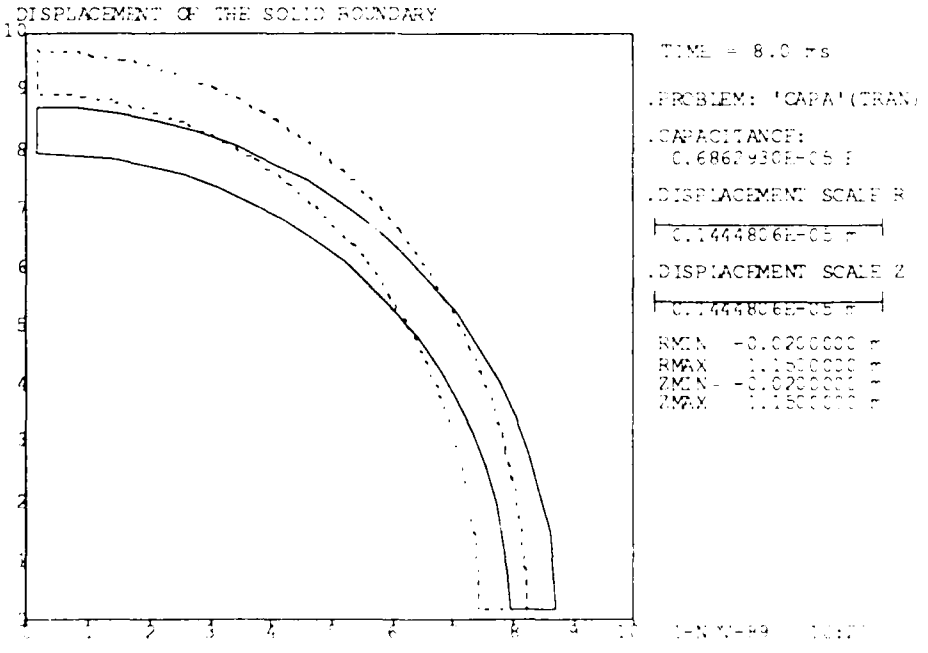

Figure 4.5.3: Problem 5 - Deformations at 0.0085 s

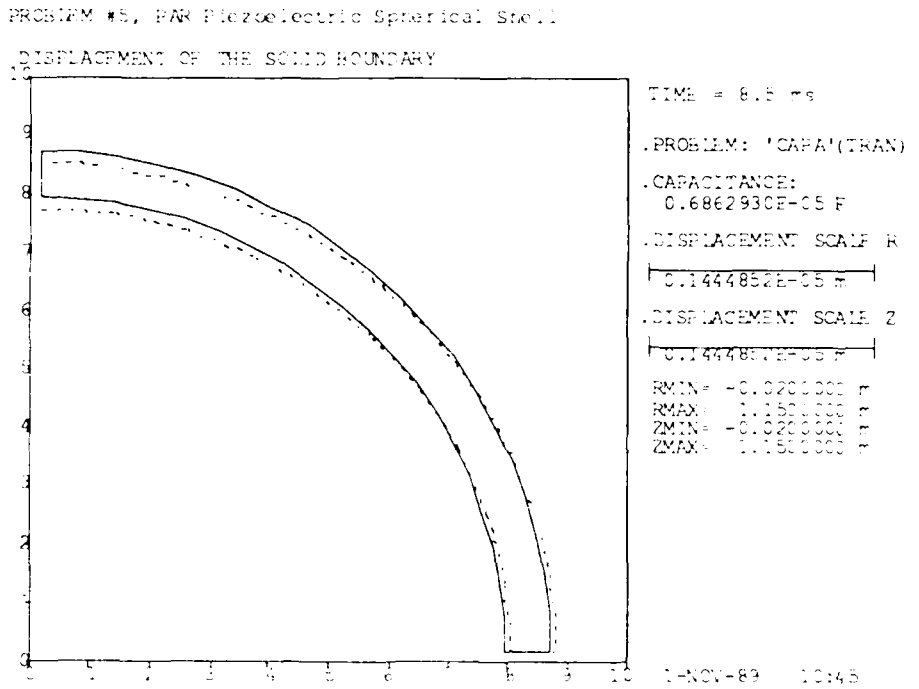

Figure 4.5.4: Problem 5 - Deformations at 0.0090 s

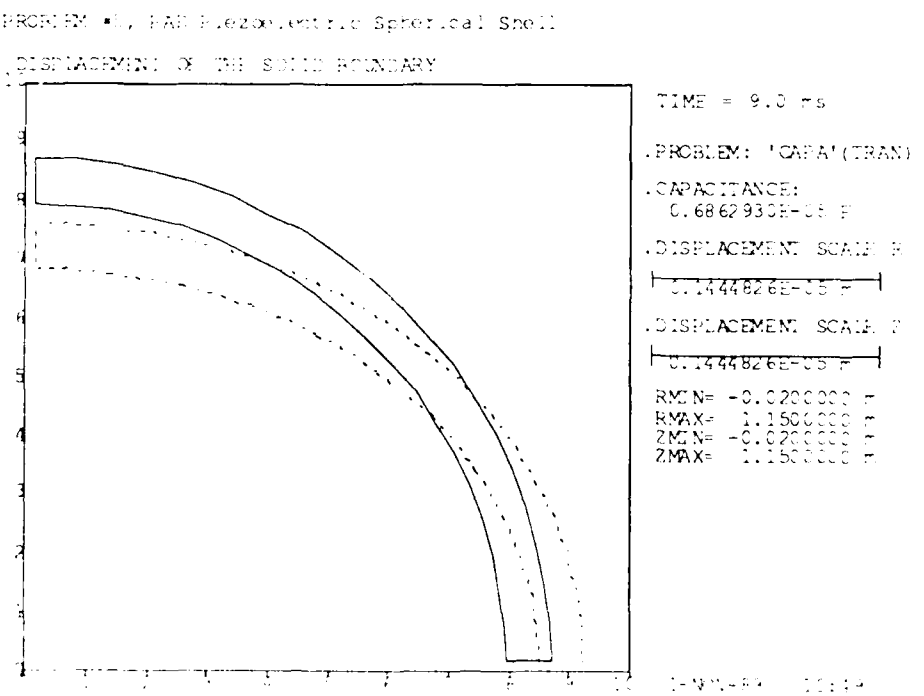

Figure 4.5.5: Problem 5 - Deformations at 0.0095 s

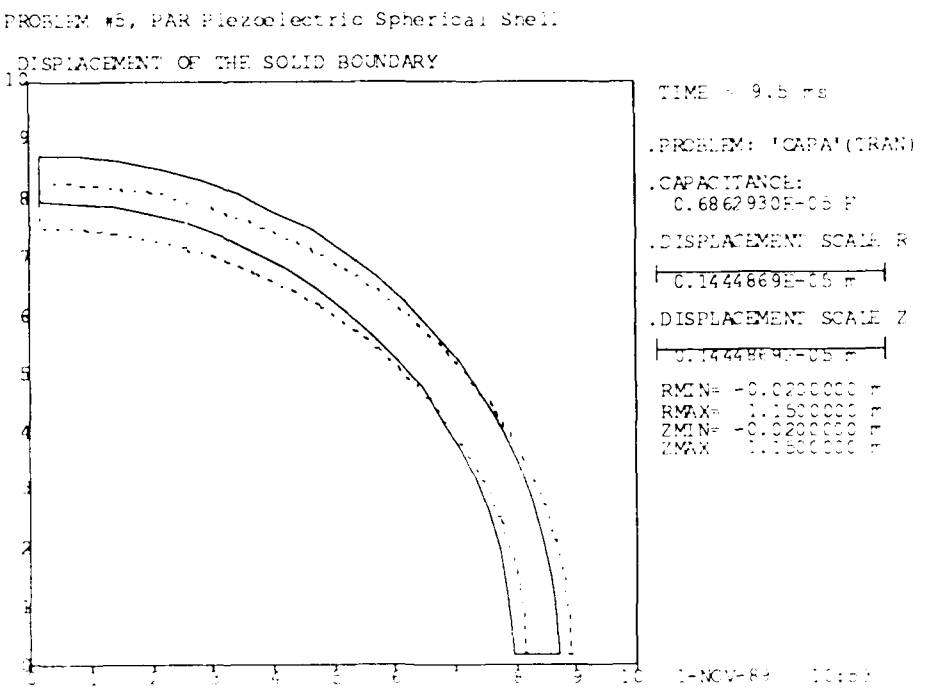

Figure 4.5.6: Problem 5 - Deformations at 0.0100 s

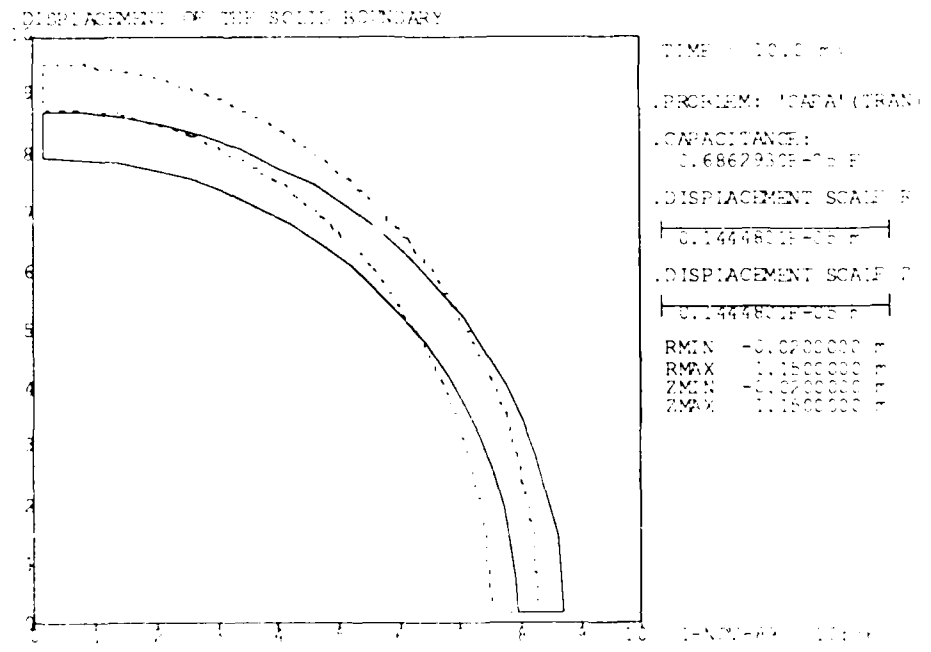

4.6 PROBLEM 6

Analysis Type: DRIVE - frequency sweep

Input File: D06.DAT

The complete F.E. model from Figure 4.0.2 is used.

Voltage fixities, the driving point and the polarity of PARQ elements are the same as for Problem 4 .

The frequency sweep is conducted in only one range of 325 Hz through 340 Hz, with a rather coarse 5 Hz step. Acoustic radiation loading is small for this mode (Mode 1), and the sweep spans the narrow resonance region.

The output data indicate that, among the frequencies surveyed, 330 Hz is closest to resonance in sea water. Mass loading due to the water lowers the resonance frequency from the in-air value of 404.4 Hz. Figures 4.6.1 and 4.6.2 show frequency dependence of admittance and transmitting voltage response, respectively. A cubic spline fit, available as an option in GRAF1, has been applied to these data.

Plots of selected data, obtained for 330 Hz excitation, are shown in Figures 4.6.3 through 4.6.7 .

Figure 4.6.1: Problem 6 - Admittance Components vs. Frequency

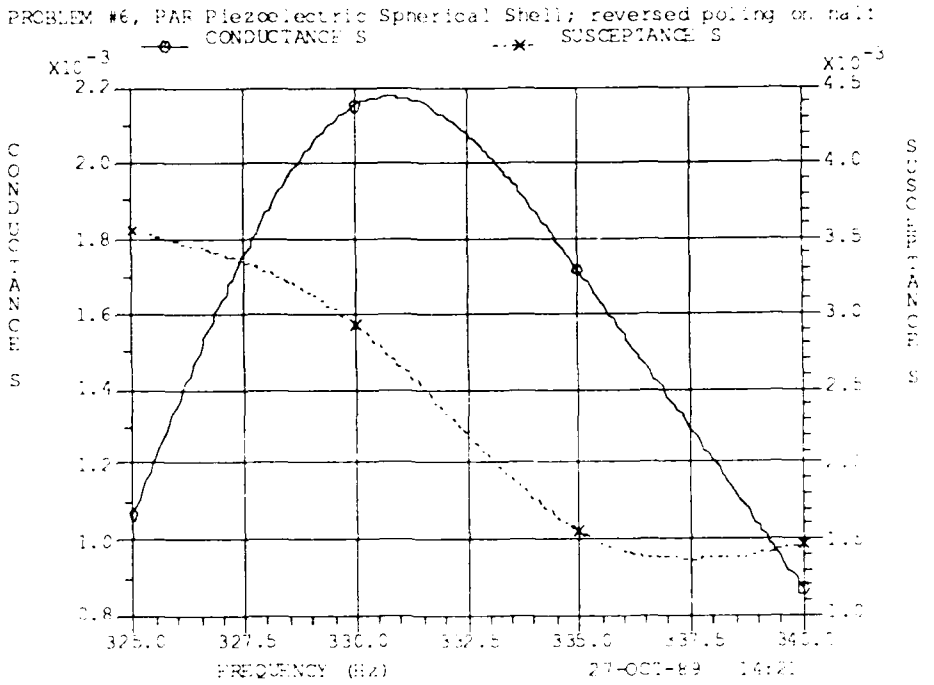

Figure 4.6.2: Problem 6 - Transmitting Voltage Response

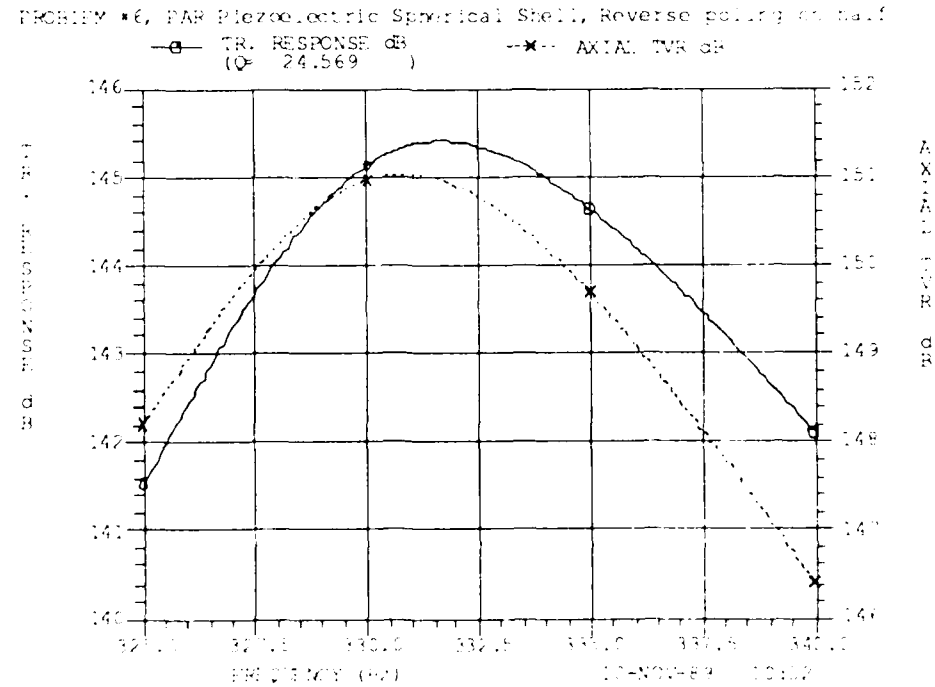

Figure 4.6.3: Problem 6 - Displacement of Solid Boundary

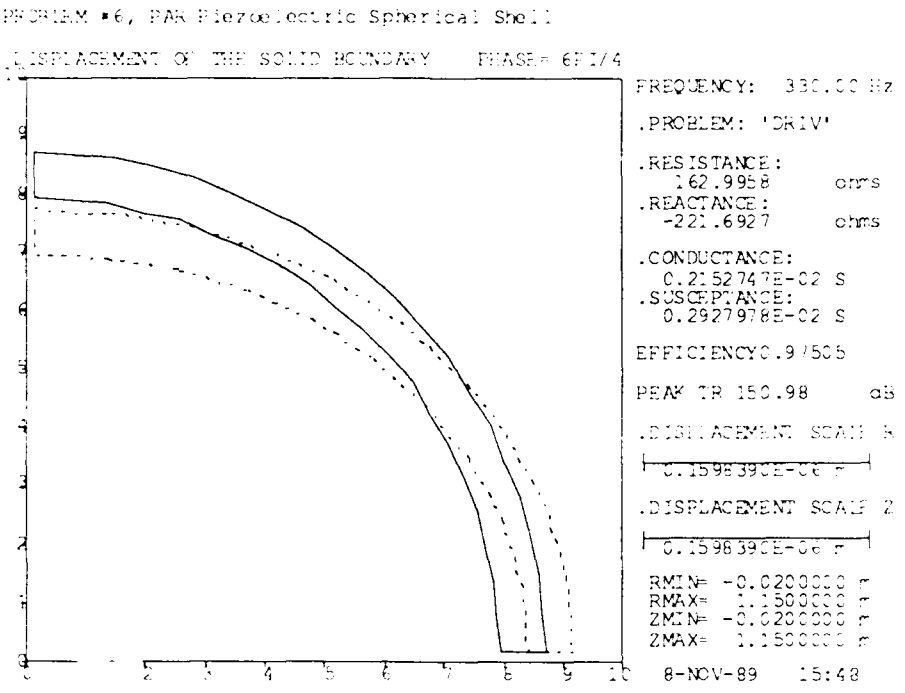

Figure 4.6.4: Problem 6 - Directional Response at 330 Hz

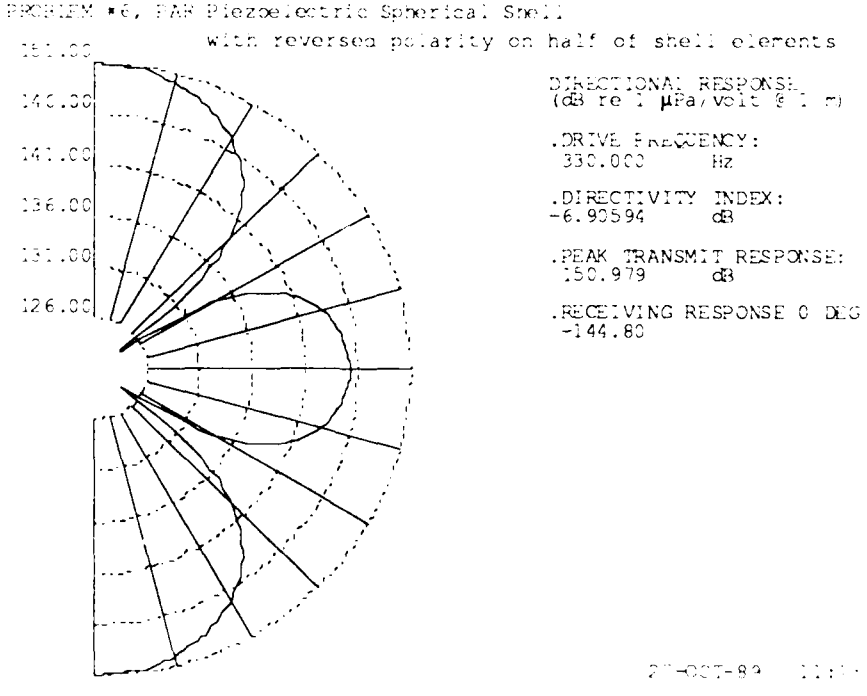

Figure 4.6.5: Problem 6 - Near-Field Pressure Contours

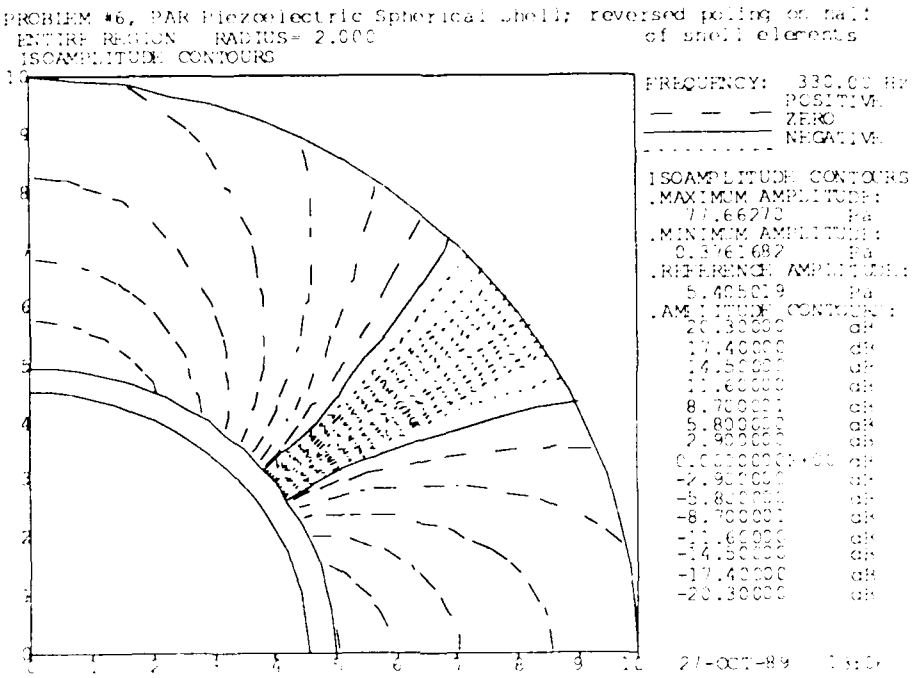

Figure 4.6.6: Problem 6 - Detail of Near-Field Pressure

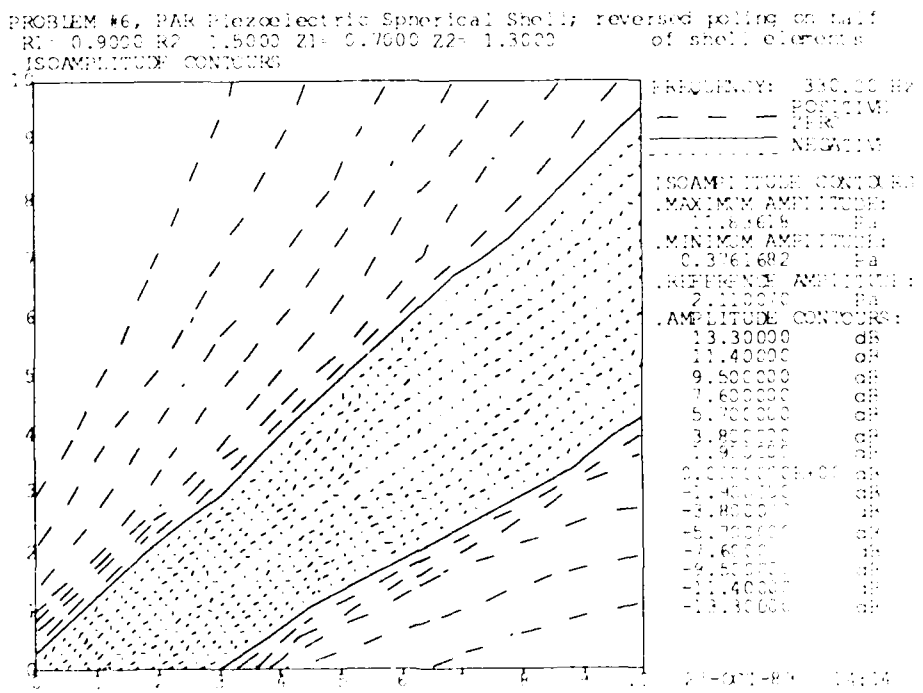

Figure 4.6.7: Problem 6 - Near-Field Pressure Gradient Contours

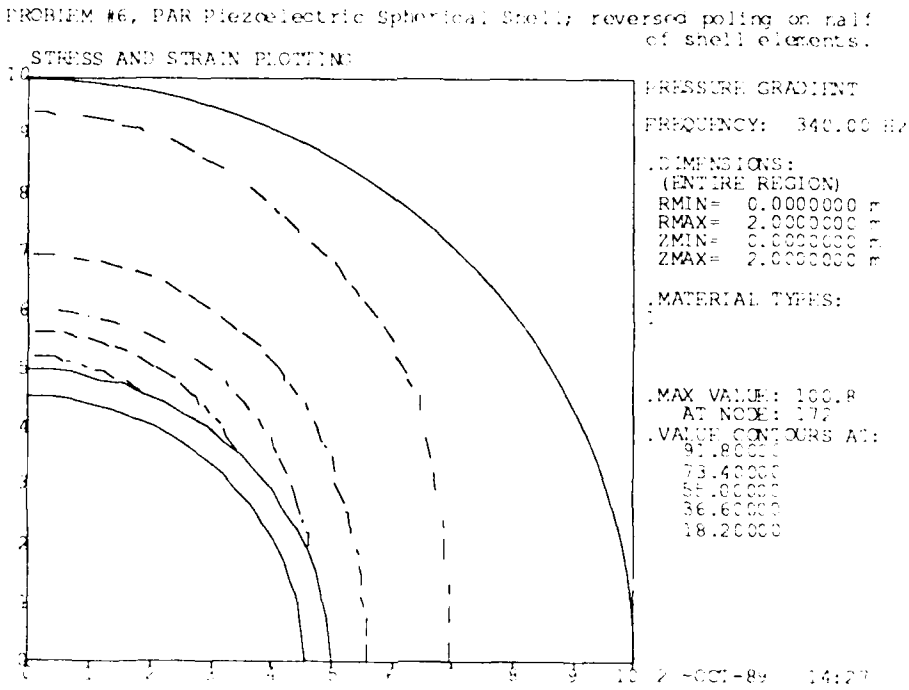

5 SERIES 2: PT PIEZOELECTRIC RING

A radial, cross-sectional diagram of the piezo-ceramic ring, immersed in a sphere of sea water, is given in Figure 5.0.1. The inner radius of the ring is 0.833 m, the outer radius is 1.0 m, and its half height is 0.333 m. It is made from 48 staves of tangentially-poled Channel 5400. The outer radius of the sea water sphere is 2 m.

The mesh of the F.E. model is shown in Figure 5.0.2, together with the element numbers. As in the case of the Series 1 model, only the upper hemisphere needs to be modelled because of symmetry. Figures 5.0.3 (a,b) give details of the node numbering of the F.E. model.

The ring is modelled by two PTQ elements. The fluid model contains both quadrilateral and triangular elements. The fluid and PT solid are connected by FTOS elements. FTOF elements are grouped along the outer boundary of the fluid. Node 303, the only node of E type, is positioned at the origin of the system of coordinates and coincides with F type Node 236, at the geometrical centre of the model. Coordinates of E-nodes are immaterial in the analysis.

The horizontal symmetry plane requires proper boundary conditions for solid elements; cross-plane (Z) displacements for Nodes 98, 99 and 132 are fixed to zero.

Figure 5.0.1: Series 2 Problems - Cross-Sectional Diagram of Free-Flooded Ring in Sea Water

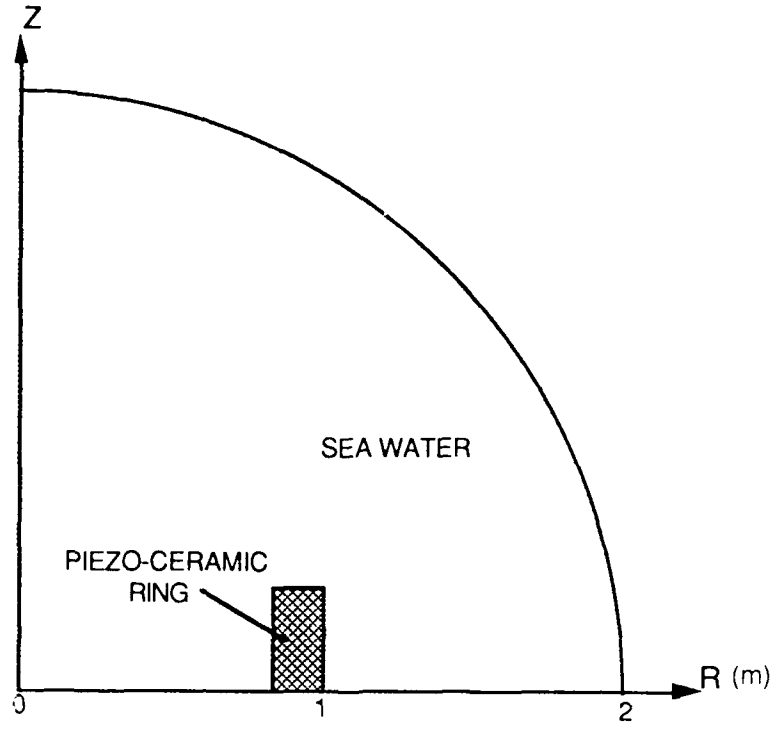

Figure 5.0.2: Series 2 Problems - Element Numbering

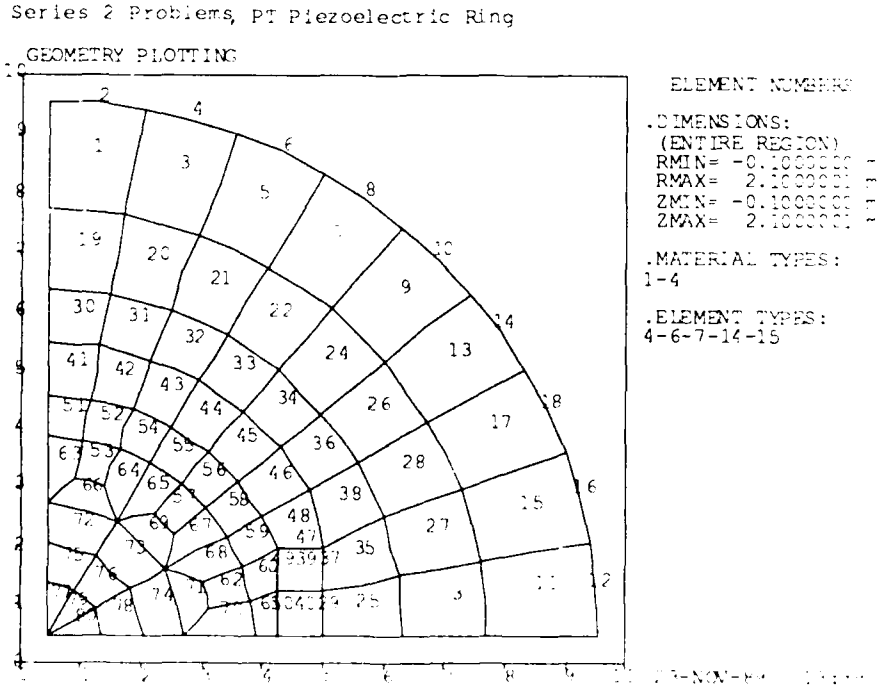

Figure 5.0.3 (a): Series 2 Problems - Outer Node Numbering

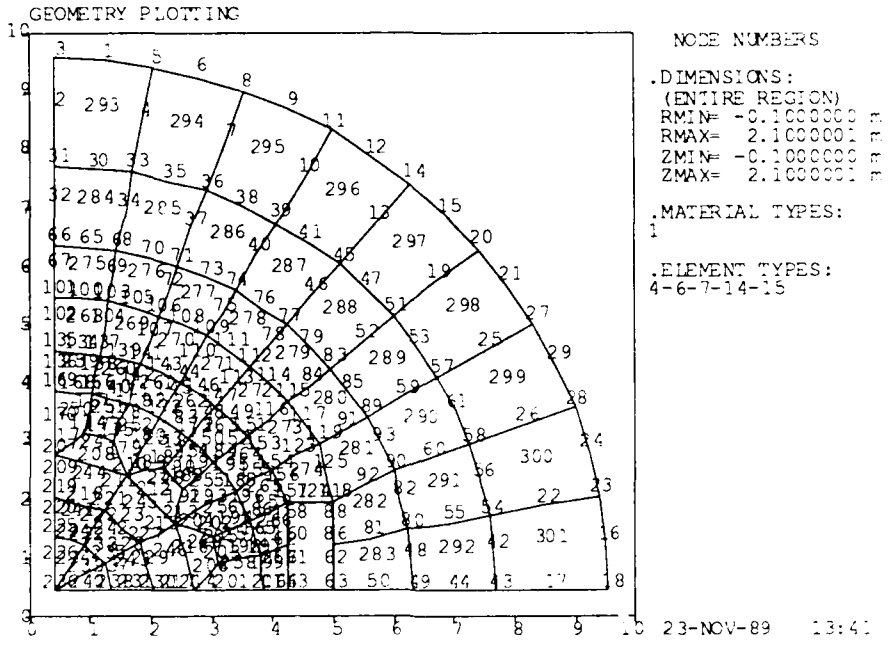

Figure 5.0.3 (b): Series 2 Problems - Inner Node Numbering Detail

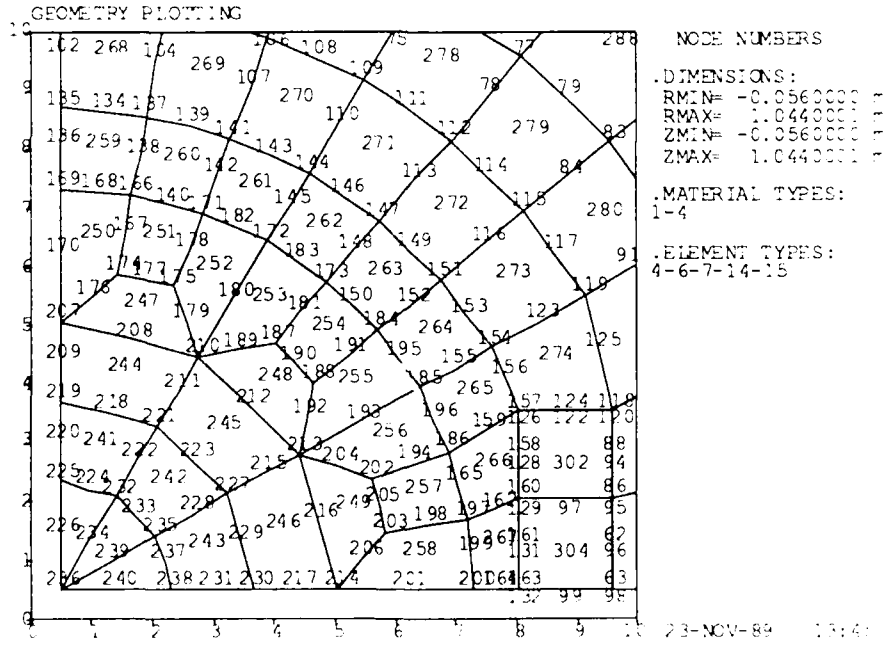

5.1 PROBLEM 7

Analysis Type: EIGEN - resonance (m = 2,0)

Input File: D07.DAT;(1,2)

The F.E. model is a subset of the full model from Figure 5.0.2 and contains the PTQ elements only.

As the resonance condition requires, a V = 0 fixity is applied to the only electrical DOF at Node 303 . The Fourier mode number m = 2 is written into the problem parameters data of Card 2 (IMODE).

Although the lower and upper bounds on the frequency estimate were set to 100 Hz and 500 Hz respectively, the predicted resonance frequency was found at 72.9 Hz, outside of the 100 to 500 Hz band. Figure 5.1.1 shows the corresponding mode shape in the Z-R plane at ϕ = 0. Tangentially, the displacement dependence is proportional to cos $m\phi$ (= cos 2ϕ in this case).

The same input data file was run with Fourier mode number m set to zero, giving a resonance frequency of 516.06 Hz. The mode shape is shown in Figure 5.1.2.

We see that the cross-sectional area of the ring remains essentially constant under vibration when m = 2, indicating the pure bending nature of the mode. On the other hand, when m = 0, the modes are extensional and the area varies in vibration, as seen in Figure 5.1.2.

Figure 5.1.1: Problem 7 - 1st Mode Shape ($m = 2$) at 72.9 Hz

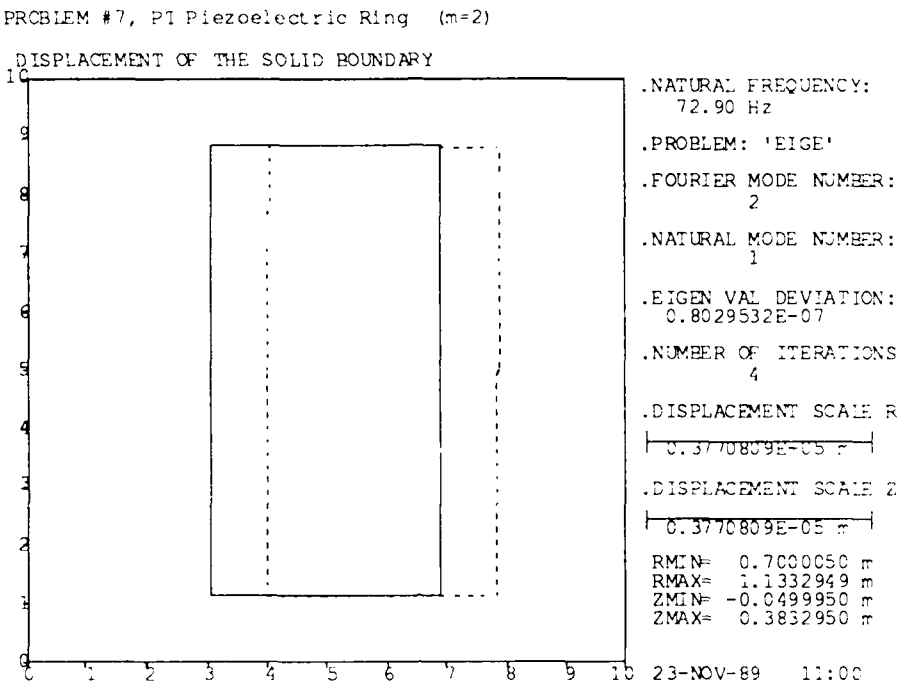

Figure 5.1.2: Problem 7 - 1st Mode Shape ($m = 0$) at 516 Hz

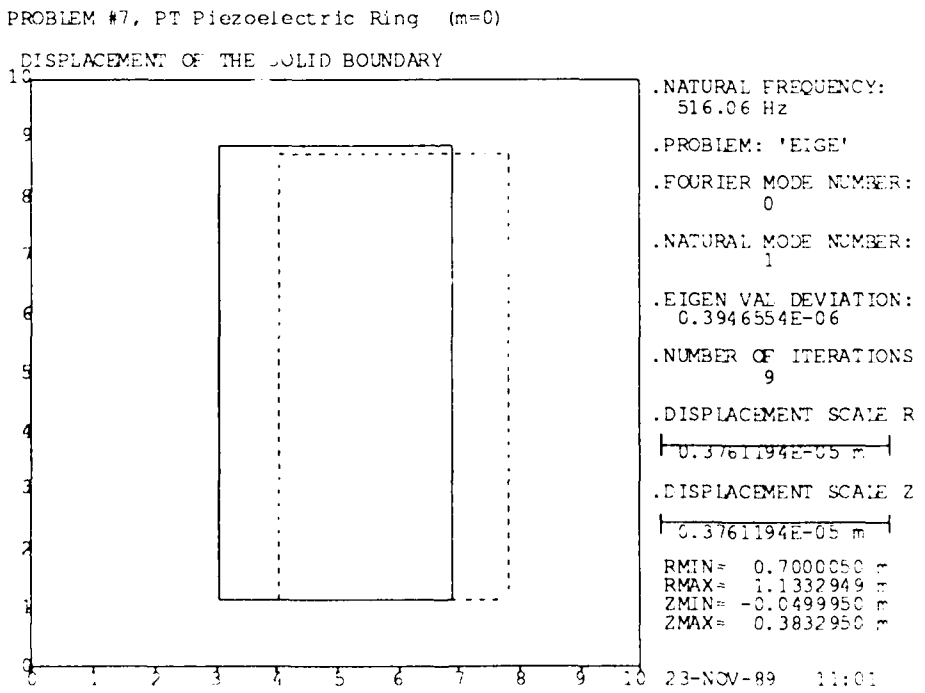

5.2 PROBLEM 8

Analysis Type: CAPAC - frequency sweep (m = 0)

Input File: D08.DAT (frequency sweep)

The F.E. model is a subset of the full model from Figure 5.0.2 and contains the two PTQ elements only.

A sinusoidal driving voltage of 1 V amplitude is specified as a fixity at Node 303 .

Similar to Problem 4 , three frequency ranges are specified for scanning. They cover the band from 508 Hz through 524 Hz. One element group composed of both PTQ elements is used (Card 11). It is not necessary to specify the coordinates of an integration line for PT elements; i. e., RR1, ZZ1, RR2, and ZZ2 are not used.

In the output data the maximum computed capacitance was found at a frequency of 516 Hz. As this is very close to the actual resonance of 516.06 Hz predicted in Problem 7, the capacitance is very high. Being an undamped driven problem, the capacitance and displacement become infinite at the resonance. A plot of the deformation at 516 Hz is shown in Figure 5.2.1 and a plot of absolute value of the capacitance versus frequency is given in Figure 5.2.2.

Figure 5.2.1: Problem 8 - Deformations at 516 Hz

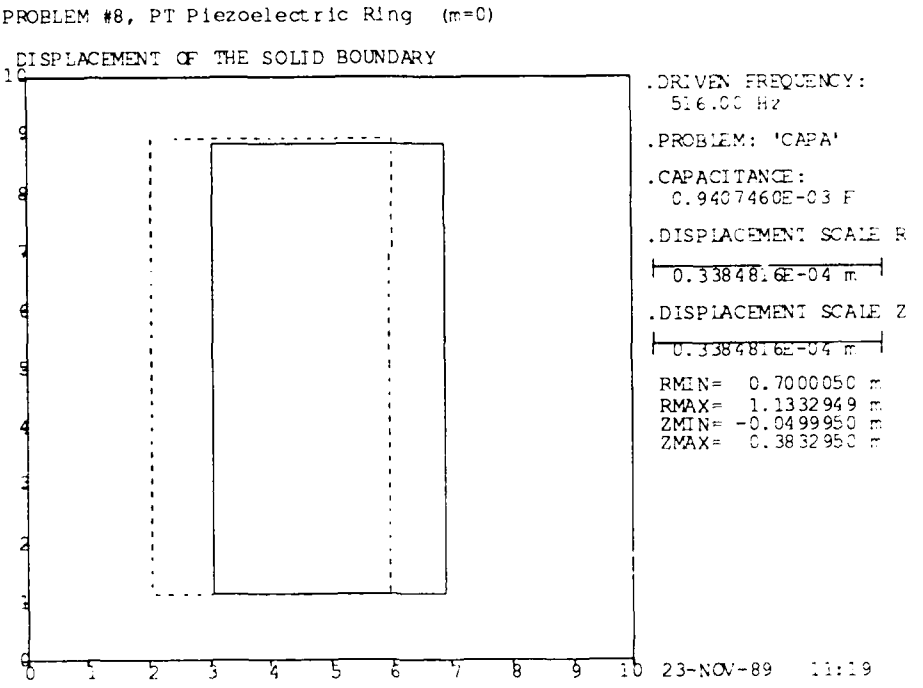

Figure 5.2.2: Problem 8 - Capacitance versus Frequency

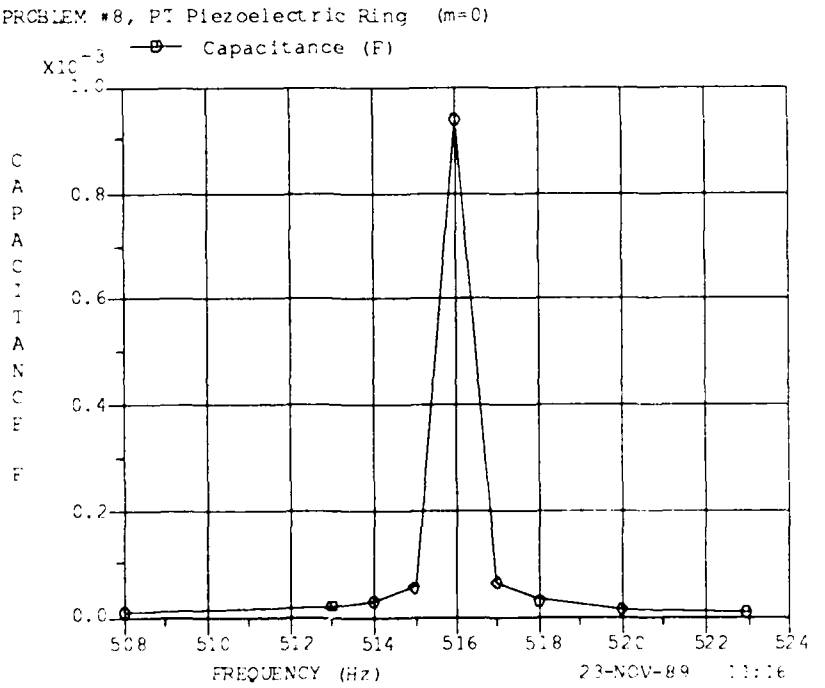

5.3 PROBLEM 9

Analysis Type: DRIVE - resonance search

Input Files: D09.DAT
D09E.DAT

The complete F.E. model from Figure 5.0.2 is used.

Two versions of the input file differ in the extra degrees-of-freedom (DOF) either being dropped (IFOU=0), or taken into account (IFOU=1) in the analysis. The extra DOF's are carried automatically when the Fourier mode number $m > 0$, and is only required for $m = 0$ if data from different Fourier modes are to be combined.

The voltage fixity is the same as in Problem 8, the E-node (#303) is fixed at 1 volt.

To locate the resonance, instead of frequency sweep as in Problem 2 , another strategy is applied for the case without the extra DOF's. Card 8 in file D09.DAT specifies only one frequency range within which the search is to be performed. The negative value of parameter F2 in Card 8 activates the resonance search mode, which continues until the maximum of a specified parameter is located with peak tolerance specified by F2I in decibels, or until I2 iteration cycles are reached. If the maximum is at one or the other end of the specified search range, the search range will be extended until a lower value is seen or until the I2 iteration cycles are completed. Various parameters, including a DOF at a specified node, may be chosen as the search parameter by specifying a non-zero value for NFUN in Card 12. Allowable values for NFUN are discussed in Reference [1.1a]. In a DRIVE analysis, radiated power (i. e., conductance, NFUN = 2) is the default parameter on which the resonance search is based; in CAPAC, it is capacitance (NFUN = 3).

The parameter NSEL in Card 12 specifies a node whose DOF values are written to the plot file for GRAF1 processing; one of these DOF's may be used in the resonance search [1.1a]. If NSEL is zero, the default node used is the first in the node list.

The output data indicate that 375 Hz is the frequency closest to resonance in sea water. Plots of selected output data are shown in Figures 5.3.1 through 5.3.6. The cubic spline fit option has been selected in GRAF1 to plot the frequency response data in Figures 5.3.3 and 5.3.4.

The case with the extra DOF's carried (D09E.DAT) was run only at 375 Hz excitation frequency. The results are identical to the previous run for that frequency.

Figure 5.3.1: Problem 9 - Deformation at 375 Hz

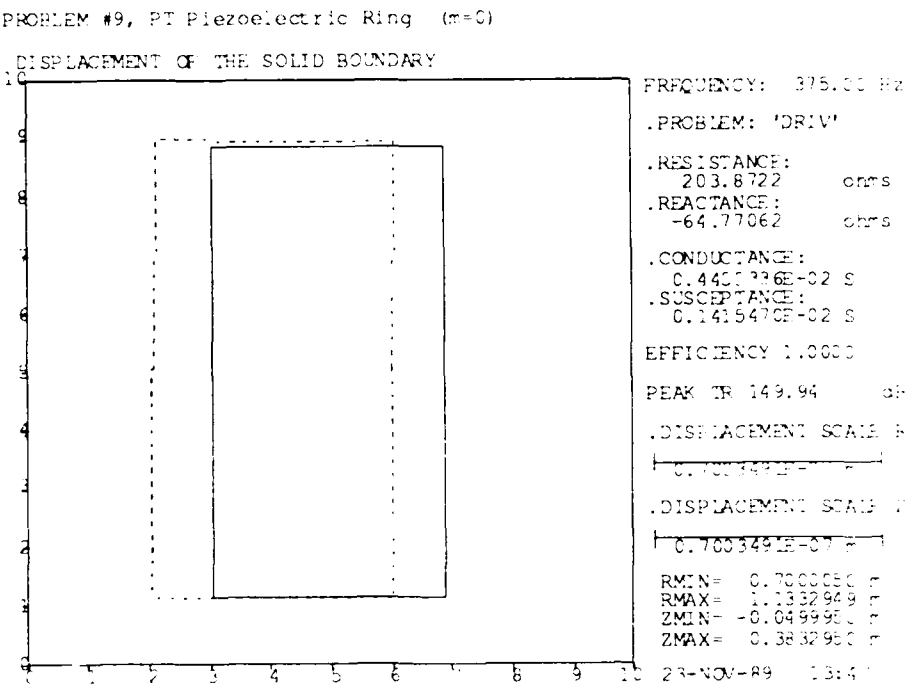

Figure 5.3.2: Problem 9 - Tangential Stress Contours

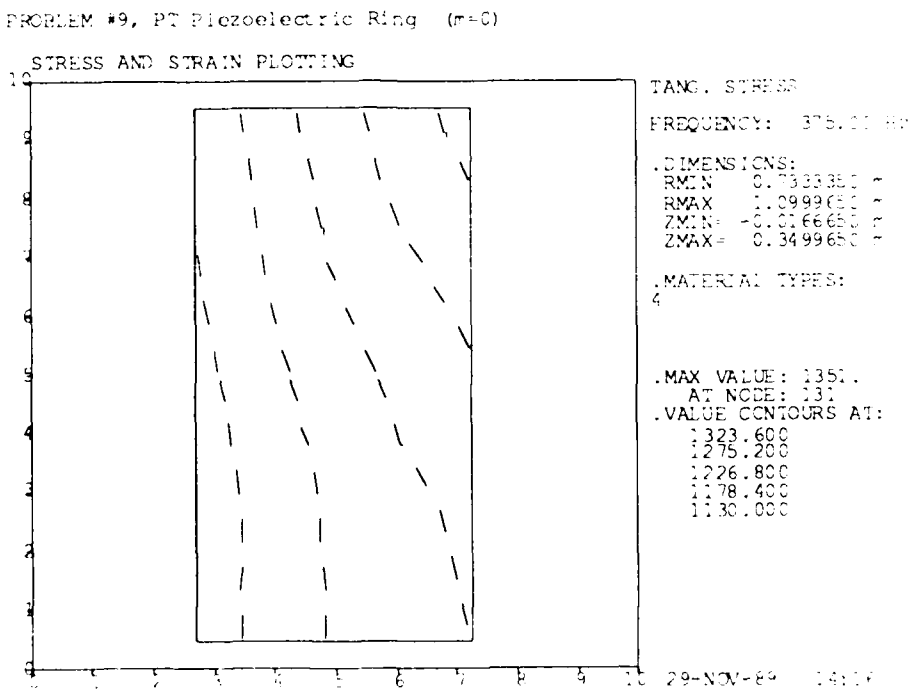

Figure 5.3.3: Problem 9 - Admittance Components vs. Frequency

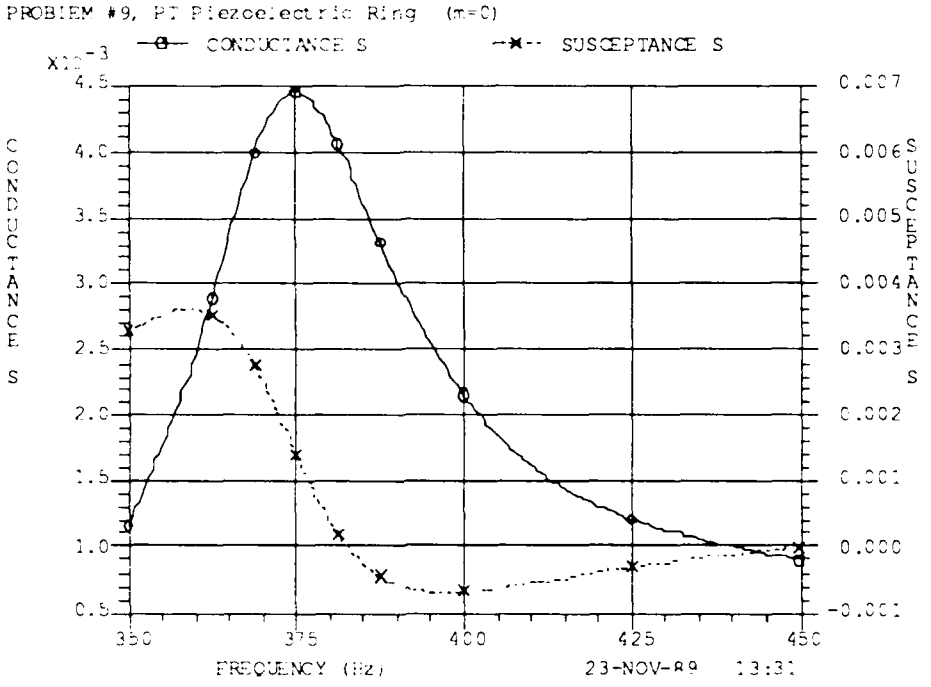

Figure 5.3.4: Problem 9 - Transmitting Voltage Response

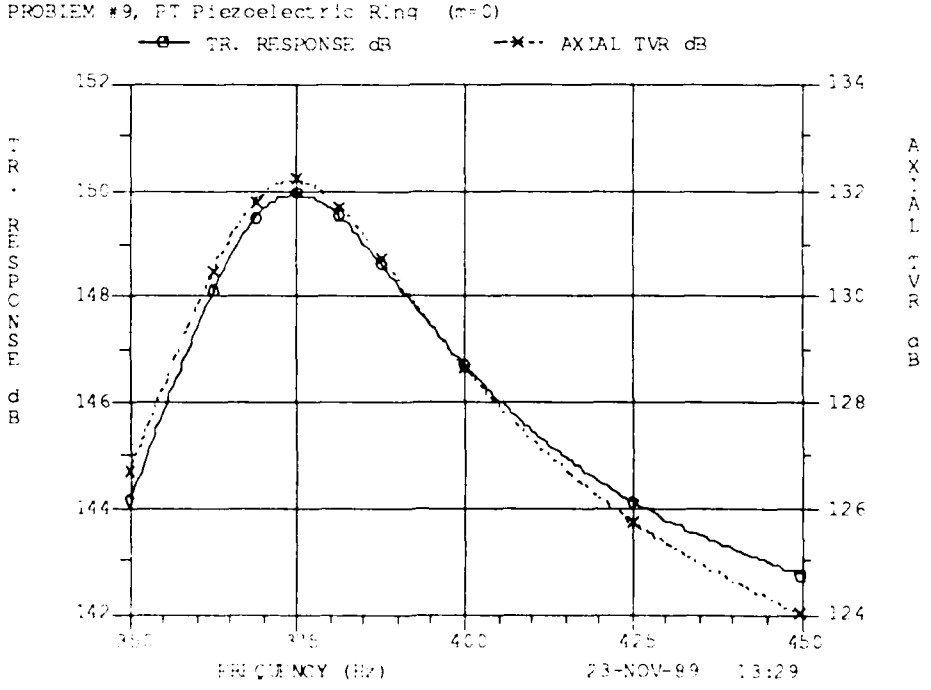

Figure 5.3.5: Problem 9 - Directivity at 375 Hz

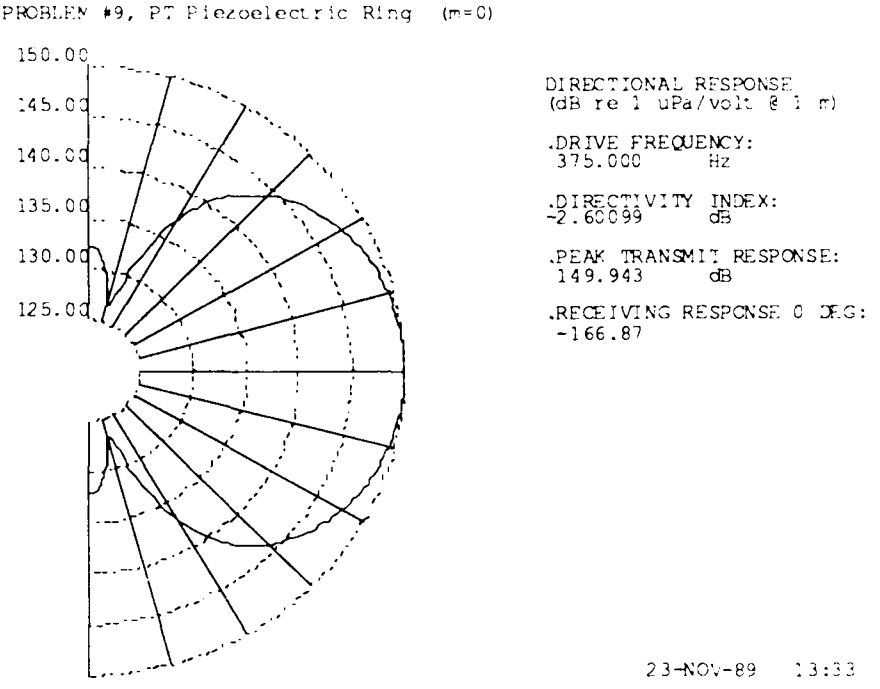

Figure 5.3.6: Problem 9 - Near-Field Pressure Contours at 375 Hz

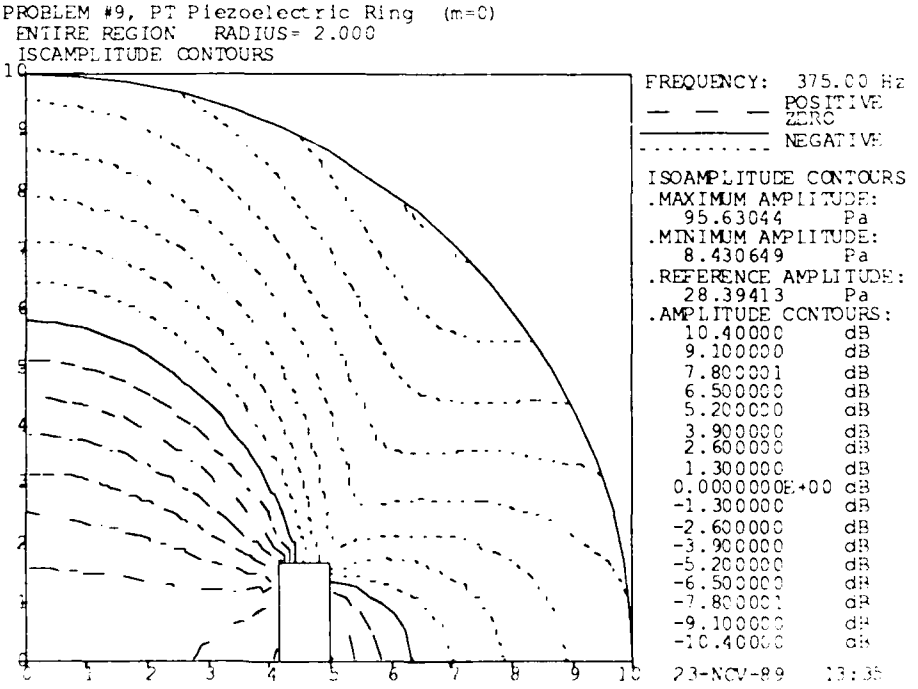

6 SERIES 3: TRILAMINAR BENDER DISK

A cross-sectional diagram of the trilaminar disk is given in Figure 6.0.1. It is made of two outer layers of PZT-4 ceramic 1 cm thick with a 2-cm aluminum layer between. The piezoelectric material on both sides of the disk is poled in the same +Z-direction. Although the structure is symmetrical geometrically with respect to the R-axis, it cannot be considered electrically symmetrical due to the chosen piezoelectric polarity, and as a result the complete structure has to be analyzed.

SLIDER elements are inserted between the PZT-4 and the aluminum. Physically, they can be considered as representing the adhesive joints bonding the materials together, and are only necessary if the adhesive contributes a significant compliance to the structure. Otherwise, the model can be simplified by eliminating the SLIDERs and allowing the aluminum to share the adjoining A-nodes of the PZT-4. The SLIDER elements can serve three purposes:

- they can "soften" the junction of two structural components;
- they provide for connection of two dissimilar nodes, such as H and A types, where both must exist because of the elements that they serve; and
- they can be used to apply damping in complex driven analyses (damping applications are covered in Problem 18)

The mesh of the F.E. model is shown in Figure 6.0.2. There was no necessity of using triangular elements to model the structure; they were chosen in order to demonstrate their use.

Figures 6.0.3 and 6.0.4 (a,b) give details of element and node numbering, respectively. The axial scale has been expanded to allow the numbers to be read more easily.

Figure 6.0.1: Series 3 Problems - Cross-Sectional Diagram

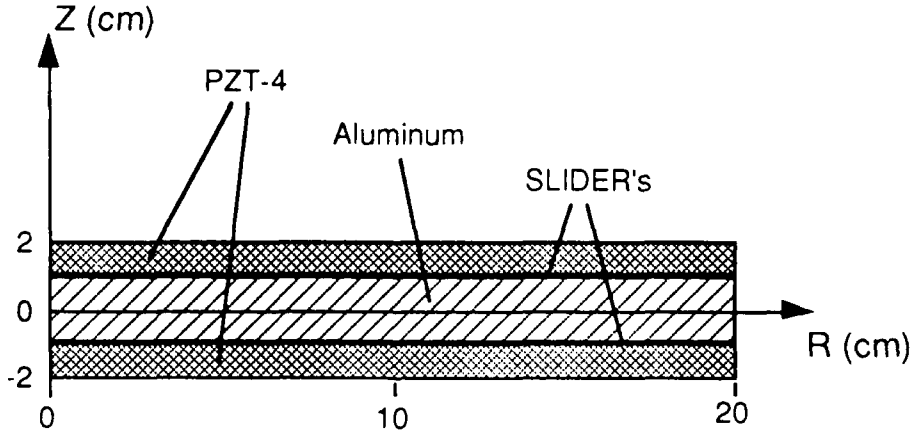

Figure 6.0.2: Series 3 Problems - F.E. Model

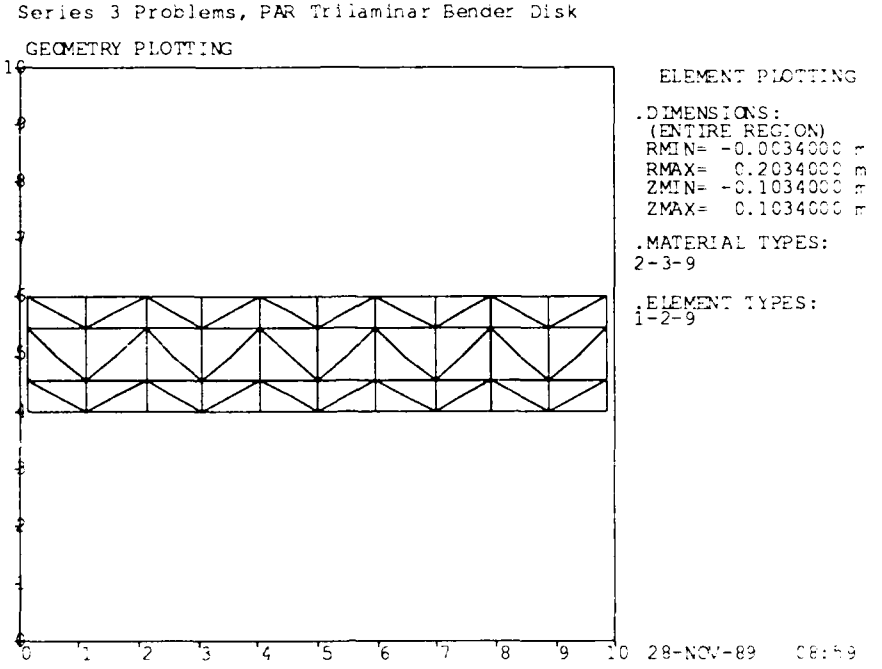

Figure 6.0.3: Series 3 - Element Numbering

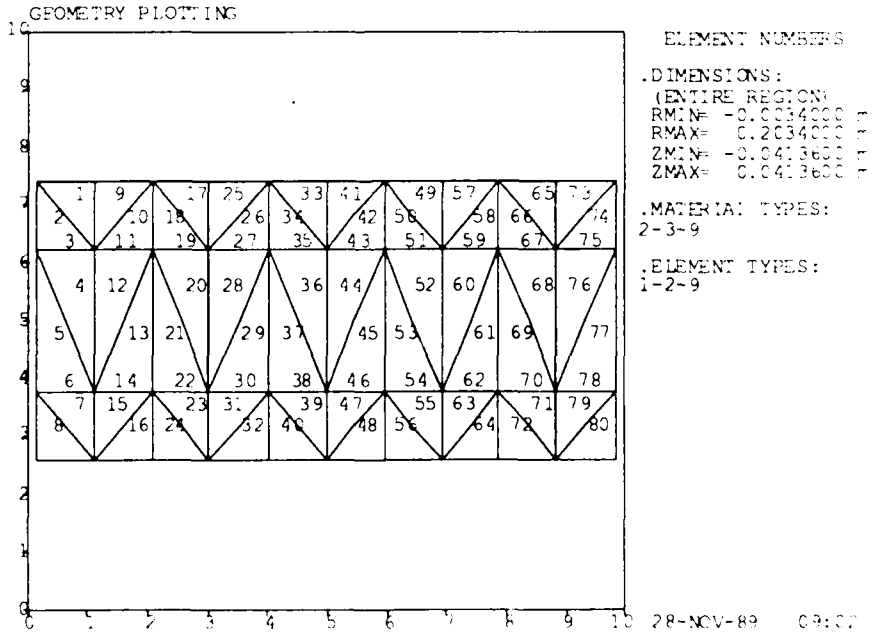

Figure 6.0.4(a): Series 3 - Node Numbering, Aluminum Layer

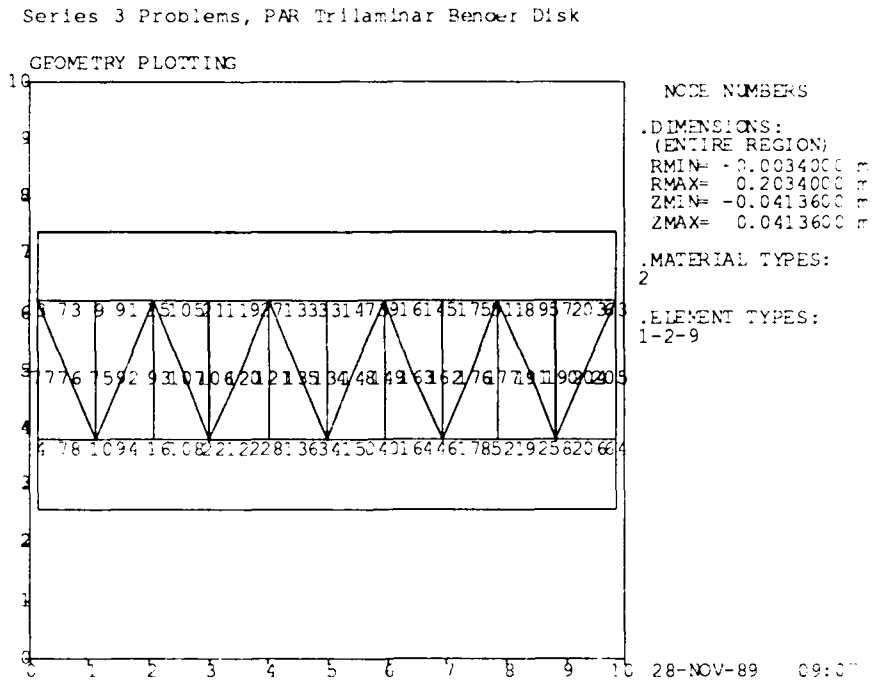

Figure 6.0.4 (b): Series 3 - Node Numbering, Piezoelectric Layers

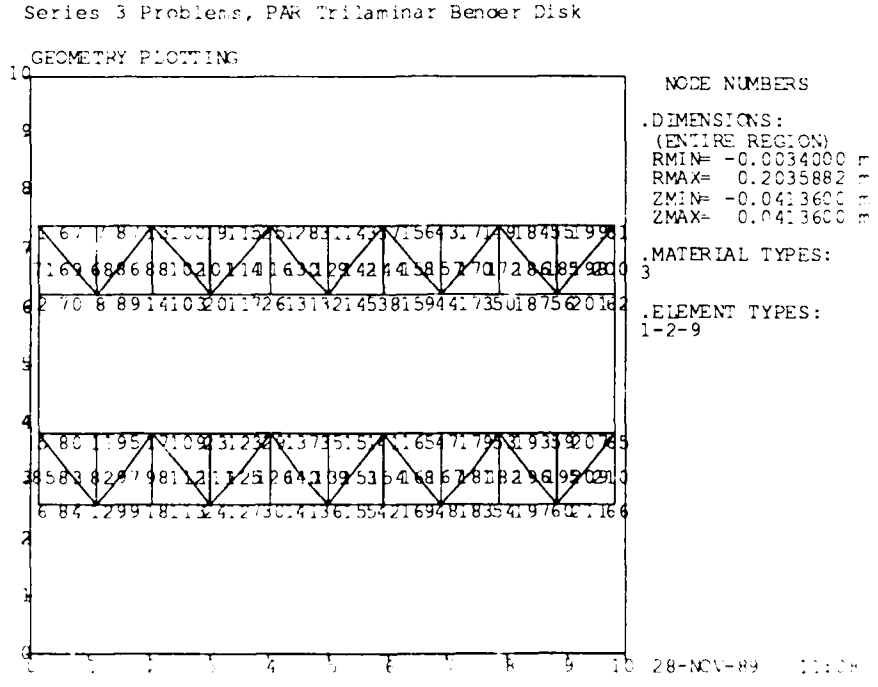

6.1 PROBLEM 10

Analysis Type: STATC - electric stresses

Input File: D10.DAT

The complete F.E. model from Figure 6.0.2 is used.

A 1-volt fixity is applied to all A-nodes on the top and the bottom surfaces of the disk. A zero-volt fixity is applied to all A-nodes attached to the SLIDER elements. The SLIDER stiffness is set at 1.0E+15 Pa in all three moduli. Node 77 is restrained in the Z-direction.

A plot of the deformation of the disk is shown in Figure 6.1.1. In Figure 6.1.2, an expanded axial scale is used to show radial strain contours in the materials; the solid contour line is the line of zero strain, long dashed lines are positive strain contours, and the short dashed lines are negative contours. The waveyness in the contours is an artifact caused by the use of the triangular elements.

Figure 6.1.1: Problem 10 - Electrical Deformation with a Hard SLIDER

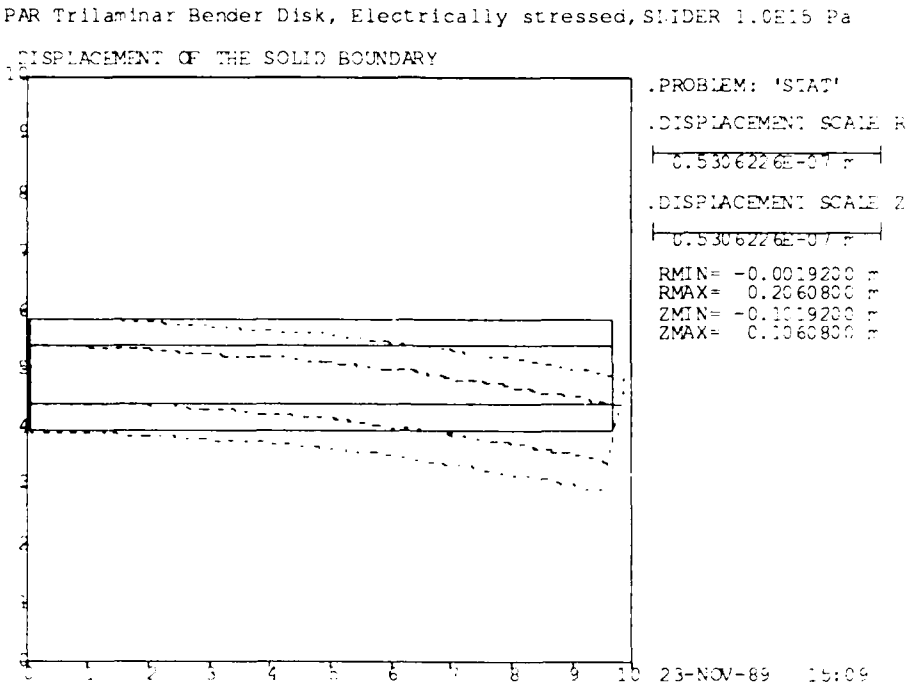

Figure 6.1.2: Problem 10 - Radial Strains

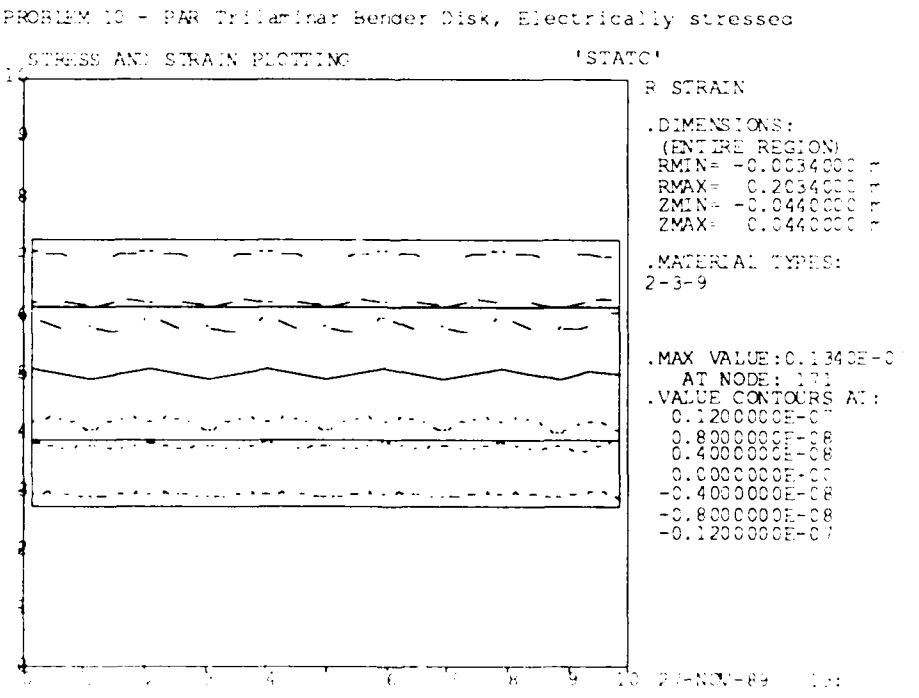

6.2 PROBLEM 11

Analysis Type: STATC - thermal stress

Input File: D11.DAT

The complete model from Figure 6.0.2 is used.

A zero-volt fixity is applied to all A nodes on the top and bottom surfaces of the piezoelectric layers. The SLIDER stiffness is set at 1.0E+15 and Node 77 is restrained in the Z-direction, as in Problem 10.

The element data contains extension Cards 5 (b) specifying element temperature differences from zero strain: +20° C for elements of the top piezoelectric layer, –20° C for the bottom piezoelectric layer. The temperature of the aluminum disk is left unchanged from its zero strain state.

Figures 6.2.1 and 6.2.2 show output data for the thermally stressed disk that corresponds to Figures 6.1.1 and 6.1.2 for the electrically stressed disk. We note that the form of the deformation is essentially the same in both cases but the strain is very different: There are three lines of zero strain (solid lines) in the latter case but only one in the former. Adjacent parts of the materials undergo opposite strains. The hydrophone sensitivity printed on Figure 6.2.1 is meaningless in this situation.

Figure 6.2.1: Problem 11 - Thermal Deformation with a Hard SLIDER

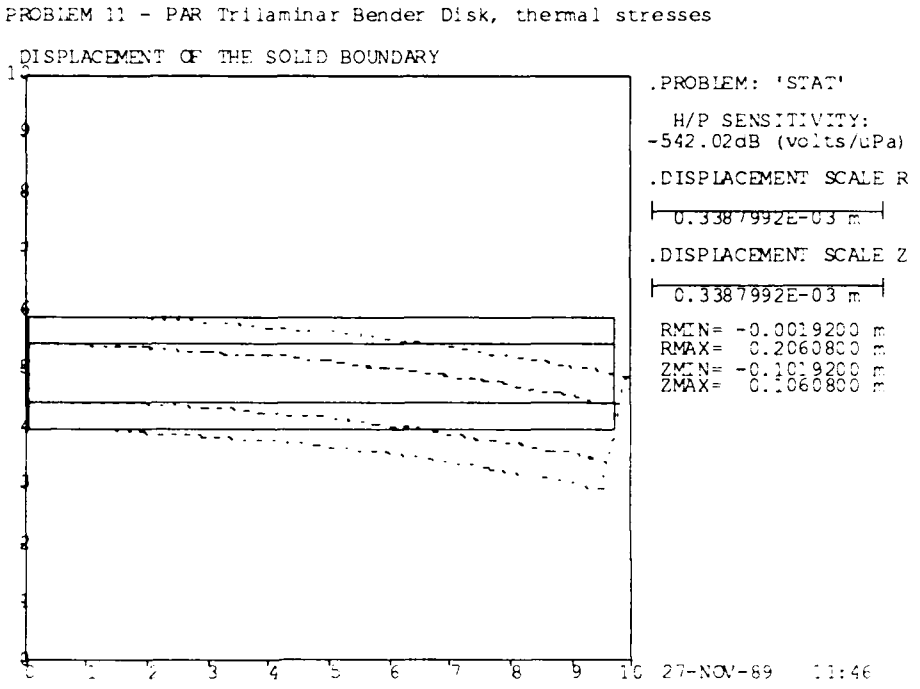

Figure 6.2.2: Problem 11 - Radial Strains

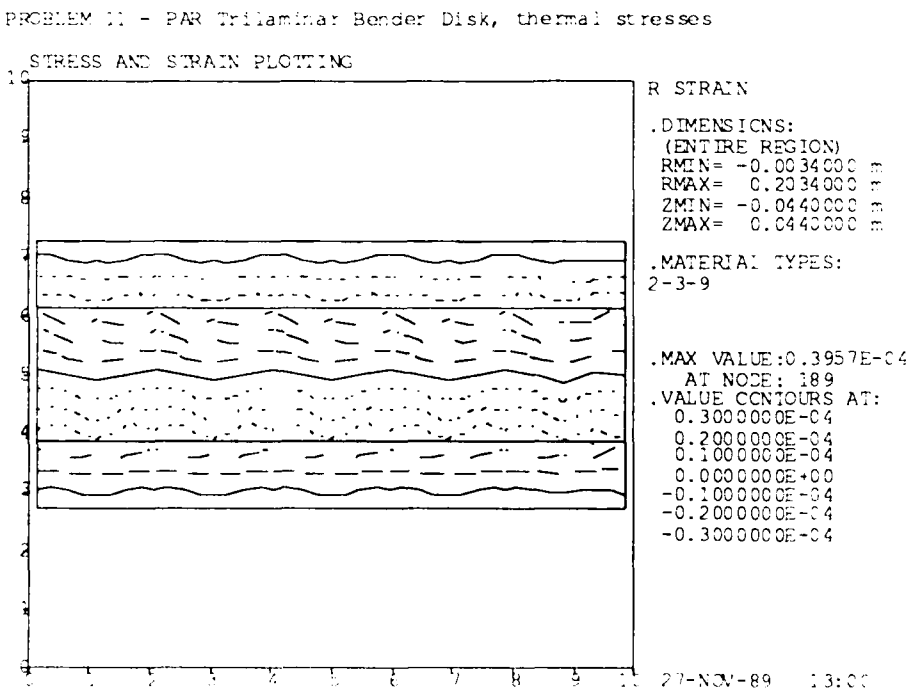

6.3 PROBLEM 12

Analysis Type: CAPAC - without slider softening (a)
- with full slider softening (b)
- with partial slider softening (c)

Input Files: D12A.DAT
D12B.DAT
D12C.DAT

The complete F.E. model from Figure 6.0.2 is used.

A sinusoidal 100-Hz drive with an amplitude of 1 volt is applied to all A nodes on the top and bottom surfaces of the disk. All A nodes attached to the SLIDER elements share a 0-volt fixity. No structural nodes are restrained in the Z-direction.

Two element groups, one for each piezoelectric layer, are used. Three SLIDER conditions are analysed. The material properties of the SLIDER elements in Case (a) make the aluminium-piezoelectric connection stiff ($c_{11} = c_{22} = c_{33} = 1.0E+15$), as in Problem 10. In Case (b) the connection remains stiff in the Z-direction while allowing free sliding in the R-direction ($c_{22} = c_{33} = 0.$). Case (c) is an intermediate condition ($c_{22} = c_{33} = 1.0E+11$), providing some shear compliance in the R-ø plane.

Plots of deformations at 100 Hz are shown in Figures 6.3.1 to 6.3.3 for the three cases (a), (b), and (c), respectively. The clamping effect of the aluminum plate on the piezoelectric layers is reflected in the reduced capacitance as the sliders become stiffer.

An 'EIGE' run was carried out for the hard slider, Case (a), predicting a resonance of 1647.8 Hz. Deformations are shown in Figure 5.3.4. Since no node is fixed, the first mode will always be at zero frequency, hence the data indicate a NATURAL MODE NUMBER of '2'.

Figure 6.3.1: Problem 12 - Deformations without Slider Softening

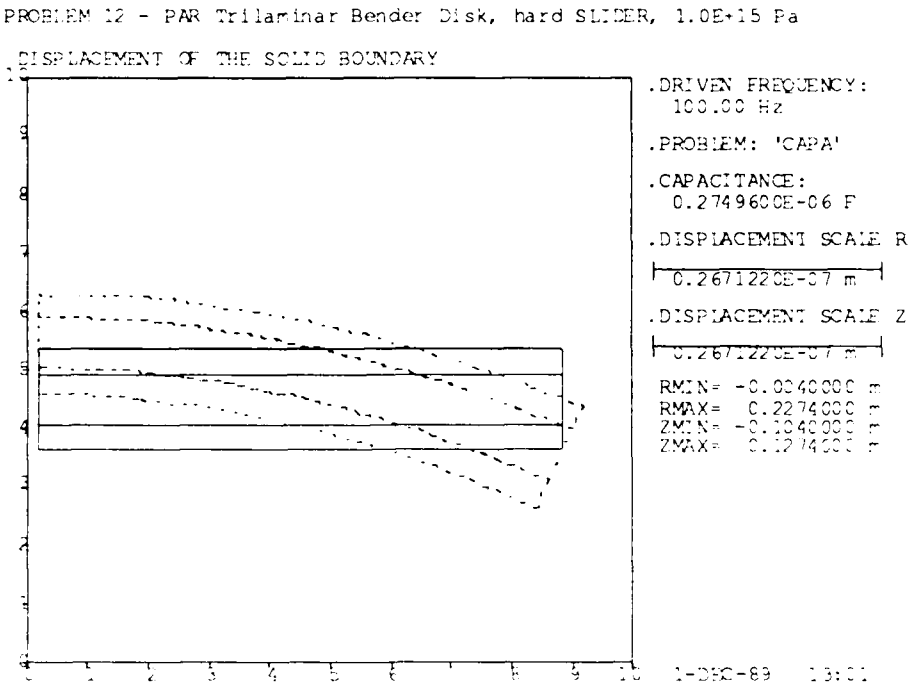

Figure 6.3.2: Problem 12 - Deformations with Slider Softening

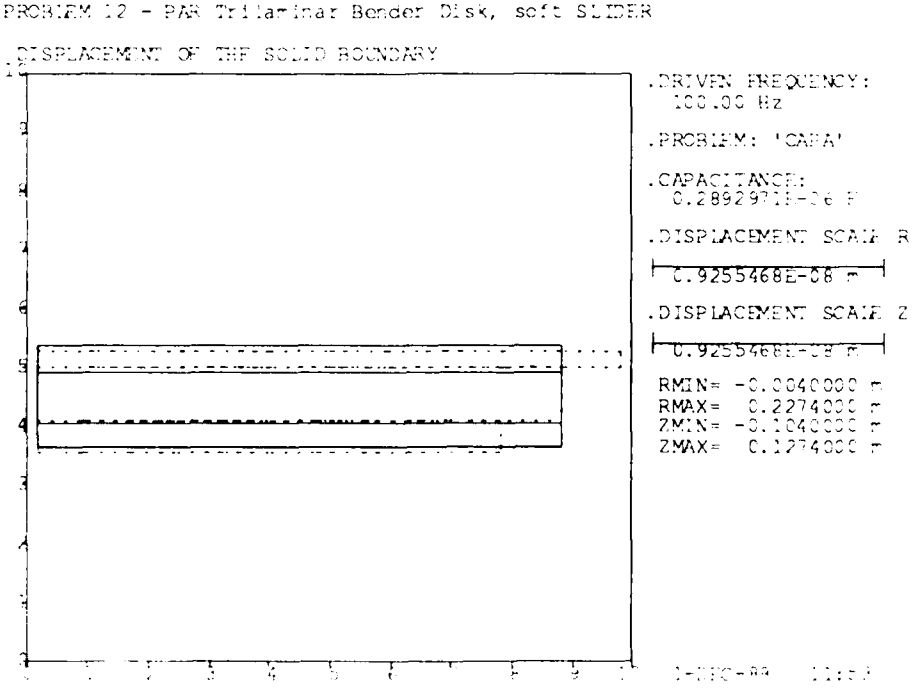

Figure 6.3.3: Problem 12 - Deformations with Partial Slider Softening

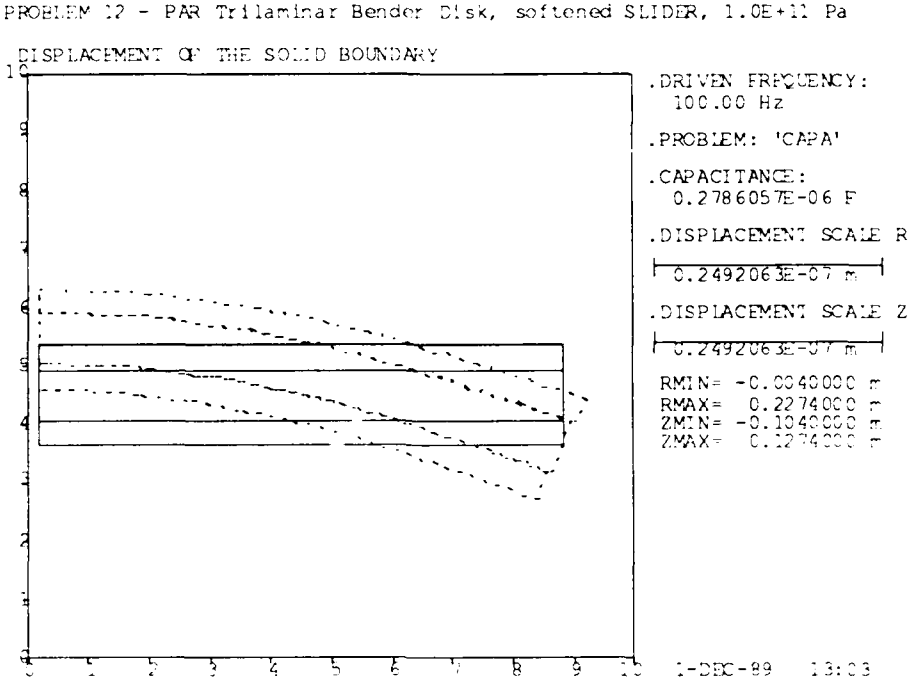

Figure 6.3.4: Problem 12 - First Mode Shape

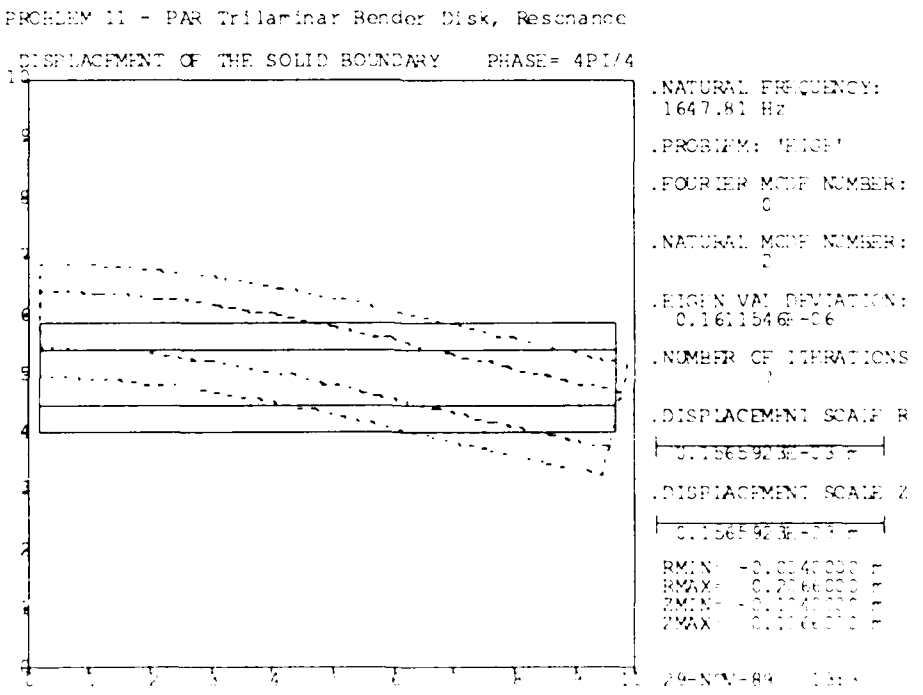

7 SERIES 4: SHELL THIN DISK/TUBE

This series of problems demonstrates the application of SHELL (Type 10) elements in modelling a thin aluminum disk and a thin-walled aluminum tube. A cross-sectional diagram of the disk is given in Figure 7.0.1 and of the tube in Figure 7.0.2. The radius of the disk is 10 cm, and the tube is 10 cm long and 5 cm in radius. In both cases the shell thickness is 2 mm, and is manifest in the material properties as discussed in the Theoretical Manual [1.2]. The properties specified for aluminum in program MATER (See [1.6], [1.7]) are Young's modulus = 7.16E10 Pa, density = 2700 kg/m^3, Poisson's ratio = 0.344 and coefficient of thermal expansion = 23.4E–6 /°C.

The F.E. model of the disk with node and element numbering, is shown in Figures 7.0.3 and 7.0.4, respectively. The corresponding F.E. model for the tube is given in Figures 7.0.5 and 7.0.6. GRAF1 has no provision for indicating the thickness of a shell.

Figure 7.0.1: Series 4 Problems - Disk Radial Cross-Section

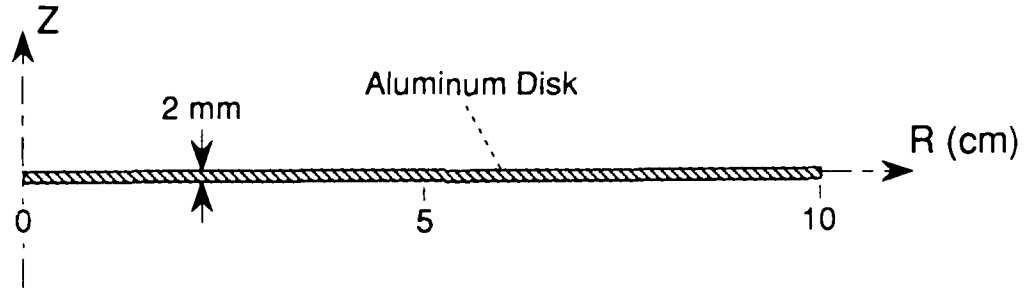

Figure 7.0.2: Series 4 Problems - Tube Radial Cross-Section

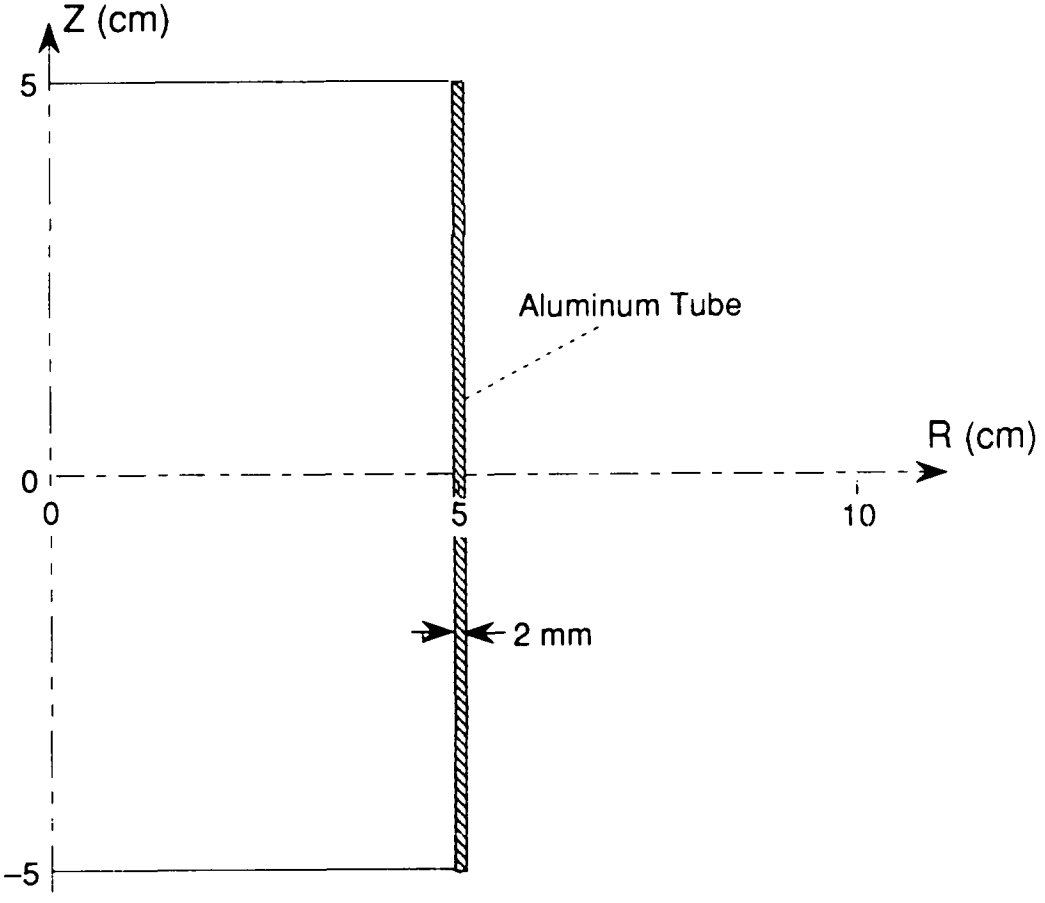

Figure 7.0.3: Series 4 Problems - Disk Node Numbering

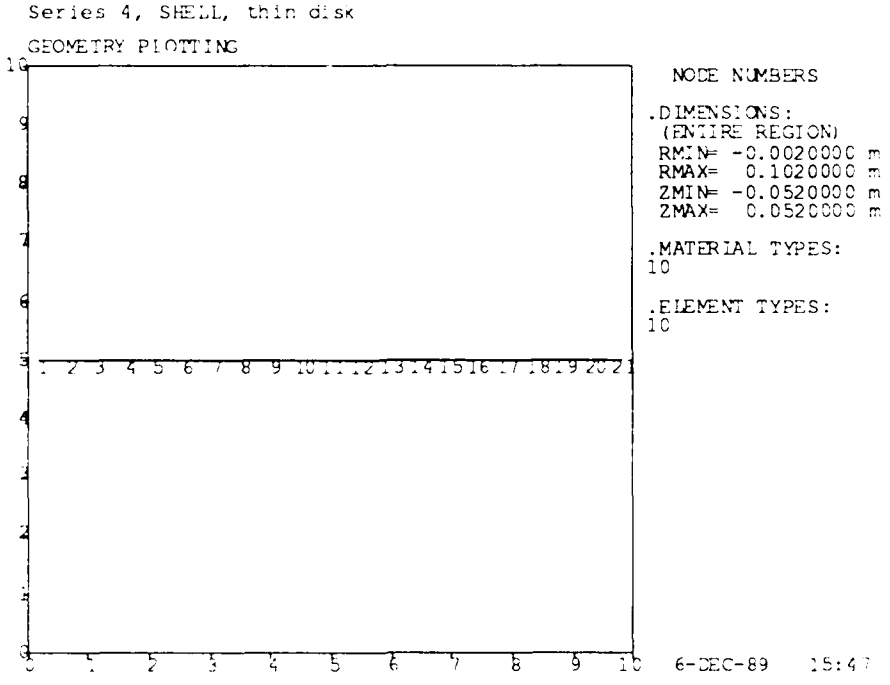

Figure 7.0.4: Series 4 Problems - Disk Element Numbering

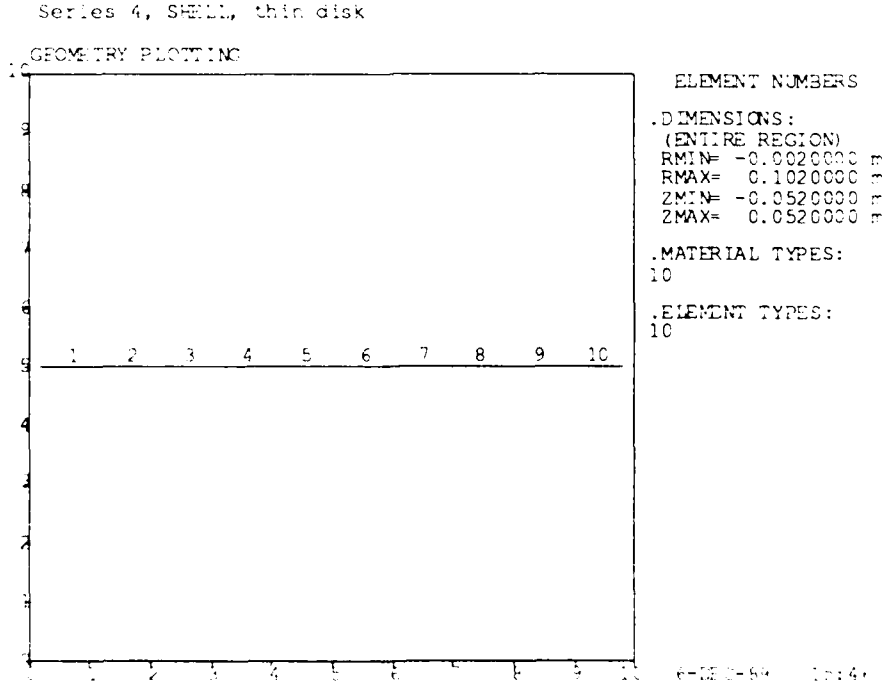

Figure 7.0.5: Series 4 Problems - Tube Node Numbering

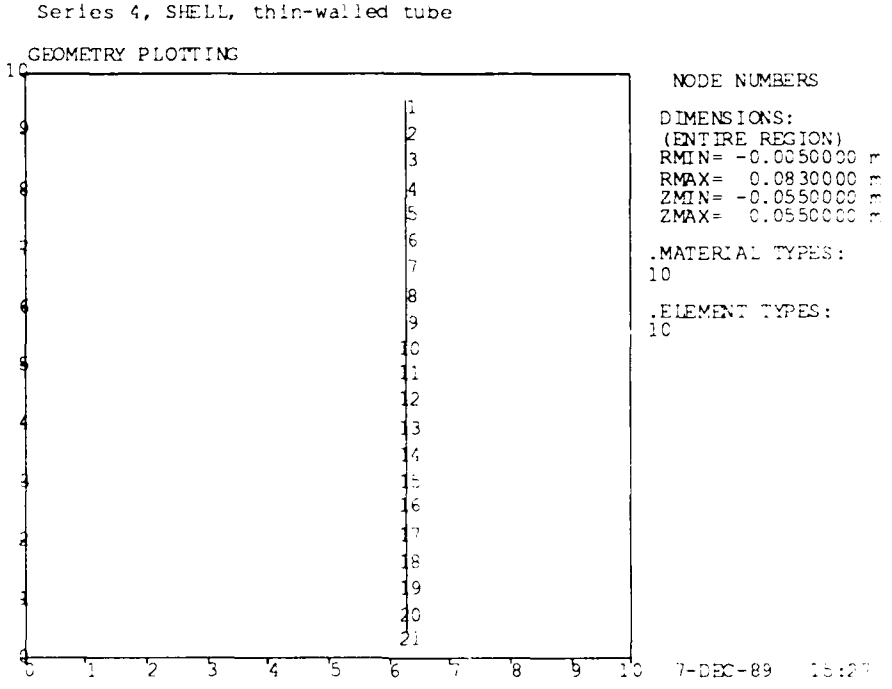

Figure 7.0.6: Series 4 Problems - Tube Element Numbering

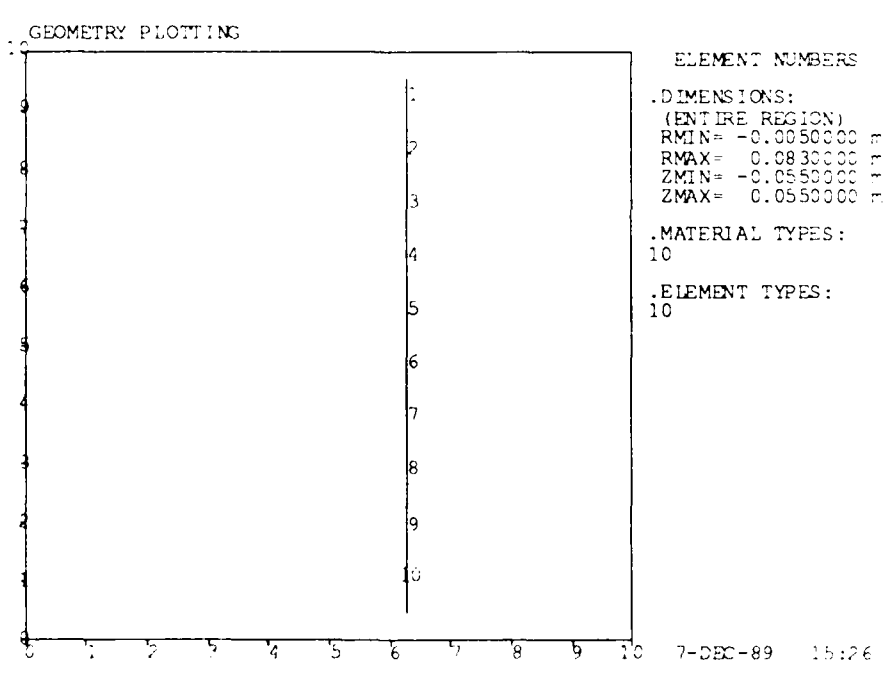

7.1 PROBLEM 13

Analysis Type: EIGEN - flexural (disk) and hoop (tube) modes

Input Files: D13.DAT (disk)
D13R.DAT (tube)

All entries into the material property table of the aluminum SHELL elements, according to the data requirements [1.1a], [1.7], depend on the shell thickness.

For the disk, the search for resonances is confined to the frequency band between 350 Hz and 450 Hz. As in Problem 2, ERVAL and ERVEC (Card 7) were each reduced to 1.0E–6 to ensure accurate convergence [4.2]. The resonance frequency was located at 458.35 Hz. A plot of the corresponding mode shape is shown in Figure 7.1.1, where the vibration is displayed at five phase angles, $\pi/4$ radians apart. (The $2\pi/4$ vibration curve lies along the disk, so is not seen.) Further testing of flexural and extensional modes in the thin disk are reported in [4.2]

For the tube, since hoop-type modes are expected to fall within a much higher frequency range, a 15,000 Hz through 16,500 Hz band is used. Also, a number of modes are expected in close proximity, so the tolerance for convergence of eigenvalues (ERVAL on Card 7) is lowered to 1.0E-8 and the tolerance for convergence of eigenvectors, ERVEC is 1.0E-6. Similarly, in anticipation of an increase in the number of necessary iteration cycles, the "stop iteration number", ITSP is increased to 50.

When the ends of the tube are fixed in Z and β (rotations), two modes were found in the search range. The first mode is antisymmetrical at 15,839 Hz and the second is symmetrical at 16,403 Hz. A plot of the first mode shape is shown in Figure 7.1.2. Extending the search range, we find a pure hoop mode at 17,456 Hz as Mode 4. The end fixities simulate the constraints in an infinite tube, and calculation of this resonance from simple elastic theory gives 17,457 Hz.

When there are no fixities, three modes occur in the search range, two symmetrical modes at 15,838 and 16,396 Hz, and one antisymmetrical mode at 16,314 Hz. The first mode shape is shown in Figure 7.1.3.

In the free tube, no real mode displays pure hoop vibration, but when rotations are suppressed by artificially applying β fixities of zero to all nodes, a hoop mode is found at 15,924 Hz. The mode shape, shown in Figure 7.1.4, displays both radial and axial vibration. If, in addition to the β fixities, the axial motion is suppressed by Z fixities applied to the ends of the tube, the pure hoop mode at 17,456 is again observed, now as Mode 1.

Figure 7.1.1: Problem 13 - Disk, First Flexural Mode Shape

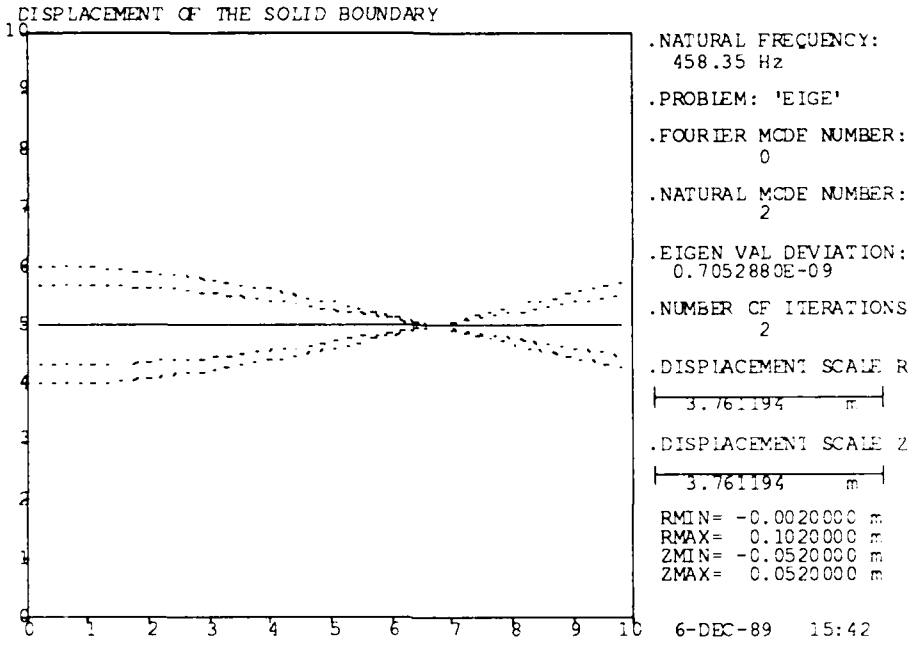

Figure 7.1.2: Problem 13 - Tube, First Mode Shape, Fixed Ends

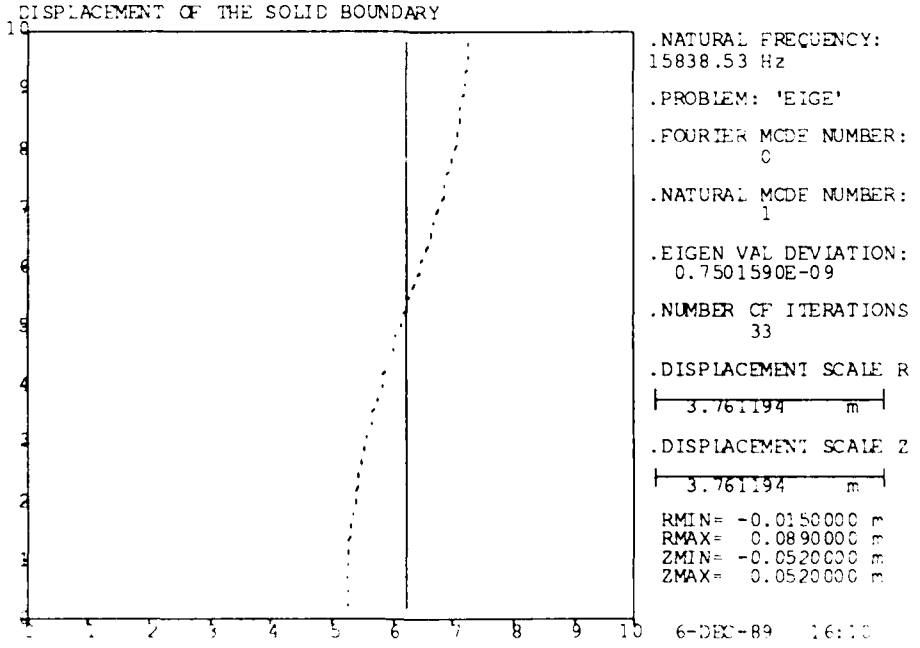

Figure 7.1.3: Problem 13 - Tube, First Mode Shape, Free Ends

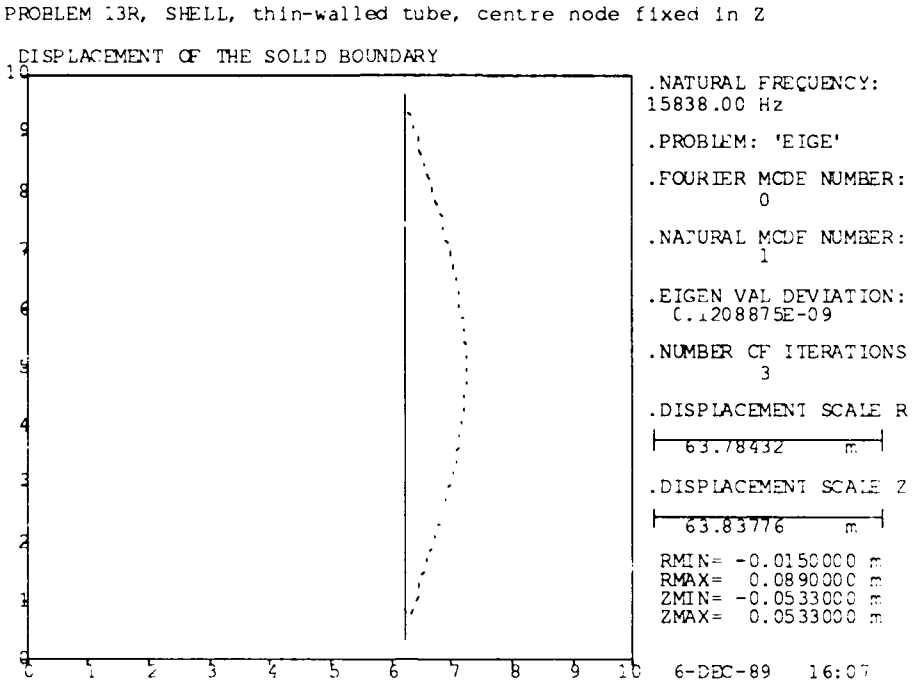

Figure 7.1.4: Problem 13 - Tube, Hoop Mode Shape, Fixed Rotations

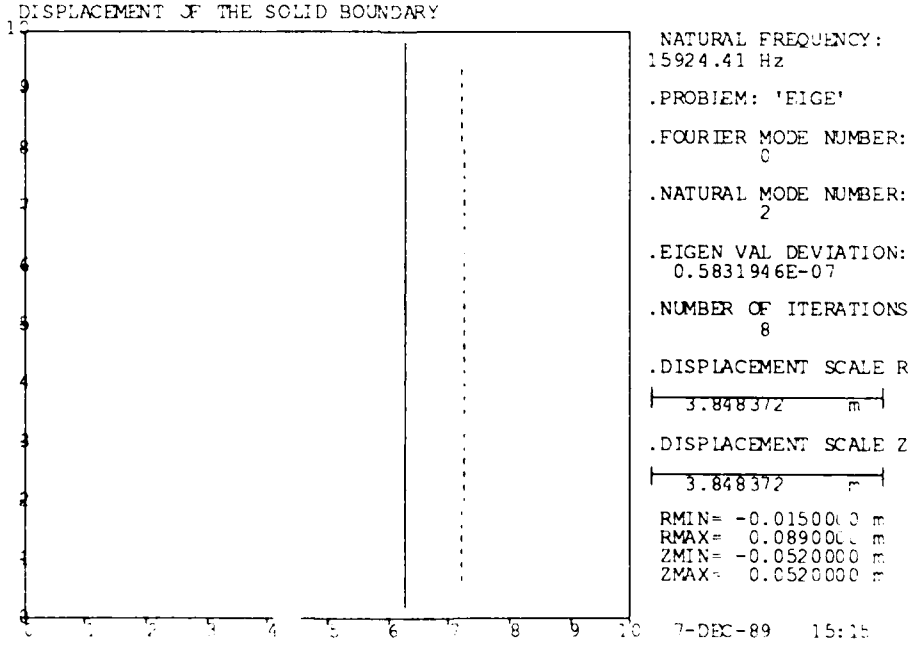

7.2 PROBLEM 14

Analysis Type: STATC - transverse temperature differential (a), and nodal load (b)

Input Files: P14A.DAT
P14B.DAT

Only the disk structure is used in these problems.

In Case (a) a 20° C transverse temperature difference is assumed across the shell thickness, with the higher temperature on the top surface of the disk. The data format requires that, for the right side of the element (as seen from the first node on the element) being hot, the temperature difference is positive. In this case the left side is hotter, so a negative value of DELDT is used on the element extension data, Card 5b.

A plot of the thermally deformed disk is shown in Figure 7.2.1.

In Case (b) the disk is clamped around its periphery by specifying zero u,v,w, and β fixities at Node 21 . A 10-N force is applied as a load fixity at Node 1 in the +Z-direction.

A plot of the deformed disk is shown in Figure 7.2.2. In both Figures 7.2.1 and 7.2.2, the printed hydrophone sensitivity is meaningless.

Figure 7.2.1: Problem 14 - Disk Thermal Deformations

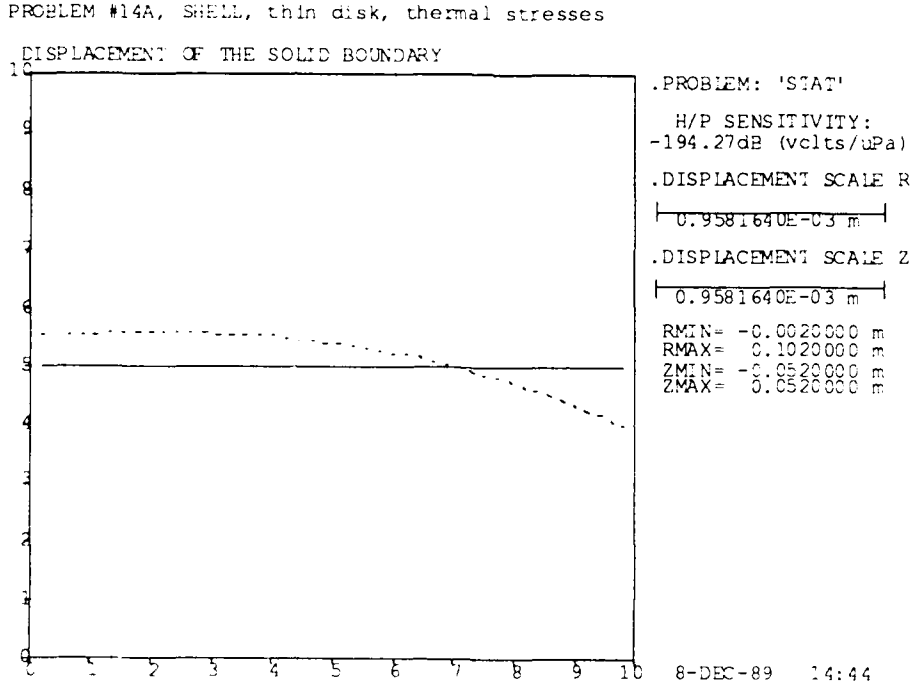

Figure 7.2.2: Problem 14 - Disk Forced Deformations

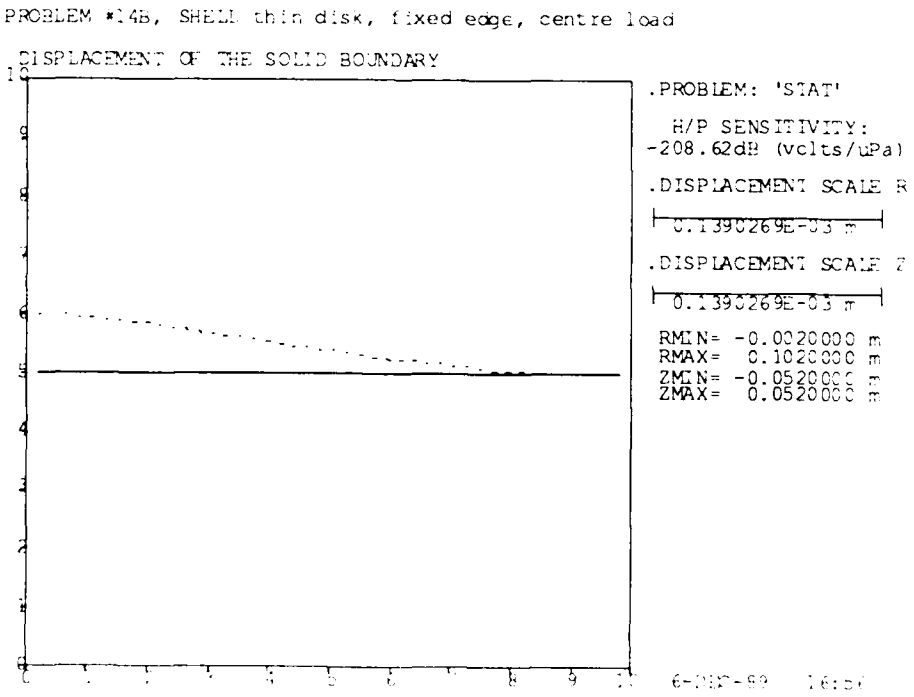

8 SERIES 5: ANALYTICAL FLUID PROBLEM

A cross-sectional diagram of the structure modelled in this series is given in Figure 8.0.1. It is a 10 cm diameter piston that vibrates axially in an infinite hard baffle. The half-space over the piston and baffle is sea water. The outer radius of the sea water sphere used in the analysis is 0.165 m.

The mesh of the F.E. model with node numbers is shown in Figure 8.0.2, while Figure 8.0.3 gives the element numbering. The piston is modelled with six SHELL (Type 10) elements.

The model shown in Figures 8.0.2 and 8.0.3 has been changed from that in the original Examples Manual [1.1c]. The main change has been to reduce the number and size of the fluid elements to increase accuracy and to reduce the run time. Testing that resulted in these changes is reported in Ref. [4.2]

Figure 8.0.1: Series 5 Problem - Diagram of Piston in Infinite Baffle

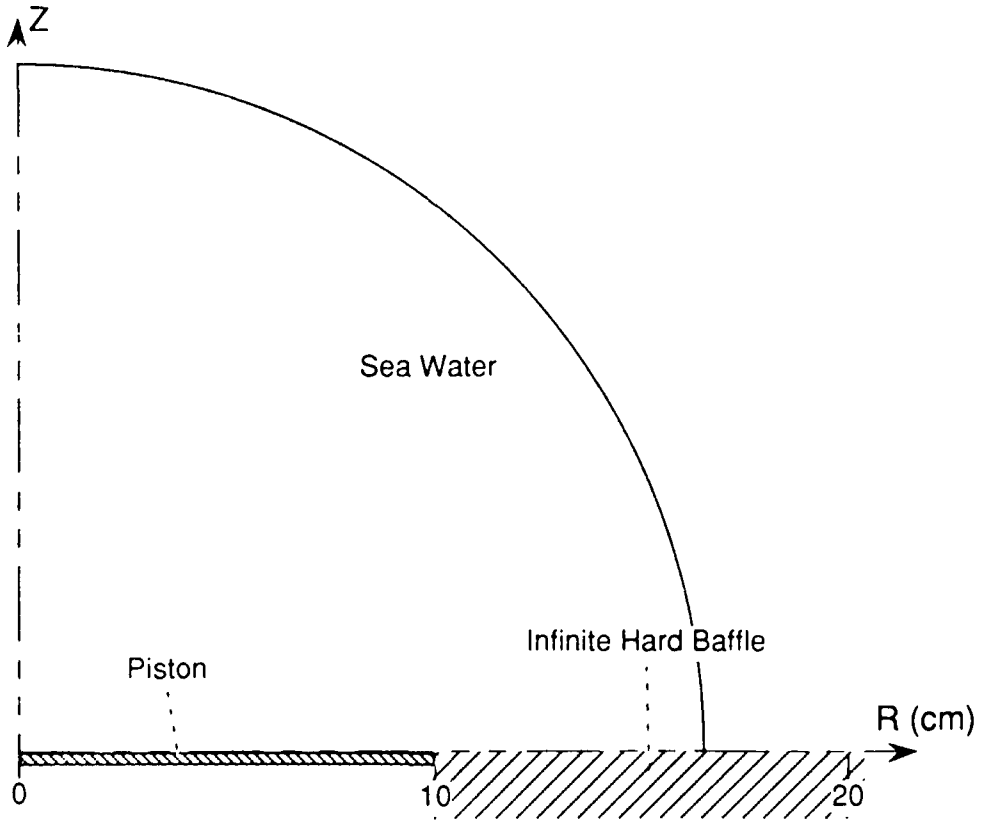

Figure 8.0.2: Series 5 Problems - Node Numbering

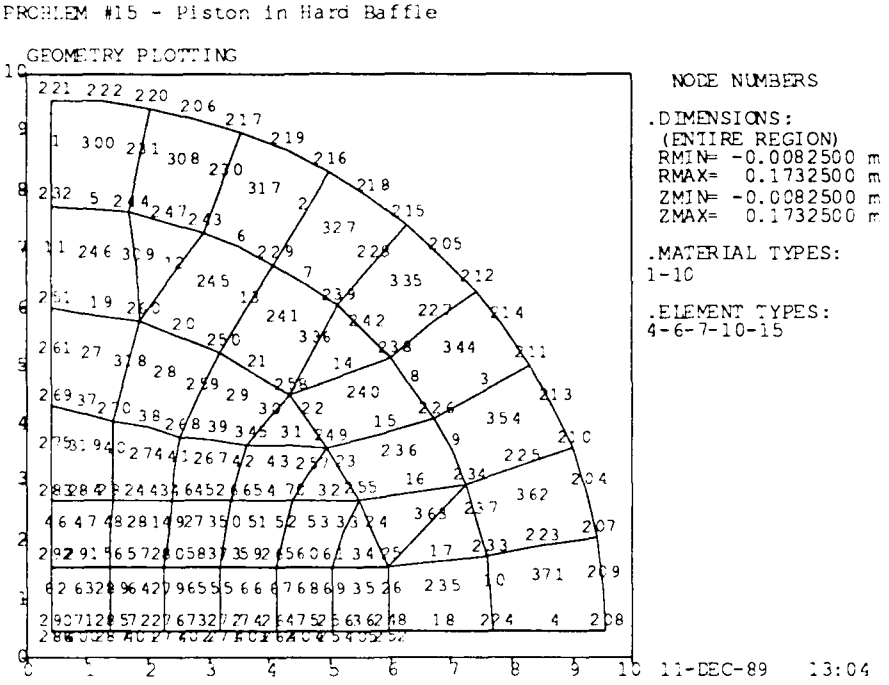

Figure 8.0.3: Series 5 Problems - Element Numbering

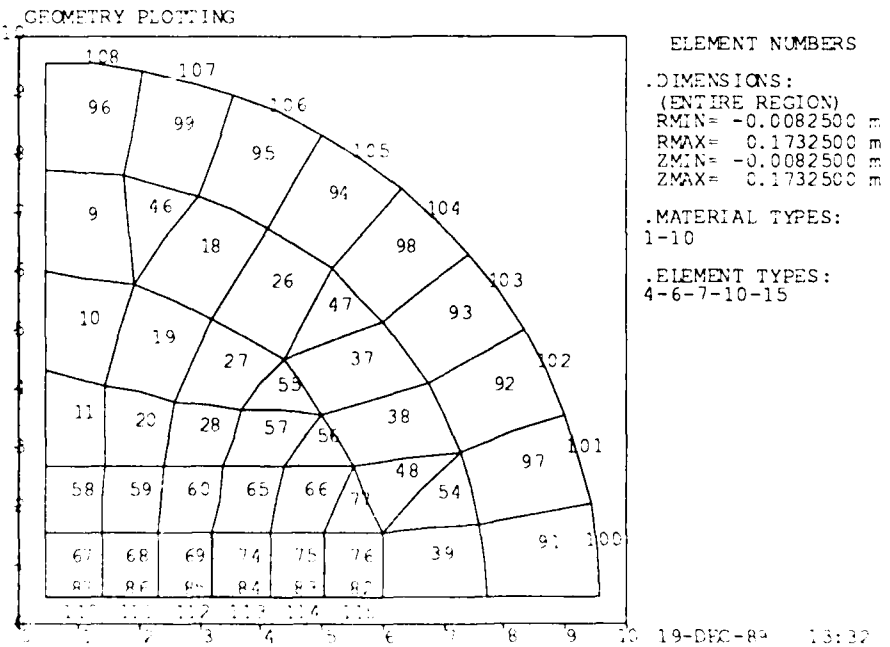

8.1 PROBLEM 15

Analysis Type: DRIVE - piston in infinite hard baffle

Input File: D15S.DAT

The piston is driven at a vibration amplitude of 1 mm by applying fixities in the Z-direction on all H nodes of the SHELL elements. Only one excitation frequency of 12,000 Hz is used in the analysis.

Test results reported in [4.2] show that this model is acoustically accurate at frequencies up to 18,000 Hz. It was shown that FLUID element dimensions should not exceed 0.4 wavelength at the highest frequency where accurate results are sought.

A plot of far-field directivity at 12,000 Hz is shown in Figure 8.1.1. The peak pressure of 269.28 dB re1μPa @1m is the same as predicted by analytical theory [4.2]. When an acoustic radiation problem is analysed as a hemisphere, a mirror of symmetry is assumed, hence the directivity pattern is repeated for the lower hemisphere. Under these conditions, a hard baffle condition on the symmetry plane is automatic. A soft baffle could be created by imposing pressure fixities of zero on all fluid nodes on the plane, but this soft baffle would extend only to the spherical boundary of the near-field region analysed.

Figure 8.1.2 shows near-field pressure contours at 12,000 Hz.

Figure 8.1.1: Problem 15 - Piston Directivity at 12,000 Hz

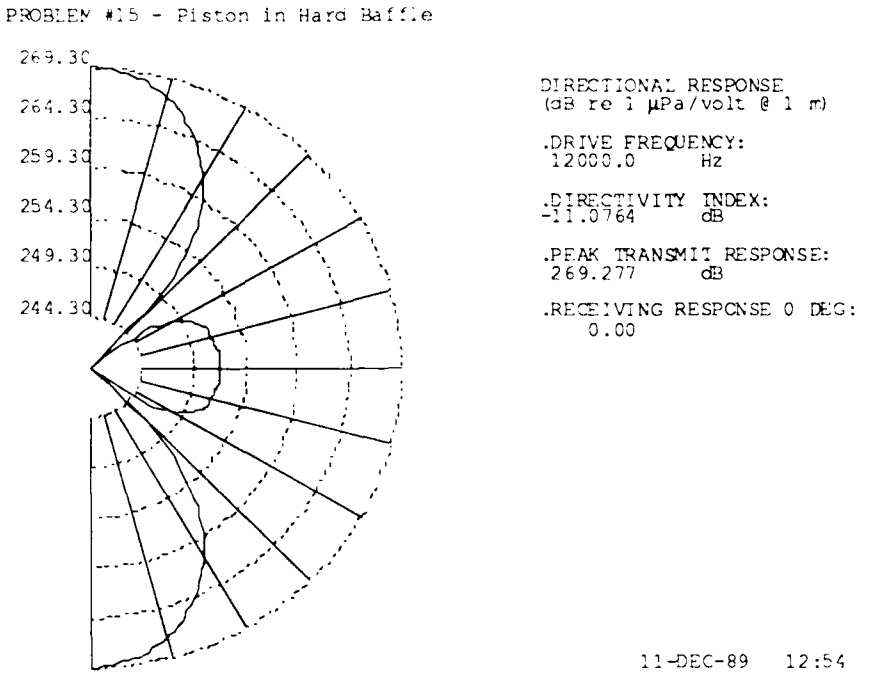

Figure 8.1.2: Problem 15 - Near-Field Pressure Contours at 12,000 Hz

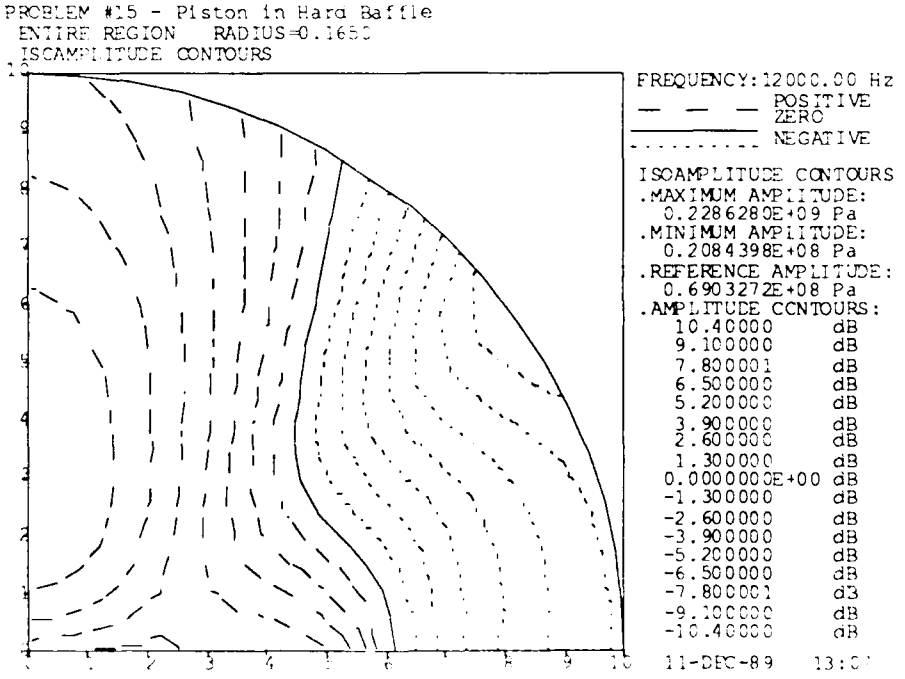

9 SERIES 6: MEMBRANE

This series demonstrates the use of MEMBRANE elements to separate two dissimilar fluids, namely, a 20-cm diameter spherical air bubble pulsating in sea water. Figure 9.0.1 is a cross-sectional diagram of the structure analysed. Unlike solid elements, FLUID elements cannot be adjoined by sharing common nodes along the boundary; MEMBRANE elements must be used with FTOS elements on each side to couple to the respective fluids.

The mesh of the F.E. model is shown in Figure 9.0.2. The membrane material properties correspond to 0.1 mm thick rubber with modulus of elasticity E = 2.06E7 Pa, Poisson's Ratio = 0.499 , and density = 1000 kg/m^3. The material properties of the air within the bubble are determined assuming that the bubble is placed at 10 metres depth, where the absolute hydrostatic pressure in the water is two atmospheres. Values for density and bulk modulus are 2.585 kg/m^3 and 0.285E+6 Pa, respectively. The adiabatic bulk modulus of the air is used, as this is a dynamic problem; for static problems, the isothermal bulk modulus would be used.

Figures 9.0.2 (a,b,c) and 9.0.3 (a,b) give details of node and element numbering. For clarity, numbers of the FTOS elements joining the membrane to the water are not shown, as they are in the same location as the membrane element numbers. Their numbers are 10, 22, 34, 46, 58, and 70, from the R-axis to the Z-axis.

Figure 9.0.1: Series 6 Problems - MEMBRANE on Air Bubble in Water

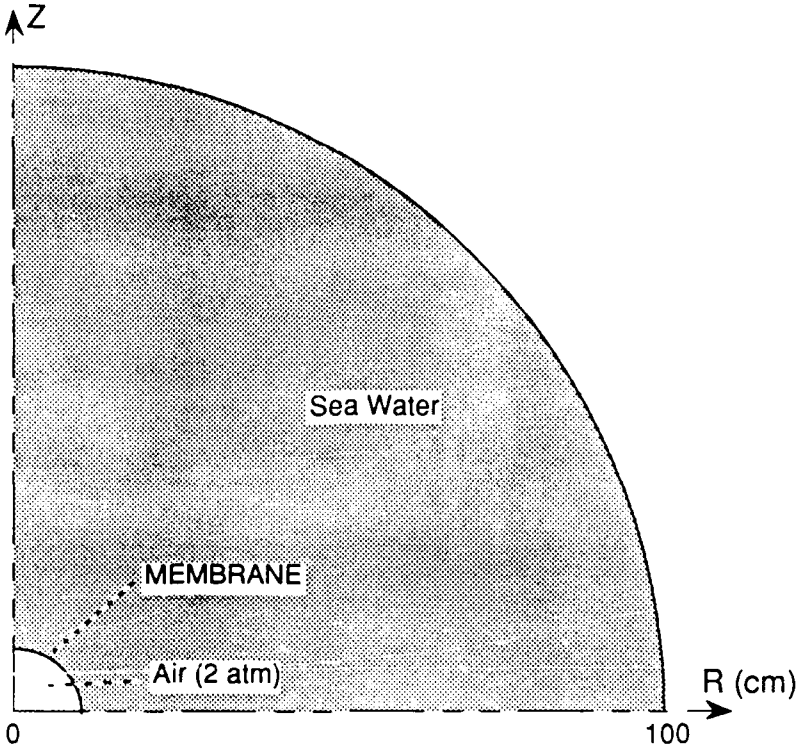

Figure 9.0.2 (a): Series 6 Problems - Outer Fluid Node Numbering

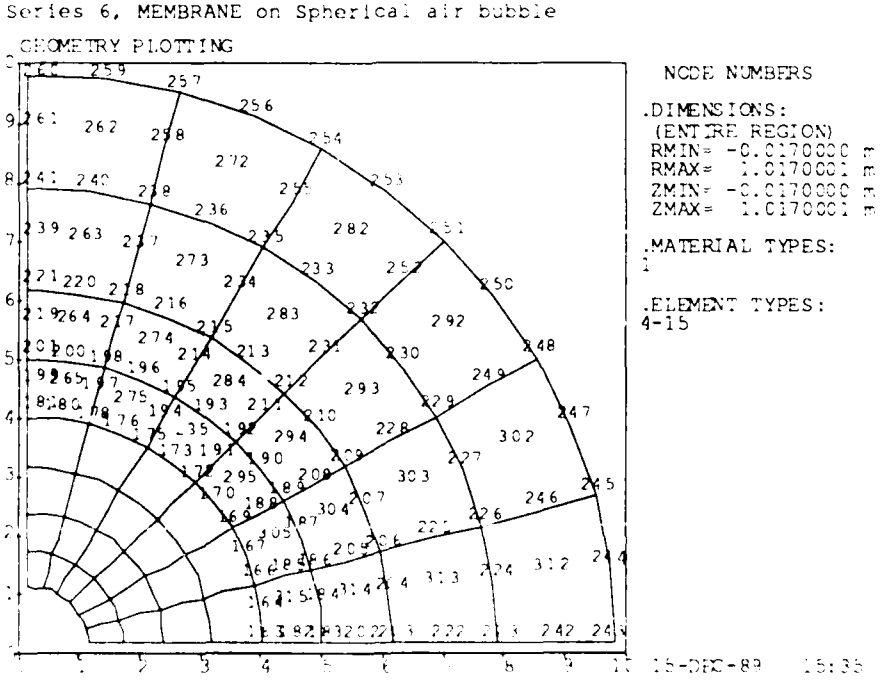

Figure 9.0.2 (b): Series 6 Problems - Middle Fluid Node Numbering

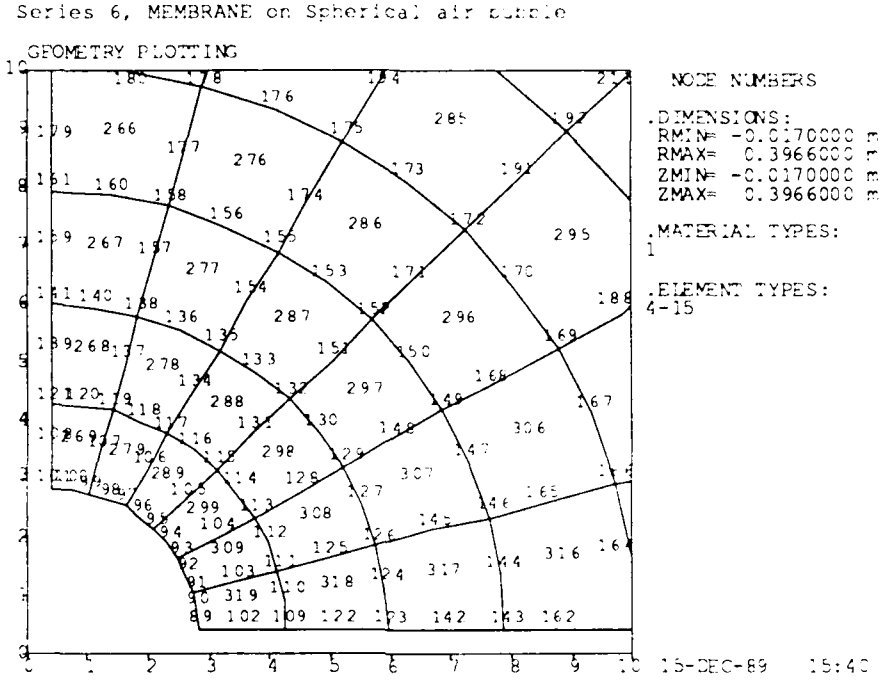

Figure 9.0.2 (c): Series 6 Problems - Air & Membrane Node Numbering

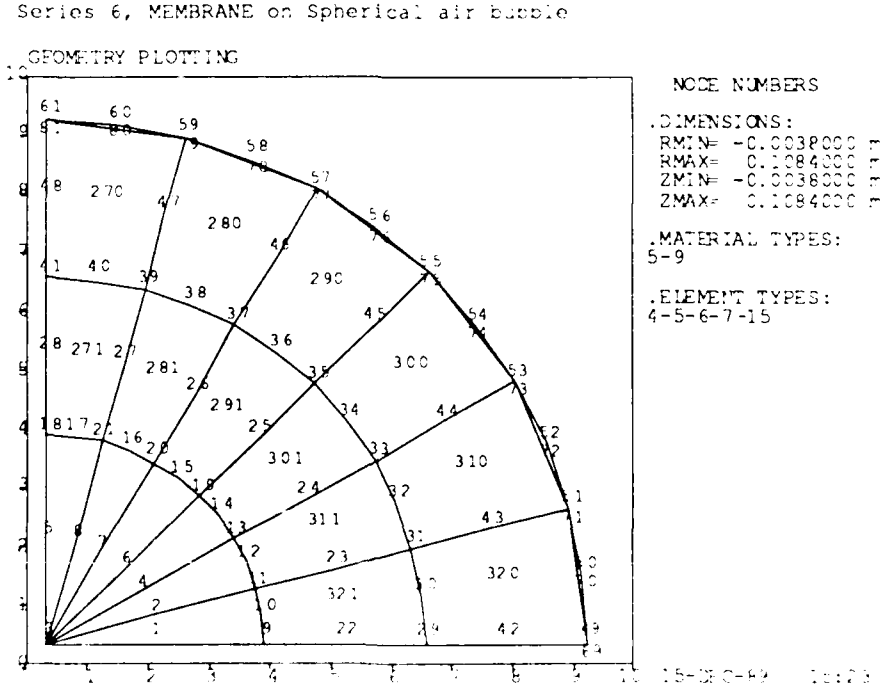

Figure 9.0.3 (a): Series 6 Problems - Outer Element Numbering

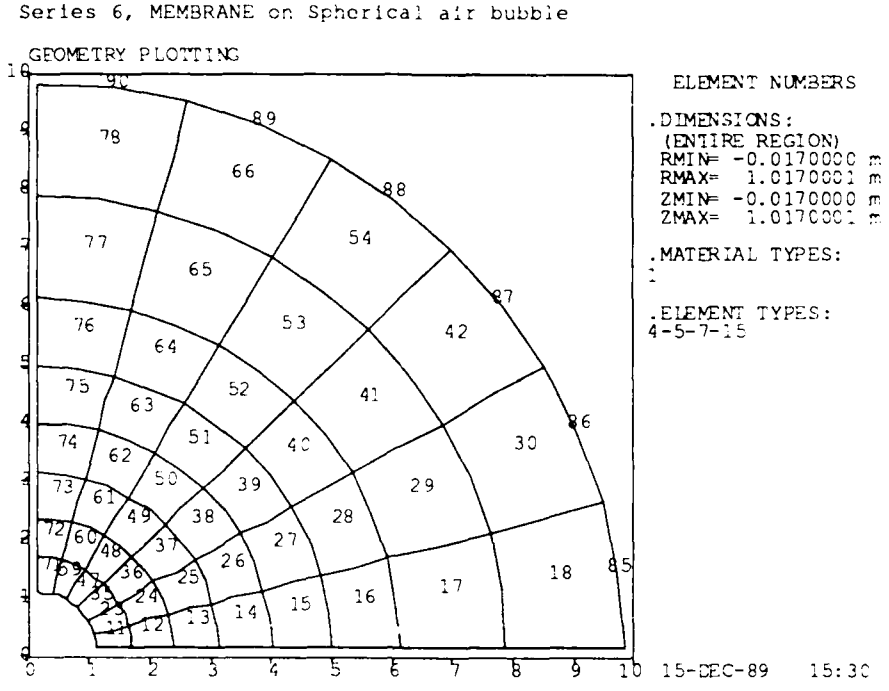

Figure 9.0.3 (b): Series 6 Problems - Inner Element Numbering

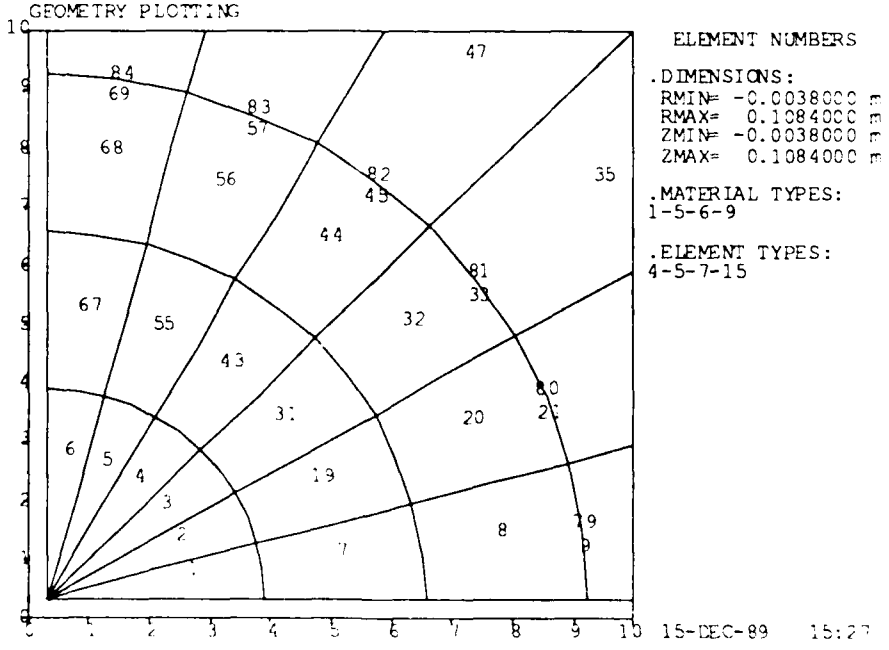

9.1 PROBLEM 16

Analysis Type: DRIVE - spherical air bubble

Input File: D16.DAT

Since only the upper hemisphere of the complete structure is analyzed, Node 69 on the symmetry plane must be restrained in the Z-direction.

Reference [4.2] reports extensive testing of the modelling of an air bubble in water, using variations of Problem 16. A shortcoming in the modelling capability of MAVART was discovered: Pressures are not transferred from one fluid medium to another through a MEMBRANE having FTOS elements on each side. Pressure on one side will deform the membrane, resisted only by the membrane stiffness, and not by any reactive force imposed by the fluid on the other side. Results are similar if SHELL or SOLID elements are used in place of the MEMBRANE elements. Modelling of the pressure in both fluids appears to be correct when the membrane is deformed by a loading force on the MEMBRANE nodes. Presumably, this statement can be generalized to say that the modelling is correct when the deformation of the structure is due to forces arising within the solid structure that separates the two fluids.

A spherically radial, harmonic force was applied to the membrane by placing Z and R fixities on the nodes, with values to simulate a uniform (pressure-like) force. Fixities on the end nodes of each element are half that on the centre node, as they are applied twice, once for each element in which they appear. The fixity at Node 69 on the symmetry plane is halved again to simulate the uniform force.

Frequency response plots of radiated far-field pressure (dB re 1μPa @ 1m) and radial displacement of the bubble at Node 70 are given in Figure 9.1.1. The resonance frequency is 47.38 Hz with a Q of 51.57. The resonance frequency predicted by analytical theory [4.2] is 45.9 Hz with a Q of 52.0.

Near-field pressure contours are shown in Figure 9.1.2 at 47.5 Hz, near the resonance. The pressure in the air bubble is nearly constant, varying from 8296 Pa at the origin to 8292 Pa at the membrane. This is 0.58 dB less than the peak pressure in the water, which is at the membrane surface.

Figure 9.1.1: Problem 16 - Far-Field Pressure and Radial Displacement of a Resonant Air Bubble in Water

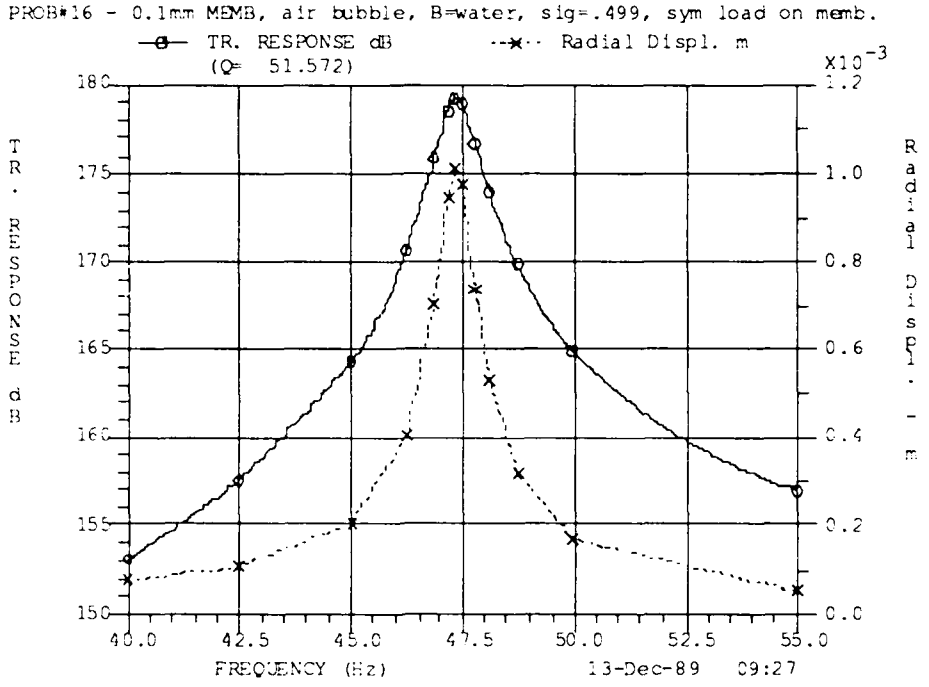

Figure 9.1.2: Problem 16 - Near-Field Pressure Contours at 47.5 Hz

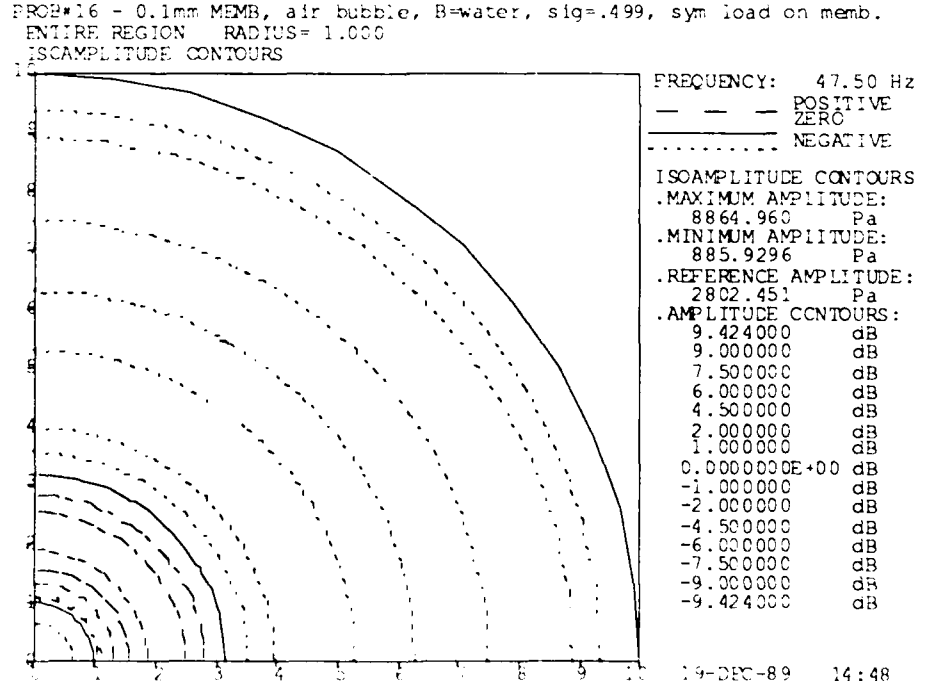

10 **SERIES 7: RING**

To demonstrate the use of RING elements, the same tubular shell structure is used as in Problem 13, with RING stiffeners added. A representative cross-sectional diagram is given in Figure 10.0.1. The node numbering is the same as in Figure 7.0.2. Ten RING elements (#11 to #20) are added to the structure of Figure 7.0.3, and are located at the odd-numbered H nodes of the shell. The cross-section of a single ring is 5 mm high and 2 mm thick. The end nodes, 1 and 21 are stiffened with single ring ribs, while the rest of the appropriate nodes receive double reinforcing.

Figure 10.0.1: Series 7 Problems - SHELL Tube with RING Stiffening

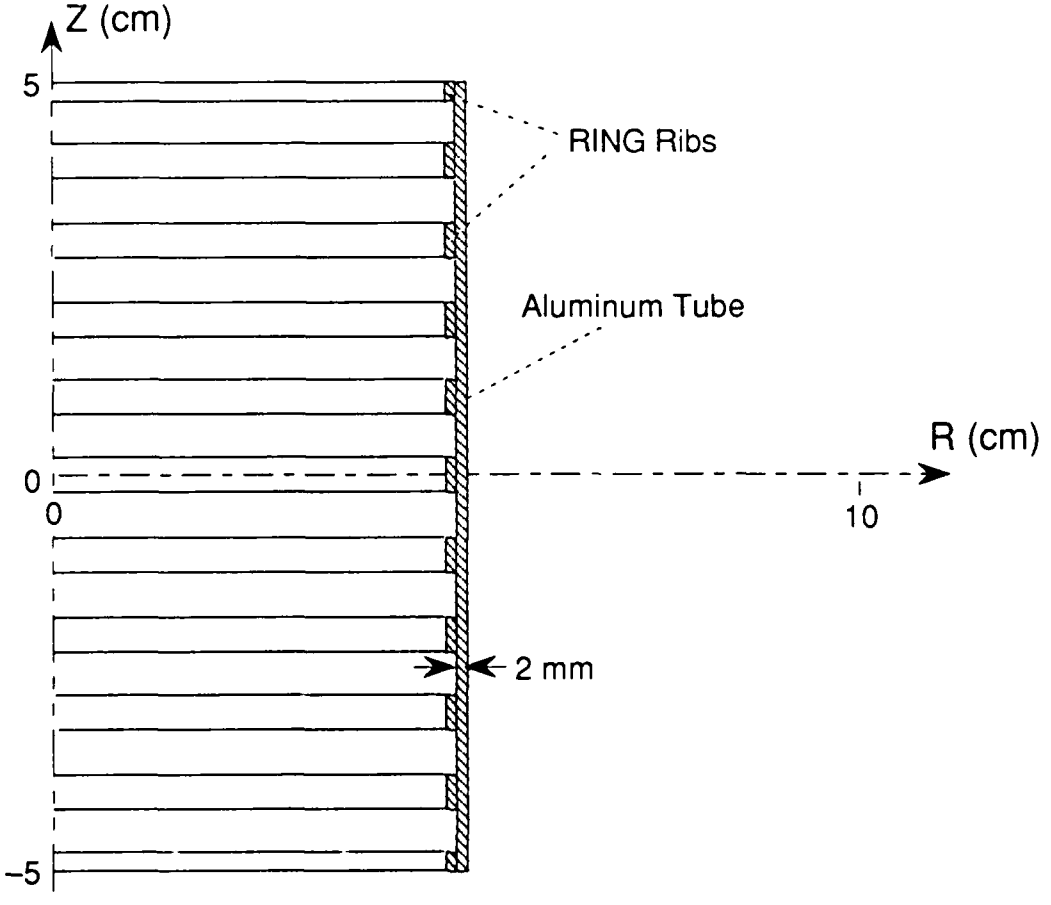

10.1 PROBLEM 17

Analysis Type: EIGEN - RING-stiffened SHELL tube,
(a) with no additional inertia,
(b) with nodal masses.

Input Files: D17A.DAT
D17B.DAT

In Case (a), the original structure of Figure 7.0.1 (Problem 13) is stiffened with aluminum RING elements added to odd-numbered H nodes of the shell. No inertia term (density) is specified in the material properties data for the ring, so that the stiffness alone may be modelled. The end nodes, 1 and 21 are free to move only in the R-direction, corresponding to the condition of Figure 7.1.2. The parameter POLANG in the element data for RING elements defines the number of elementary rings assigned to any given RING element; thus, POLANG is unity for elements 1 and 10, and 2 for the remaining RING elements.

In Case (b), nodal masses corresponding to the masses of each respective RING element are specified at the appropriate nodes. This essentially takes the place of the density term that could have been included in the material data for the RING. Note that the total mass of the ring is added to each DOF on which it is effectively acting. If the inertial moments of the RING elements are to be modelled, the density must be included in the material data, as the added masses cannot represent inertial moments.

In both cases the radial displacement of Node 1 is used as the normalizing DOF and is set to 1. The values of ERVAL and ERVEC are set to 1.0E–8 and 1.0E–6, respectively.

The results show the first natural frequency of the RING-stiffened shell to be 21,756 Hz without the nodal masses (Case (a)). After adding nodal masses, the frequency drops to 15,418 Hz (Case (b)). The mode shapes are both essentially the same, and are the same as shown in Figure 7.1.2 for Problem 13. As in Problem 13, the pure hoop mode is again Mode 4, but its frequency is lowered to 16,933 Hz.

11 SERIES 8: DAMPING APPLICATIONS

The model used in Problem 9 (Figure 5.0.1) was chosen for demonstration of damping employment in solids and fluids. Node numbering is the same as in Figure 5.0.3 (a,b). Element numbering for Problem 18A is the same as in Figure 5.0.2. For Problem 18B, an additional five VISCous fluid elements (#81 to #85) are added to the structure, using existing fluid nodes.

11.1 PROBLEM 18

Analysis Type: DRIVE - damping in the PT solid ring (a),
- damping in a VISCous fluid layer (b)

Input Files: D18A(1,2).DAT
D18B(1,2,3,4).DAT

In Case (a) the stiffness- and mass-distributed damping coefficients, μ_k and μ_m equal to 0.03 (3%), were arbitrarily chosen. Otherwise the data did not differ from those used in Problem 9. The two damping coefficients were applied separately, and resonance searches were applied in both cases in the range from 250 to 450 Hz. Transmitting voltage responses for the two types of damping are plotted in Figure 11.1.1, together with the result of Problem 9 for no damping. Corresponding efficiency plots are given in Figure 11.1.2 for the two damped cases. (The efficiency for the undamped structure is 100 percent.)

In Case (b), the material damping coefficients for the PT ring were set to zero, and a viscous dissipating fluid layer was inserted on the ring. This comprises five VISC elements, laid on F nodes of the FTOS elements.

The appropriate material properties matrix for the VISC elements was added to the data. Viscous damping is invoked by setting the "density" to 1.0 for pressure-varying damping and/or setting the stiffness coefficient c_{11} to 1.0 for pressure gradient-varying damping; these are flags and have no relevance to their normal properties. The magnitude of the damping is applied in the same way as for solid material damping: μ_k for stiffness-distributed damping and μ_m for mass-distributed damping, although these parameters are no longer fractions between zero and one. The four types of viscous damping were applied separately to the model and a resonance search was done in the same range as for material damping. Values of μ_k and μ_m were selected so as to yield efficiencies near 80% at the 375-Hz resonance.

Plots of the transmitting voltage responses with viscous damping are compared to those for the undamped structure in Figures 11.1.3 to 11.1.6. The corresponding efficiencies are plotted in Figure 11.1.7.

Figure 11.1.1: Problem 18(a) - Transmitting Voltage Responses of a Free-Flooding Ring with Different Material Damping

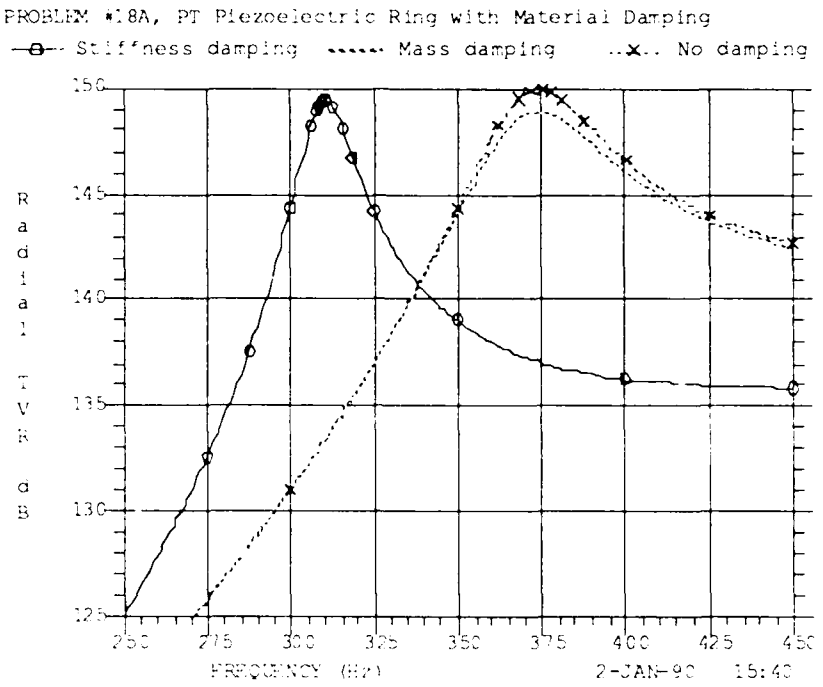

Figure 11.1.2: Problem 18(a) - Efficiencies with Material Damping

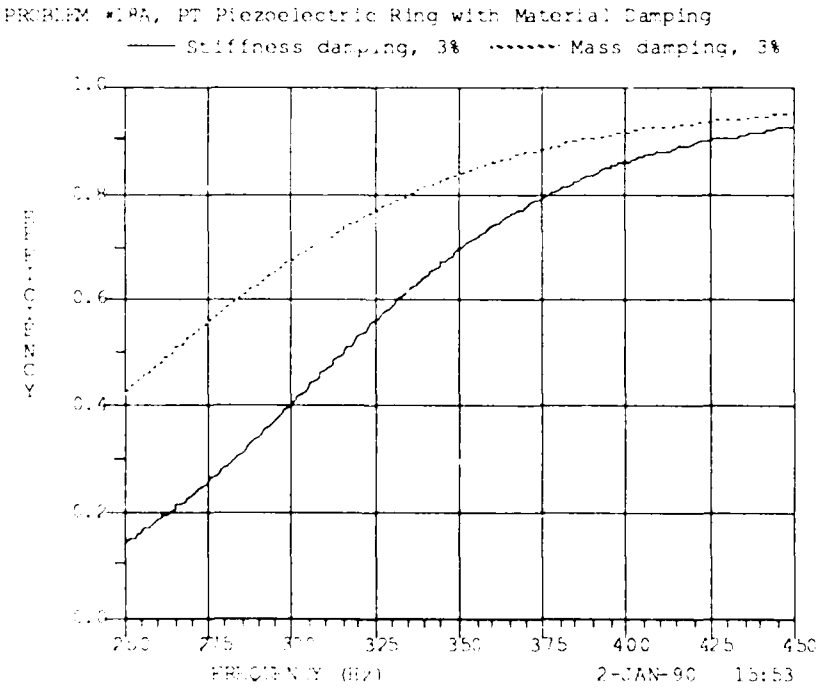

Figure 11.1.3: Problem 18(b) - Transmitting Voltage Response for a Free-Flooding Ring with Viscous Pressure Damping, μ_k = 2.0E+8

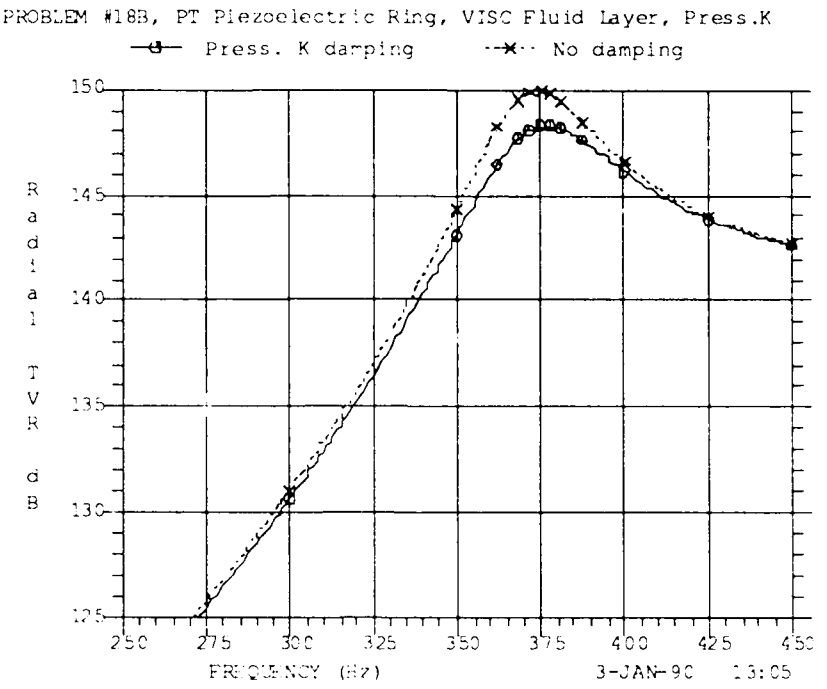

Figure 11.1.4: Problem 18(b) - Transmitting Voltage Response for a Free-Flooding Ring with Viscous Pressure Damping, μ_m = 30.

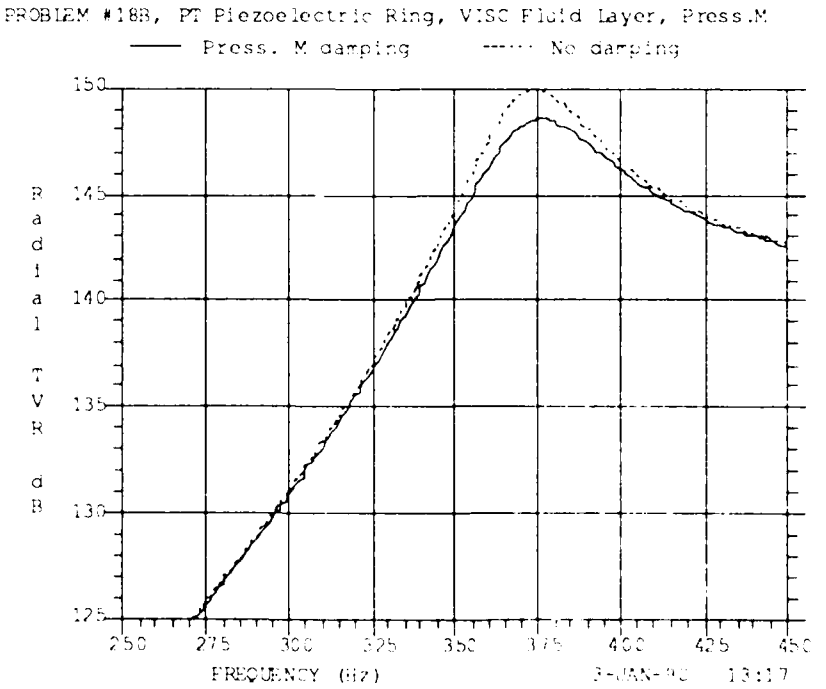

Figure 11.1.5: Problem 18(b) - Transmitting Voltage Response for a Free-Flooding Ring with Pressure Gradient Damping, μ_k = 1.5E+7

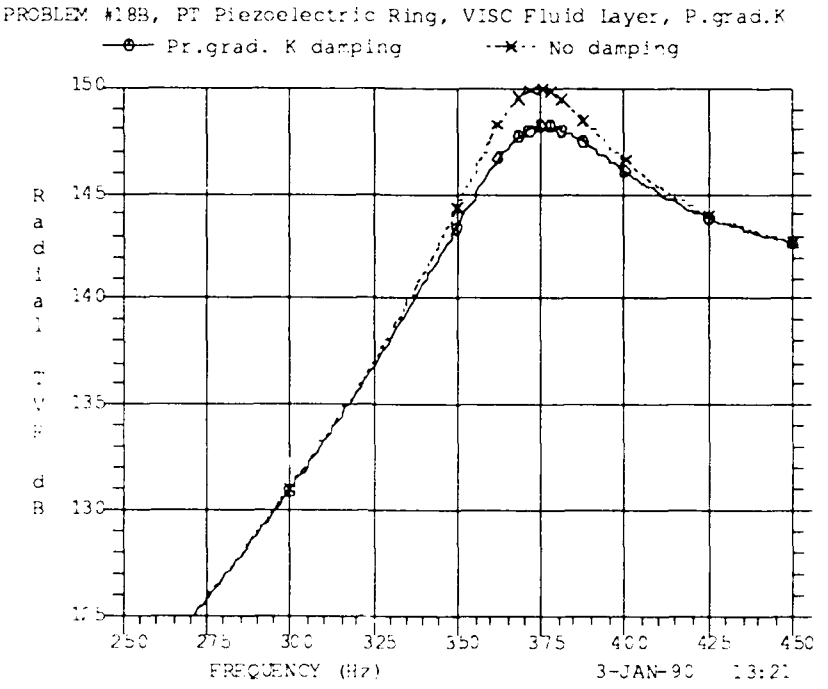

Figure 11.1.6: Problem 18(b) - Transmitting Voltage Response for a Free-Flooding Ring with Pressure Gradient Damping, μ_m = 3.

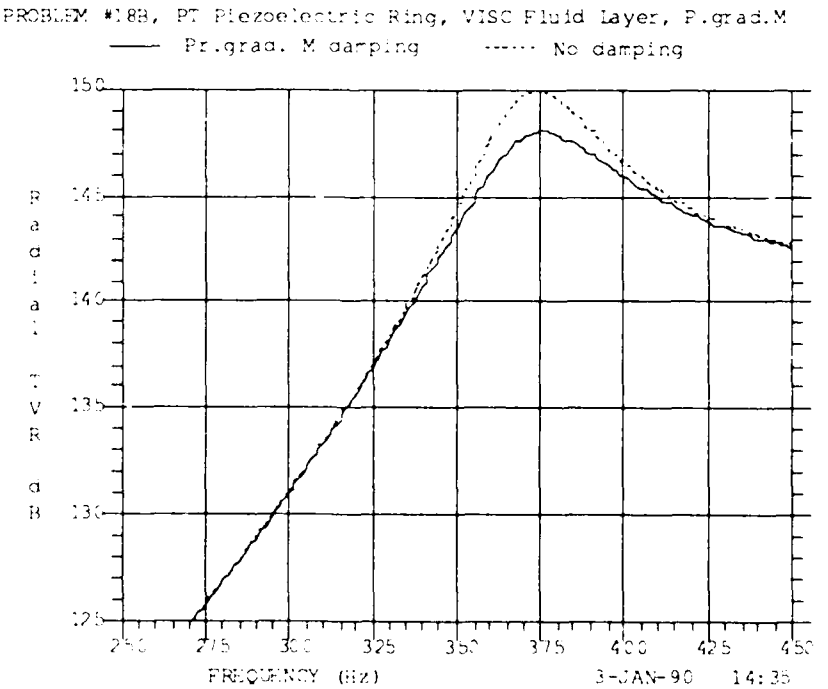

Figure 11.1.7: Problem 18(b) - Efficiencies for a Free-Flooding Ring with Different Types of Viscous Fluid Damping

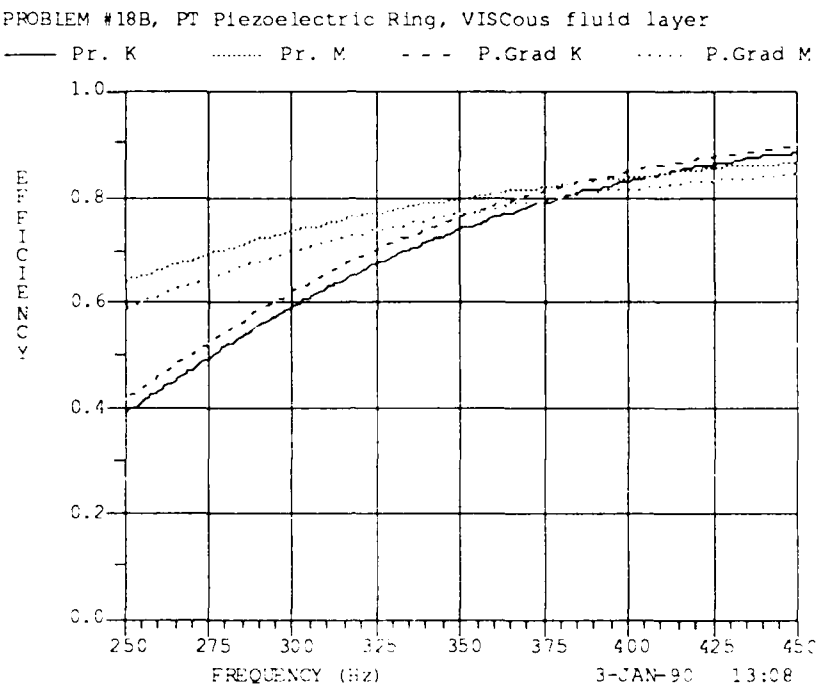

We note that the solid material stiffness damping has a profound effect on the resonance frequency of a free-flooding ring, while the other forms of damping have virtually no effect on the frequency. In all cases, the dependence of efficiency on frequency is greater for stiffness damping than for mass damping. Further investigation of damping in a free-flooding ring transducer will be reported in a future DREA Note.

12 SERIES 9: RING ARRAY, RIGID NODE

Two PT rings, each made of 48 staves of Channel 5400 ceramic, are immersed in sea water and separated by an aluminum ring as shown in Figure 12.0.1. The mesh of the F.E. model is given in Figure 12.0.2. Figures 12.0.3 (a-d) and 12.0.4 (a,b) give details of node and element numbering, with the radial dimensions expanded relative to the axial dimensions. The E-type Nodes 975 and 987 coincide with F-type Node 376, and are placed at the origin of the system of coordinates.

For this edition of the Examples Manual, the model was changed by deleting the four outer layers of fluid elements from the original model. This reduces the size of the problem with a possible improvement in accuracy as noted under Problem 15. Also, the eight elements representing the two PT rings have been placed in two element groups, one for each ring (NELG = 2 on Card 10). When all eight elements are placed in one group, the radiated power, admittance and efficiency are in error.

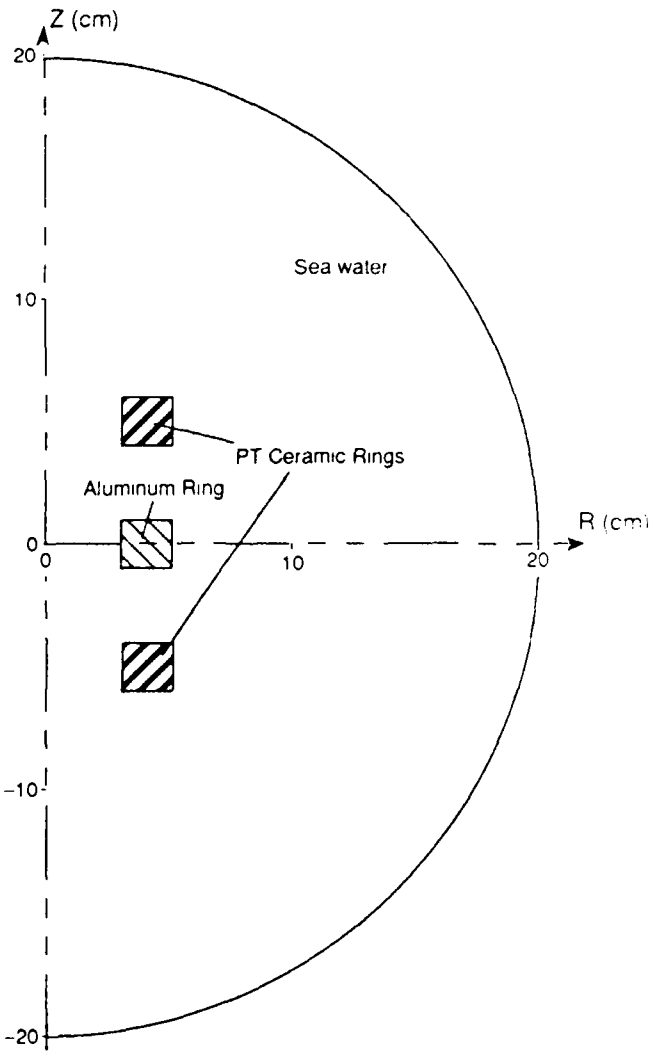

Figure 12.0.1: Series 9 Problems - Cross-Sectional Diagram of Model

Figure 12.0.2: Series 9 Problems - F.E. Mesh

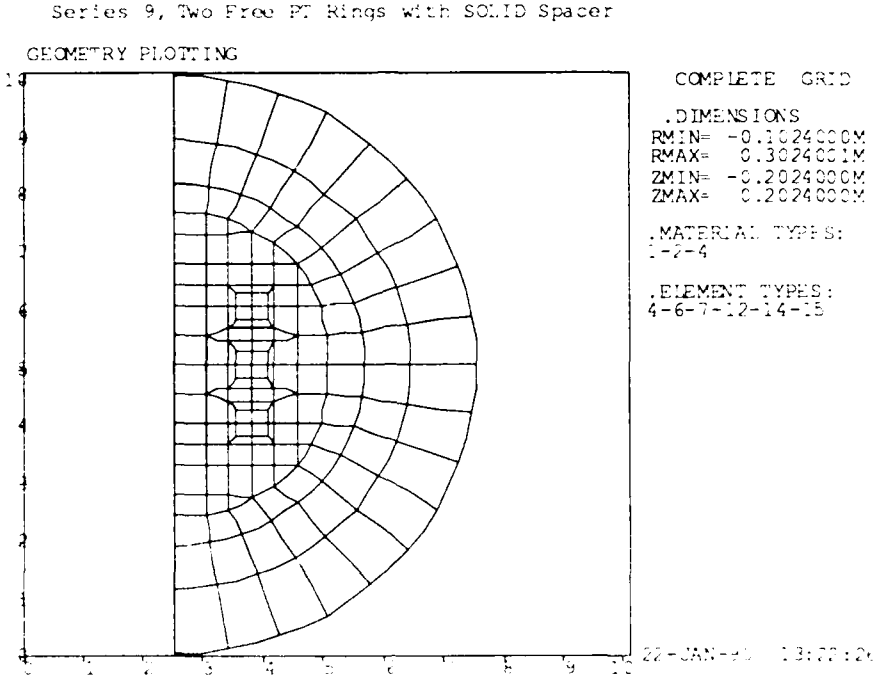

Figure 12.0.3 (a): Series 9 Problems - Outer Node Numbering

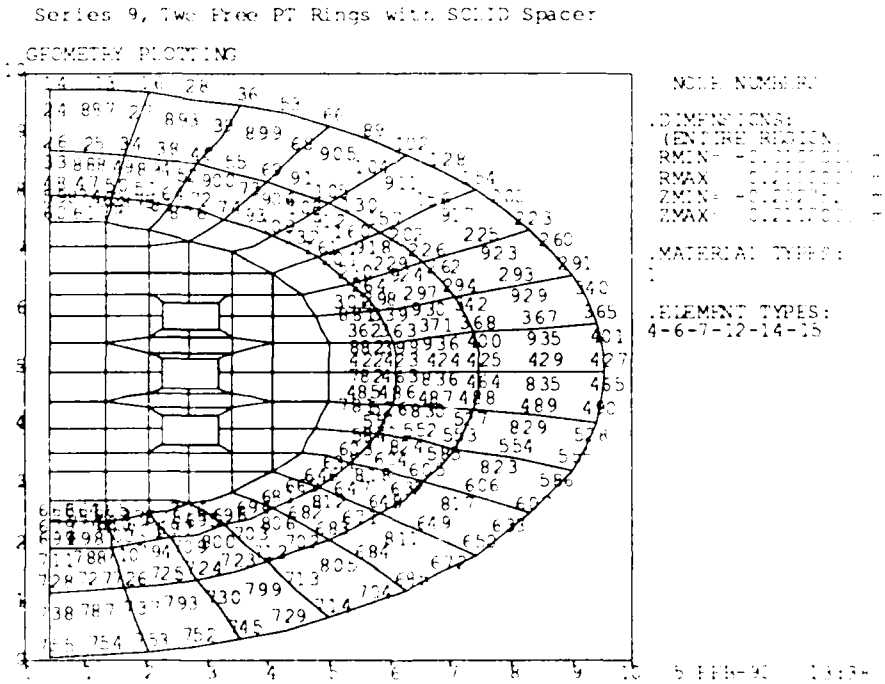

Figure 12.0.3 (b): Series 9 Problems - Middle Node Numbering

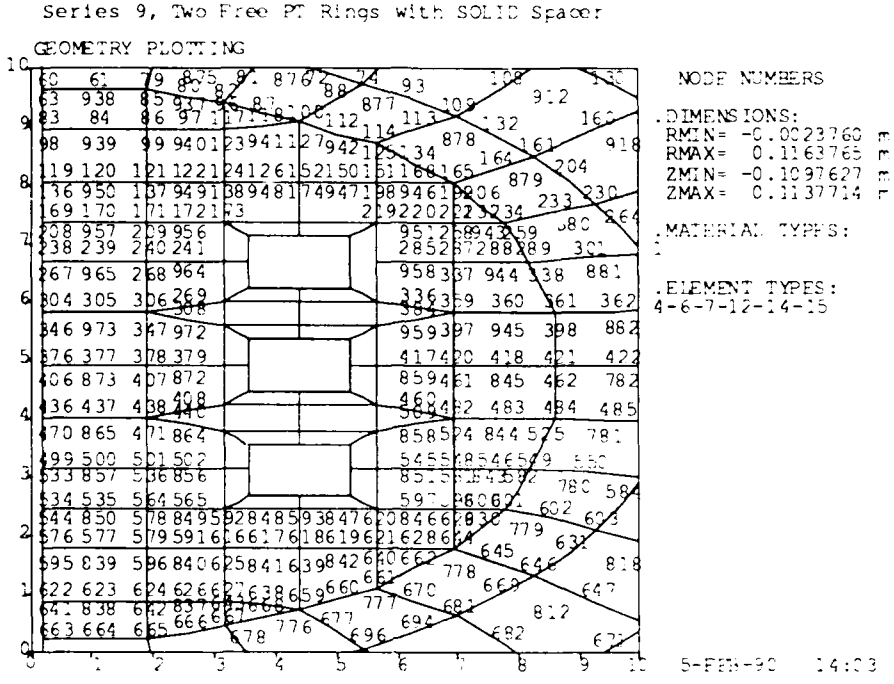

Figure 12.0.3 (c): Series 9 Problems - Inner Fluid Node Numbering

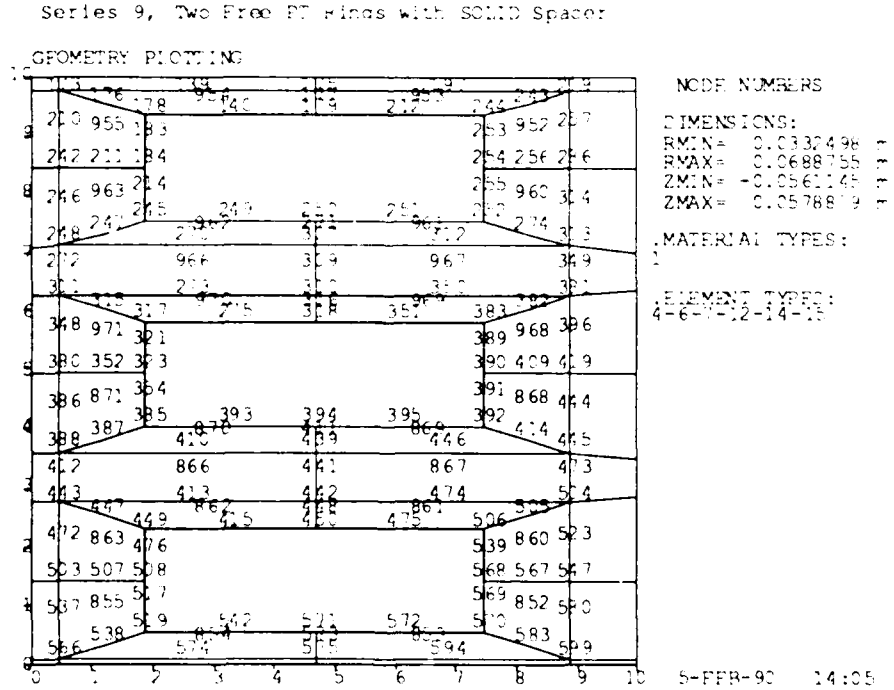

Figure 12.0.3 (d): Series 9 Problems - Solid Node Numbering

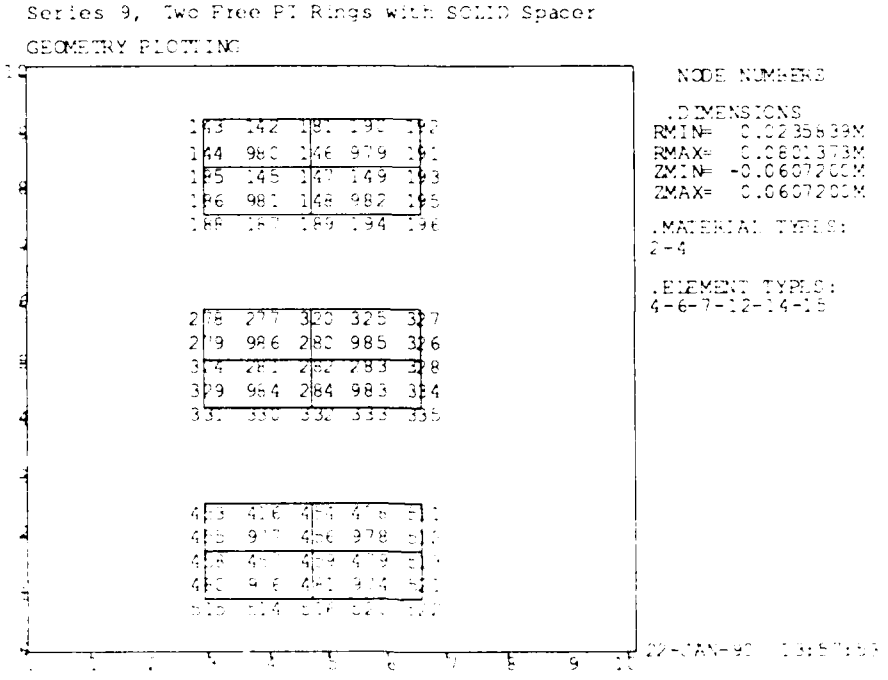

Figure 12.0.4 (a): Series 9 Problems - Outer Element Numbering

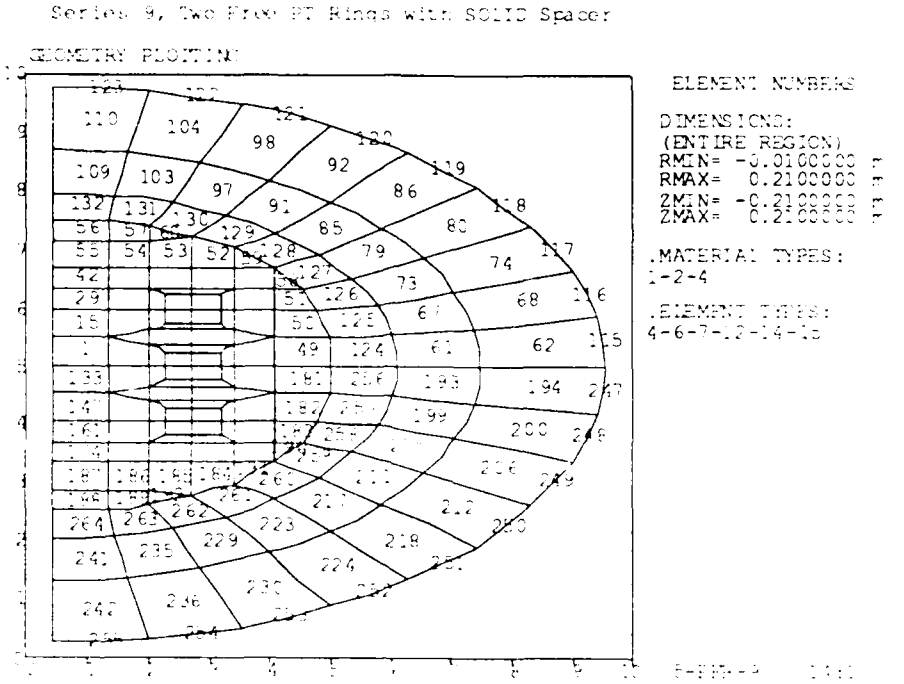

Figure 12.0.4 (b): Series 9 Problems - Inner Element Numbering

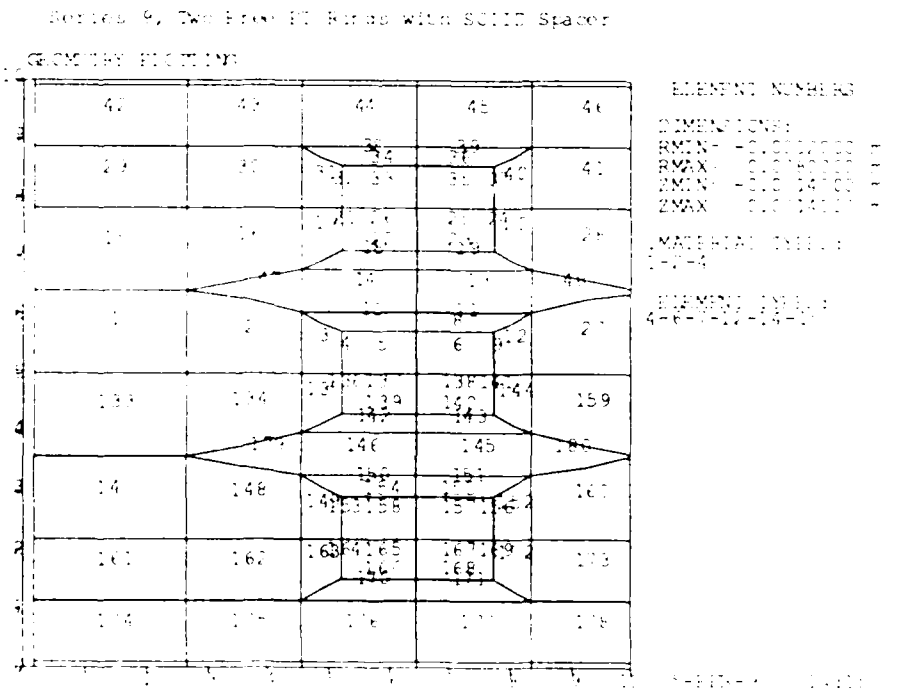

12.1 PROBLEM 19

Analysis Type: DRIVE - two free flooding PT rings with SOLID spacer

Input Files: D19A.DAT

First, the original model shown in Figures 12.0.3 and 12.0.4 is analyzed. A 6000 Hz, 1 V amplitude excitation is applied to both E-type nodes, a change from the 100 Hz drive originally applied. The inner mid-plane nodes of each PT ring and the spacer are restrained in the Z-direction, i.e., Nodes 185, 458, and 324.

Plots of displacement, far-field directivity, and near-field pressure contours are shown in Figures 12.1.1 through 12.1.3, respectively.

Note: Substructuring was included in the previous version of MAVART, but was never implemented by DREA. With the availability of more powerful computers, it was decided to delete this capability from the code as offering limited advantages, not worth expending resources to implement. Hence, in this edition of the Examples Manual, Problem 19B, which related to substructuring, has been deleted.

Figure 12.1.1: Problem 19(a) - Displacement at 6000 Hz

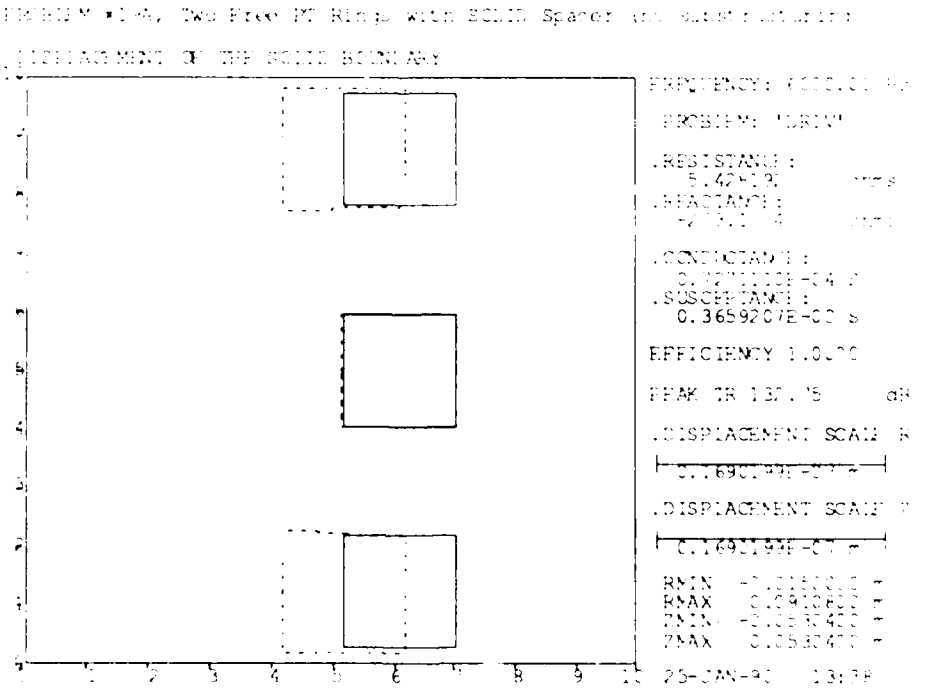

Figure 12.1.2: Problem 19(a) - Far-Field Directivity at 6000 Hz

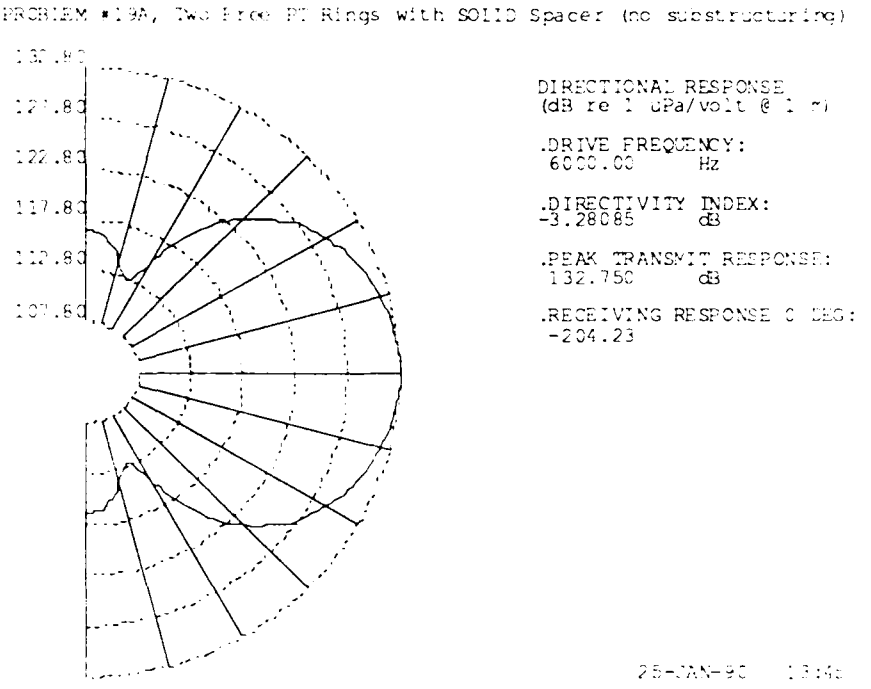

Figure 12.1.3: Problem 19(a) - Near-Field Pressure Contours

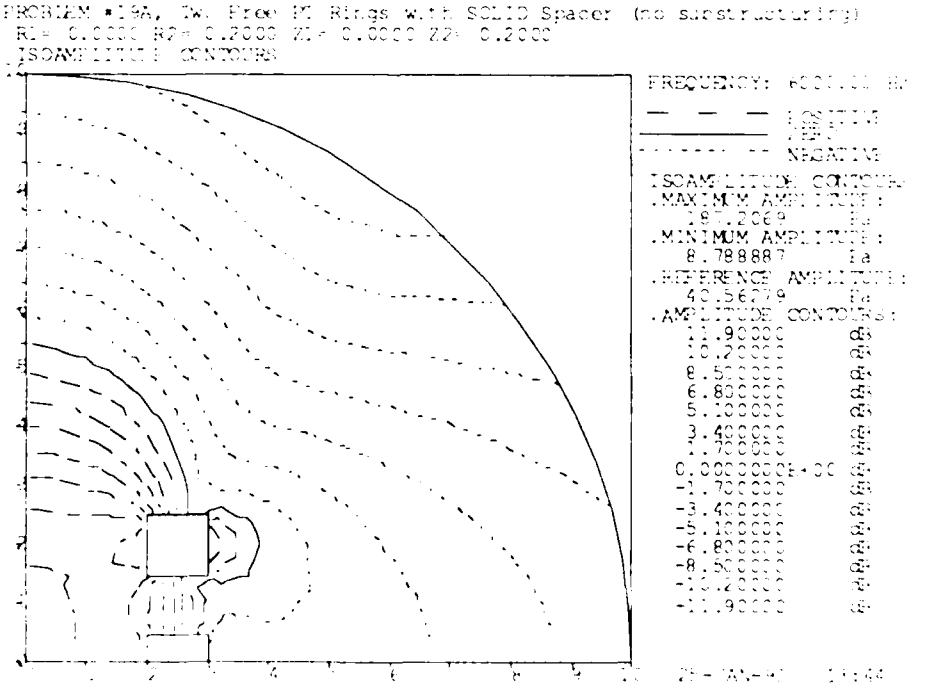

12.2 PROBLEM 20

Analysis Type: DRIVE - two free-flooding PT rings with a RIGID node replacing the spacer

Input File: D20.DAT

Using the model from Problem 19, the aluminum spacer ring is replaced by a single R-type (rigid) node. Of all the S nodes of the spacer, only the central Node 282 is retained and changed to R-type. The R node becomes a common solid node for all the FTOS elements surrounding the spacer, while the F nodes remain the same as in Problem 19. Again, the same nodes of the PT rings as well as the R node are restrained in the Z-direction. The same excitation as in Problem 19 is used.

Results of the analysis are practically the same as in Problem 19(a). Figure 12.2.1 shows a plot of near field pressure contours for comparison to Figure 12.1.3.

Figure 12.2.1: Problem 20 - Pressure Contours with a Rigid Node as the Spacer Ring

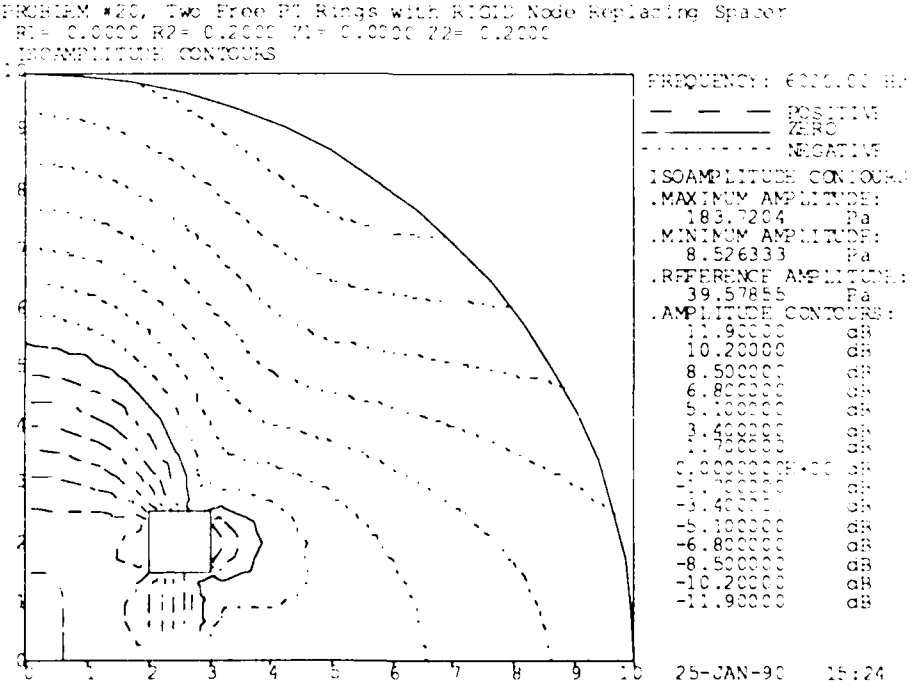

13 SERIES 10: TORSIONAL PROBLEMS

An aluminum cylinder 20 cm in diameter and 40 cm long is used to demonstrate torsional problems. A diagram of the structure is given in Figure 13.0.1. The F. E. mesh is shown in Figure 13.0.2 with element numbers, and node numbers are given in Figure 13.0.3.

Since real torsional vibration modes cannot couple to a fluid acoustically, fluids will never be used meaningfully in a torsional problem.

Driving of torsional deformations piezoelectrically has not yet been demonstrated. This will require axial/radial poling with a tangential driving field or tangential poling with axial/radial driving fields, implying either E-nodes in PAR elements or A-nodes in PT elements. In either case, some modification to the PAR and/or PT elements may be necessary.

Figure 13.0.1: Series 10 - Solid Cylinder Model for Torsional Problems

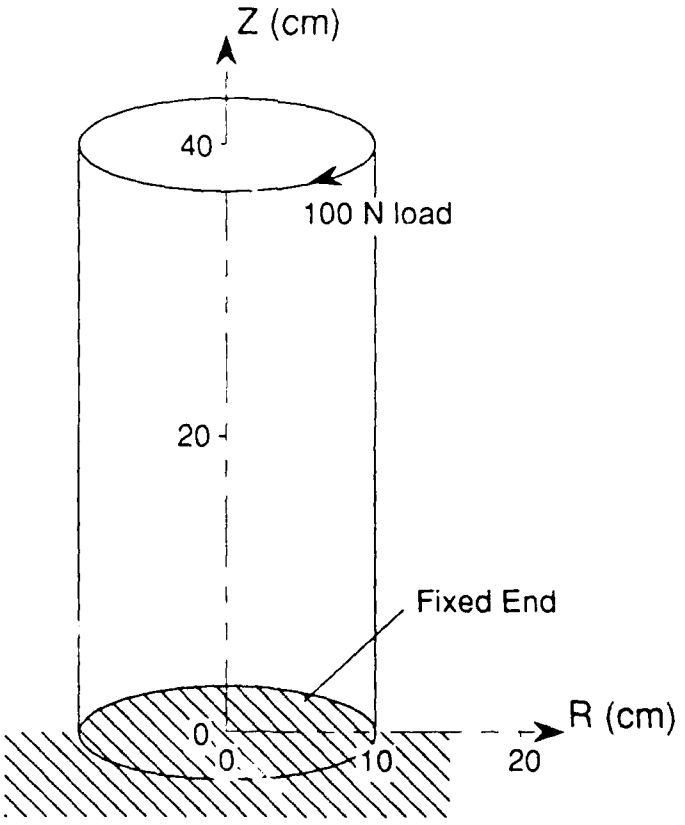

Figure 13.0.2: Series 10 - Element Numbering

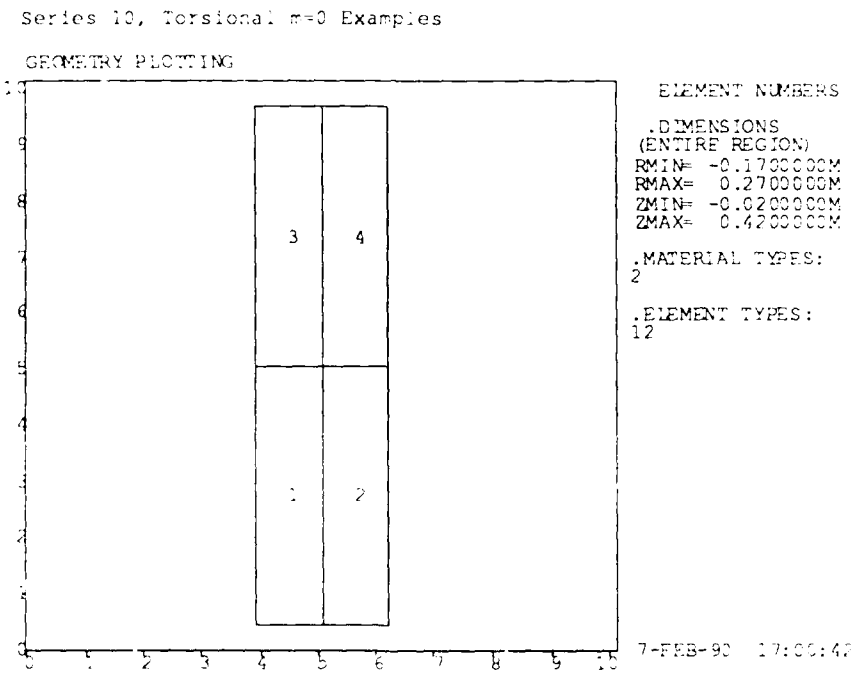

Figure 13.0.3: Series 10 - Node Numbering

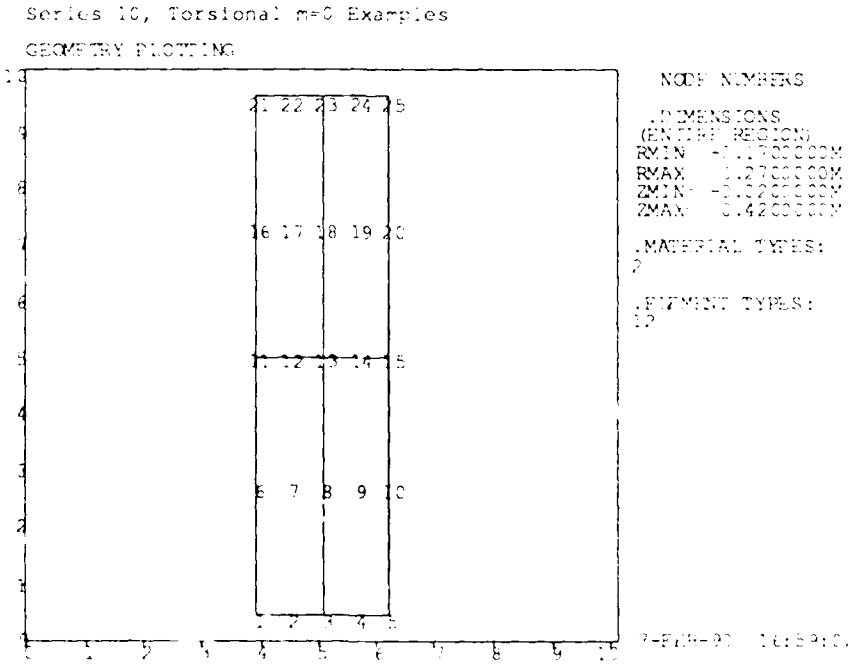

13.1 PROBLEM 21

Analysis Type: STATC - Torsional load

Input File: D21.DAT

Torsional analysis is invoked by setting MSYM = –1 in Card 2, with the Fourier mode number IMODE = 0. The nodes on one end of the cylinder are fixed in R, Z, and ø, and a 100 N torsional load is applied at Node 25 on the other end of the cylinder. As this load is at a radius of 0.1 m, the torque is 10 Nm.

From simple elastic theory, the displacement in radians for a circular cylinder of radius a and length L, subjected to a torque T is given by

$$\phi = 2TL / (G\pi a^4) \qquad (13.1)$$

where G = 0.2664E11 Pa is the shear modulus of the aluminum. Eq. 13.1 predicts a tangential displacement of 0.9559E–6 radian at the end of the cylinder for a uniform torque of 10 Nm. MAVART predicts a displacement of 0.9927E–6 rad at Node 25, and 0.9152E–6 rad at Node 23, which is at mid-radius. This variation is due to the load being applied on the outer radius, and not uniformly across the end of the cylinder.

The graphics program GRAF1 does not support plotting of torsional displacements, hence no graphic output is displayed.

13.2 PROBLEM 22

Analysis Type: EIGEN - Torsional modes

Input File: D22.DAT

A modal analysis was conducted on the model depicted in Figure 13.0.1. The same zero fixities were applied and the 100 N load was removed, so the vibrating structure is a fixed-free cylinder. Torsional modes will occur when the cylinder length is an odd multiple of one quarter wavelength. The shear velocity is given by $c_s = \sqrt{(G/\rho)}$, where ρ = 2700 kg/m^3 is the density of the aluminum. The calculated fundamental frequency for the 0.4 m long cylinder is 1963.1 Hz. MAVART predicts 1963.7 Hz, in very close agreement.

14 SUMMARY

1. With few exceptions, all example problems from the Examples Manual [1.1c] have been run successfully on the μVAX 3900 at DREA, using the latest version of MAVART (MAVART9) with the SPARSPAK solver. Some of the problems' input data required modification or minor correction to yield satisfactory results.

2. A few deficiencies in MAVART have been uncovered in this work:

   (a) Pressures arising in a fluid on one side of a solid enclosing structure are not properly transferred to a fluid on the other side of the structure via the FTOS / structure / FTOS interfaces. On the other hand, if the driving forces arise within the structure, then pressures on both sides are correct (Problem 16).

   (b) It is not clear whether piezoelectric drive of torsional deformations can be accommodated without some modification to the PAR and/or PT elements (Series 10 problems).

3. The post-processor program GRAF1 has been used to display a broad range of analysis data from all example problems except the torsional problems. As well, GRAF1 has been used to display model geometry for all examples.

15 RECOMMENDATIONS

1. The deficiency in FTOS modelling capability should be corrected during the next contract for MAVART modifications.

2. An example problem that demonstrates piezoelectric drive of torsional deformations should be added to the Series 10 Problems. If necessary, MAVART should be modified to allow such a driving mode.

3. The DREA post-processor GRAF1 should be updated to support plotting of tangential displacements for both torsional problems and for problems where the Fourier symmetry m is greater than zero.

16 REFERENCES

[1.1] (a) *User's Manual for Program MAVART*, (b) *Theoretical Manual for Program MAVART*, (c) *Examples Manual for Program MAVART Vol. I & II*, DREA Contractor Report CR/87/442, E. L. Skiba, Ontario Research Foundation, June, 1987.

[1.2] *User's Guide for Program GRAF1*, David R. Chang, B. A. Armstrong, B. L. Fanning, G. W. McMahon, and Y. R. Bonin, DREA Note SP/89/12, September 1989.

[1.3] *Programmer's Guide for Program GRAF1*, David R. Chang, B. A. Armstrong, B. L. Fanning, G. W. McMahon, and Y. R. Bonin, DREA Note SP/89/12, September 1989.

[1.4] *GRID: A Fortran Program for using a Digitizing Table to Enter a Finite Element Grid*, Bruce A. Armstrong, DREA Tech. Memo. 84/Y, November 1984.

[1.5] *A User's Manual for MOD, a Fortran Program for Modifying Finite Element Grids for MAVART*, B. A. Armstrong, DREA Research Note RN/SP/84/3, May 1984.

[1.6] *A User' Guide to the MAVART Finite Element Package*, B. A. Armstrong, DREA Research Note RN/SP/84/5, July 1984.

[1.7] *On the Input Material Properties Data Required by MAVART*, D. F. Jones, DREA Note SP/87/10, December 1987.

[1.8] *Changes to GRID and MOD, Fortran Programs for Creating and Modifying MAVART Data Files*, B. L. Fanning, DREA Note SP/86/2, December 1986.

[1.9] *Modifications to MAVART 8.0 and Supporting Programs*, B. L. Fanning, DREA Note SP/88/3, February 1988.

[4.1] *Piezoelectric Technology, Data for Designers*, Clevite Corporation, Piezoelectric Division (1965).

[4.2] *MAVART Testing - Part I*, G. W. McMahon, DREA Note SP/89/8, July 1989.

[4.3] *Research and Development of Spherical Transducers, Final Development Report*, H. Jaffe, F. Rosenthal, and H. Baerwald, Clevite Research Center, ONR Contract Nonr 1825(00), April 1957.

UNCLASSIFIED

SECURITY CLASSIFICATION OF FORM

(highest classification of Title, Abstract, Keywords)

DOCUMENT CONTROL DATA

(Security classification of title, body of abstract and indexing annotation must be entered when the overall document is classified)

1. ORIGINATOR (the name and address of the organization preparing the document. Organizations for whom the document was prepared, e.g. Establishment sponsoring a contractor's report, or tasking agency, are entered in section 8.)

Defence Research Establishment Atlantic and
Acres International

2. SECURITY CLASSIFICATION (overall security classification of the document, including special warning terms if applicable)

Unclassified

3. TITLE (the complete document title as indicated on the title page. Its classification should be indicated by the appropriate abbreviation (S,C,R or U) in parentheses after the title.)

Examples Manual for Program MAVART

4. AUTHORS (Last name, first name, middle initial. If military, show rank, e.g. Doe, Maj. John E.)

McMahon, G.W. (DREA) and Skiba, E.L. (Acres International)

5. DATE OF PUBLICATION (month and year of publication of document)	6a. NO. OF PAGES (total containing information. Include Annexes, Appendices, etc.)	6b. NO. OF REFS (total cited in document)
August 1990	100	12

6. DESCRIPTIVE NOTES (the category of the document, e.g. technical report, technical note or memorandum. If appropriate, enter the type of report, e.g. interim, progress, summary, annual or final. Give the inclusive dates when a specific reporting period is covered.)

Technical Memorandum

8. SPONSORING ACTIVITY (the name of the department project office or laboratory sponsoring the research and development. Include the address.)

Defence Research Establishment Atlantic
P.O.Box 1012, Dartmouth, Nova Scotia B2Y 3Z7

9a. PROJECT OR GRANT NO. (if appropriate, the applicable research and development project or grant number under which the document was written. Please specify whether project or grant)	9b. CONTRACT NO. (if appropriate, the applicable number under which the document was written)
DRDM01	

10a. ORIGINATOR 'S DOCUMENT NUMBER (the official document number by which the document is identified by the originating activity. This number must be unique to this document.)	10b. OTHER DOCUMENT NOS. (any other numbers which may be assigned this document either by the originator or by the sponsor)
DREA Technical Memorandum 90/204	

11. DOCUMENT AVAILABILITY (any limitations on further dissemination of the document, other than those imposed by security classification)

(X) Unlimited distribution
( ) Distribution limited to defence departments and defence contractors; further distribution only as approved
( ) Distribution limited to defence departments and Canadian defence contractors; further distribution only as approved
( ) Distribution limited to government departments and agencies; further distribution only as approved
( ) Distribution limited to defence departments; further distribution only as approved
( ) Other (please specify):

12.. DOCUMENT ANNOUNCEMENT (any limitations to the bibliographic announcement of this document. This will normally correspond to the Document Availability (11). However, where futher distribution (beyond the audience specified in 11) is possible, a wider announcement audience may be selected.)

UNCLASSIFIED

SECURITY CLASSIFICATION OF FORM

DCD03 2/06/87

13. ABSTRACT (a brief and factual summary of the document. It may also appear elsewhere in the body of the document itself. It is highly desirable that the abstract of classified documents be unclassified. Each paragraph of the abstract shall begin with an indication of the security classification of the information in the paragraph (unless the document itself is unclassified) represented as (S), (C), (R), or (U). It is not necessary to include here abstracts in both official languages unless the text is bilingual).

This document is the third in a set of documents that provides information on the Finite Element Model for the Analysis of Vibration and Acoustic Radiation of Transducers (MAVART). The set comprises: 1. Theoretical Manual for Program MAVART, 2. User's Manual for Program MAVART, and 3. Examples Manual for Program MAVART. The program MAVART is resident at the Defence Research Establishment Atlantic (DREA) and has been developed under several research contracts to Canadian industry from 1976 to the present (1990). The original set of documents formed Contractor Report DREA CR/87/442 and they are now being extensively revised.

This Examples Manual attempts to demonstrate and exercise all of the capabilities and features of MAVART. As well, the DREA postprocessing program GRAF1 has been used to display the data for the example problems.

14. KEYWORDS, DESCRIPTORS or IDENTIFIERS (technically meaningful terms or short phrases that characterize a document and could be helpful in cataloguing the document. They should be selected so that no security classification is required. Identifiers, such as equipment model designation, trade name, military project code name, geographic location may also be included. If possible keywords should be selected from a published thesaurus, e.g. Thesaurus of Engineering and Scientific Terms (TEST) and that thesaurus-identified. If it not possible to select indexing terms which are Unclassified, the classification of each should be indicated as with the title).

Transducers
Hydrophones
Finite Elements
Vibration Analysis
Projectors
Mathematical Modelling
Acoustic Radiation